Emergent relationships between the functional diversity of marine zooplankton and ecosystem functioning in the global ocean

Running title: Global zooplankton functional diversity and marine ecosystem functioning

List of authors: Fabio Benedetti[1*], Jonas Wydler[2,3], Corentin Clerc[1], Nielja Knecht[1,4], Meike Vogt[1]

Institutional affiliations

1. *Environmental Physics, Institute of Biogeochemistry and Pollutant Dynamics, ETH Zürich, 8092 Zürich, Switzerland*
2. *Eawag, Swiss Federal Institute of Aquatic Science and Technology, 8600, Dübendorf, Switzerland*
3. *University of Zürich, Department of Geography, 8057 Zürich, Switzerland*
4. *Stockholm Resilience Centre, Stockholm University, Stockholm, Sweden*

ORCID

- *F.B. (0000-0002-7554-3646)*
- *J.W. (0009-0001-3808-9800)*
- *C.C. (0000-0002-8436-4391)*
- *N.K. (0000-0002-4105-3251)*
- *M.V. (0000-0002-0608-1935)*

*Contact information: Dr. Fabio Benedetti (fabio.benedetti@unibe.ch; +41 44 632 09 72)

Abstract

Copepods are a major group of the mesozooplankton and thus a key part of marine ecosystems worldwide. Their fitness and life strategies are determined by their functional traits which allow different species to exploit various ecological niches. The range of functional traits expressed in a community define its functional diversity (FD), which can be used to investigate how communities utilize resources and shape ecosystem processes. However, the spatial patterns of copepod FD and their relation to ecosystem functioning remain poorly understood on a global scale. Here, we use estimates of copepod community composition derived from species distribution models in combination with functional traits and indicators of ecosystem functioning to investigate the distribution of multiple facets of copepod FD, their relationships with species richness and ecosystem processes. We also project how anthropogenic climate change will impact the facets of copepod FD. We find that the facets of FD respond to species richness with variable strength and directions: functional richness, divergence and dispersion increase with species richness whereas functional evenness and trait dissimilarity decrease. We find that primary production, mesozooplankton biomass and carbon export efficiency decrease with species richness, functional richness, divergence and dispersion. This suggests that ecosystem functioning may be disproportionally influenced by the traits of a few dominant species in line with the mass-ratio hypothesis. Furthermore, climate change is projected to promote trait homogenization globally, which may decrease mesozooplankton biomass and carbon export efficiency globally. The emergent covariance patterns between FD and ecosystem functions we find here strongly call for better integrating FD measurements into field studies and across scales to understand the effects of changing zooplankton biodiversity on marine ecosystem functioning.

Keywords: Zooplankton; Functional diversity; Ecosystem functioning; Climate change; Global ocean; Copepods

1. Introduction

Plankton comprise myriads of floating microscopic organisms that shape the functioning of marine ecosystems (de Vargas et al., 2015). In the plankton, copepods are small crustaceans (i.e., usually 0.2-20 mm) that dominate mesozooplankton communities in terms of abundance and species diversity (Steinberg & Landry, 2017; Brandão et al., 2021). They are pivotal players for the biologically driven transfer of carbon from the atmosphere to the deep ocean, a process known as the biological carbon pump (Turner, 2015; Steinberg & Landry, 2017). Copepods display a spectrum of functional traits and traits trade-offs allowing them to efficiently feed on motile and non-motile microplankton, marine snow and even gelatinous macrozooplankton (Kiørboe et al., 2011; Takahashi et al., 2013; Brun et al., 2017). Functional traits are characteristics that control the fitness of organisms and determine their ability to feed, grow and reproduce (Violle et al., 2007; Litchman et al., 2013). The range and composition of functional traits expressed in a community constitutes the functional dimension of biodiversity: functional diversity (FD; Mouillot et al., 2013). Copepod trait composition determines how mesozooplankton contribute to key functions of the biological carbon pump, such as phytoplankton grazing, secondary production, or the active export of organic carbon at depth (Henson et al., 2019; Brun et al., 2019; Pinti et al., 2023). For instance, large copepods egest large and fast sinking carbon-rich pellets that promote export efficiency of particulate organic carbon to depth (Stamieszkin et al., 2015; Brun et al., 2019). The efficiency of the biological carbon pump partly depends on the amount and the composition of sinking particles (Le Moigne et al., 2016; Nowicki et al., 2022) which are influenced by trait composition and thus copepod FD.

However, the FD patterns of marine copepods have seldomly been measured *in situ* and over large scales (Becker et al., 2021; Tang et al., 2022; Li et al., 2022) whereas taxonomic diversity patterns are relatively well documented (Rombouts et al., 2010; Benedetti et al., 2023). The spatial distribution of mean trait values in copepod communities is not even in the global ocean, as certain trait combinations are more suitable than others given varying environmental conditions (Brun et al., 2016; van Someren-Grève et al., 2017; Prowe et al., 2018; Benedetti, Wydler & Vogt, 2023; Djeghri et al., 2023). For example, planktonic copepods display larger body sizes in cold-water environments (Campbell et al., 2021). Moreover, strategies that optimize the survival of early life stages, such as sac-spawning, tend to prevail in tropical oligotrophic gyres where cannibalism and carnivory are more prevalent (Kiørboe & Sabatini, 1994; Woodd-Walker et al. 2002; Benedetti, Wydler & Vogt, 2023). Many species can display very similar trait combinations and thus perform similar functions so changes in the number of species or their identity can be uncoupled from changes in FD (Hillebrand et al., 2017; Blowes et al., 2019). Because of functional redundancy, we anticipate that copepods will exhibit FD gradients that diverge from richness gradients, similar to the patterns observed for numerous other marine clades, from reef fishes (Mouillot et al., 2014; McLean et al., 2021; Ferrari et al., 2023), corals (McWilliam et al., 2018), bivalves (Edie et al., 2018) to marine mammals (Albouy et al., 2017; Pimiento et al., 2021). Such studies showed that even speciose communities can be vulnerable to functional loss if functions are only carried by few species in said community (Mouillot et al., 2014; McWilliam et al., 2018; McLean et al., 2021).

Our limited understanding of zooplankton FD distribution limits our capacity to predict how changes in biodiversity affect ecosystem functions across ecosystems (Cardinale et al., 2012).

This is a major aspect to address in the context of climate change since the richness and composition of zooplankton will likely be reshuffled (Beaugrand et al., 2015; Benedetti et al., 2021). Global warming may elicit strong changes in community composition at high latitudes, as warm-water taxa migrate poleward and replace local cold-water taxa along the way (Benedetti et al., 2021). Yet, it is unknown how such changes will affect zooplankton FD. Therefore, we need to answer the following questions: How do changes in copepod species richness relate to changes in trait diversity? Where are higher levels of zooplankton FD expressed worldwide? Do higher levels of FD promote ecosystem functions such as secondary production or carbon export?

Such ecosystem functions may be positively or negatively related to marine copepod FD and they may be scale-dependent (Chalmandrier et al., 2017; Gonzalez et al., 2020; Suarez-Castro et al., 2022). On one hand, more speciose communities could harbor a wider range of functional traits (i.e., higher functional richness) enabling copepods to optimize the use of resources to be converted to biomass ("portfolio effect"; McCann, 2000). As a result, copepod biomass may increase with species richness and functional richness. On the other hand, production could be mainly carried out by a few dominant species that outcompete less fit species in the community ("mass-ratio hypothesis"; Grime, 1998). As a result, copepod biomass could scale negatively with the richness of species and traits. If ecosystem functions such as carbon export are influenced by traits distinct from those governing secondary production, then the nature and intensity of their association with copepod FD may deviate from that observed with secondary production (Yan et al., 2023). FD is multi-faceted (Villéger et al., 2008) so these relationships could vary in strength and shape depending on the facet considered (Paquette & Messié, 2010; Maureaud et al., 2019; Suarez-Castro et al., 2022). For instance, if the balance between trait combinations matters more to productivity than their absolute number, indices such a functional evenness or functional dispersion should correlate more strongly with ecosystem functions than functional richness (Brun et al., 2020; Le Bagousse-Pinguet et al., 2021). Similar to the above, if spatial gradients in trait composition are decoupled from those in trait richness, assemblages with very dissimilar trait composition (beta-FD; Villéger et al., 2011) may achieve similar levels of functional richness (McLean et al., 2021; Suarez-Castro et al., 2022). Therefore, integrating beta-FD is crucial to explore the links between FD and ecosystem functions.

The relationships between copepod FD and ecosystem functions in the global ocean can be explored in two ways. Firstly, direct measurements of ecosystem functions and fine-resolution diversity can be taken simultaneously to measure causal links between variables, using covariance coefficients or structural equation modelling (Gamfeldt et al., 2015; Lehtinen et al., 2017; Maureaud et al., 2019). Despite the substantial progress made in zooplankton field sampling (Lombard et al., 2019; Ratnarajah et al., 2023), such simultaneous and standardized measurements remain too sparse for global scale analyses. Choosing an indirect approach, we leverage the large number of species-level observations (Benedetti et al., 2021) and satellite-based or model-based indicators of ecosystem functioning to diagnose the emergent covariance between the various facets of copepod FD and ecosystem functions (Gamfeldt et al., 2015; Eriksson et al., 2024). We rely on functional trait data and global community matrices given by an ensemble of species distribution models (SDMs; Elith & Leathwick, 2009) to estimate patterns of zooplankton FD for the contemporary and future ocean. Our approach allows to assess how decades of field observations answer the following questions: (i) How do the

multiple facets of zooplankton FD relate to the global gradient of species richness on a mean annual scale (Stuart-Smith et al., 2013; Suarez-Castro et al., 2022)? (ii) What is the direction, shape and strength of the emergent relationships between zooplankton FD and indicators of ecosystem functioning? And (iii) how will zooplankton FD patterns change in the future under anthropogenic climate change (Benedetti et al., 2021)?

2. Materials and methods

2.1. Copepod community matrices for the contemporary and future ocean

We use community matrices that describe the species composition of copepod assemblages worldwide in combination with a functional trait table (see section 2.2) to estimate multiple FD indices (see section 2.3). These community matrices were generated by Benedetti, Wydler & Vogt (2023) based on habitat projections generated by an ensemble of state-of-the art SDMs following the methodology of Benedetti et al. (2021). In short, SDMs were calibrated on a global monthly scale based on species-level presence data taken in the upper 500 m as compiled in the ZooBase dataset (Benedetti et al., 2021). For each species, presences were aggregated on a monthly 1°x1° ocean cell grid following the WGS84 spatial reference system and thinned according to a 100 km radius to remove observations that fell within the same monthly cell. For the 343 species displaying at least 50 different presences, background data were generated following the target-group approach of Phillips et al. (2009). Three types of SDMs spanning various levels of complexity were used to model the species' distributions and account for the main source of uncertainty in SDMs-based studies (Thuiller et al., 2019): Generalized Linear Models (GLM), Generalized Additive Models (GAM) and Artificial Neural Networks (ANN). These SDMs were tuned to fit non-overfitting response curves that describe how each species' habitat suitability (ranging between zero and one) varies as a function of the environmental predictors included in the SDMs. Six environmental predictors were used: sea surface temperature (SST; WOA 2013v2), surface photosynthetically available irradiance (PAR), log-transformed surface nitrate concentrations (WOA 2013; Garcia et al., 2014), the excess of nitrate to phosphates relative to the Redfield ratio (N*; Sarmiento & Gruber, 2006), the excess of silicate to nitrate relative to the Redfield ratio (Si*) and log-transformed surface chlorophyll-*a* concentration (SeaWiFS). These six predictors were chosen because: (i) they were not collinear at the scale of the occurrence data (Dormann et al., 2013); (ii) they ranked within the top predictors across all species, based on tests of relative importance ranks; (iii) these variables were available for describing the future state of the ocean based on an ensemble of Earth System Models (ESMs), thus allowing to perform ensemble projections and to evaluate the impact of climate change on FD. Previous work showed that this set of predictors robustly models global zooplankton diversity patterns, and that predictor choice is a minor source of projection uncertainty relative to SDM and ESM choice (Benedetti et al., 2021, 2023). All three types of SDMs were calibrated 10 times on different random subsets of 80% the species-level datasets and evaluated against the remaining 20%. Ultimately, 303 copepod species (88% of the 343 initially considered) were robustly modelled and used to construct the species assemblages, one assemblage corresponding to one monthly 1°x1° ocean grid cell. Then, habitat suitability indices (HSI) were projected onto the 12 monthly climatologies of the predictors included in the 30 SDMs. Average monthly HSI was calculated for each type of SDMs and each species to

build the ensemble members of contemporary copepod assemblage composition (see Benedetti, Wydler & Vogt, 2023 for a full description).

To estimate the impact of anthropogenic climate change on zooplankton FD, we estimated the composition of copepod assemblages for the future ocean. Future monthly fields of the six environmental predictors were obtained from the projections of five ESMs forced by the IPCC's RCP8.5 scenario from the MARine Ecosystem Model Intercomparison Project (MAREMIP; Sailley et al., 2013) and the Coupled Model Intercomparison Project 5 (CMIP5; Taylor et al., 2012). The future monthly climatologies were obtained from the ESM's projections over the 2012-2100 period and anomalies were computed by subtracting the values of the "baseline" period (2012-2031) to the values projected for the "end-of-century" period (2081-2100). To obtain the final climatologies of the six predictors for the future state of the surface ocean, those anomalies were added to the in situ climatologies used to calibrate the SDMs. The SDMs of the 303 copepod species modelled were then projected onto these future monthly climatologies for each of the ESM separately. This way, we estimate monthly species composition in the future global ocean based on mean species HSI derived from 15 ensemble members (three SDM types and five ESMs).

2.2. Species functional traits and functional dissimilarity matrix

Computing FD estimates requires information about the functional traits of the copepod species modelled. This dataset is fully described in Benedetti, Wydler & Vogt (2023) and includes the following five functional traits based on the data available from the literature (Table S1): (i) Body size (quantitative continuous) estimated through average maximum female body size (adult stages only) in millimeter; body size is considered a master trait as it impacts all life functions, scales with most physiological rates and influences predator–prey interactions; (ii) Trophic group (categorical) which gathers the species based on their preferred food sources to indicate their role in food-web dynamics (although we acknowledge that most marine planktonic copepods are omnivorous); (iii) Feeding mode (categorical) which describes the various strategies copepods deploy to detect and capture their prey following Kiørboe (2011); (iv) Myelination (binary) which indicates the presence or absence of a lipid-rich myelin sheath around the nerves which enables faster attack or evasive reactions and thus impact feeding and mortality rates (Lenz, 2012); and (v) Spawning mode (binary) which indicates whether the copepods release their eggs in open water after fertilization (free-spawning) or are carried by females in egg sacs or egg masses (sac-spawning). We underline that these functional trait values are representative of adult stages (i.e., not the nauplii) and correspond to mean values derived from field or lab observations of diverse copepod populations from around the world. The species' trophic groups and feeding modes were fuzzy coded to represent the fact that species can display several feeding modes and trophic groups. Therefore, the final functional trait table encompasses 10 trait dimensions and cover the 303 copepod species retained for the community matrices.

FD indices require a distance matrix that indicates the pairwise functional dissimilarity of copepod species based on their combinations of traits (Mouillot et al., 2013; Benedetti et al., 2016). To obtain the latter, we computed a Gower distance matrix based on the final functional trait table, as the Gower distance can accommodate continuous, binary and categorical traits.

We used the *gawdis* R package (de Bello et al., 2021) as it enables us to specify which trait dimensions are fuzzy-coded and belong to the same trait category.

2.3. Functional diversity indices

FD is a multifaceted concept embedding changes in composition within and between assemblages (Mason et al., 2005; Villéger et al., 2011). Consequently, we chose to compute indices that describe the following facets of FD: (i) how much of the total functional space is filled by the composition of each assemblage (functional richness), (ii) how the HSI and/or inferred presences/absences of species are distributed within the functional spaces (functional dispersion, evenness, or divergence), and (iii) how much assemblages overlap in functional space (beta-FD). The FD indices used here are summarized in Table 1 and an extensive description of their computation is given in the Supplementary Methods 1.

We computed Faith's index (Faith) as a proxy for functional richness using the Gower distance matrix described above as the functional dendrogram (Faith, 1992). Standardized-effect-sizes of Faith (SES Faith) were calculated to study functional richness patterns that are not biased by differences in species richness (Schleuter et al., 2010). The SES Faith values and p-values indicate where functional richness is significantly higher or lower than the values dictated by species richness alone. SES Faith values < 0 indicate that functional clustering occurs due to environmental filtering in the copepod assemblage, whereas values > 0 indicate that functional overdispersion occurs (Mikryukov et al., 2023).

To evaluate facet (ii), we computed four complementary FD indices (Mason et al., 2005; Villéger et al., 2008): functional evenness (FEve), functional dispersion (FDis), Rao's quadratic entropy (Rao's Q) and functional divergence (FDiv). Following the guidelines of Mouillot et al. (2021), we calculated those FD indices based on the first four axes of a principal coordinate analysis (PCoA) as these retained a similar level of dissimilarity as the original Gower distance matrix (Fig. S1). Functional richness is more commonly quantified through the FRic index (Villéger et al., 2008) so we made sure that Faith provided similar functional richness patterns as standardized FRic values (Fig. S2). We preferred Faith over FRic because it is less sensible to SDM choice and because FRic is only representative of changes in species composition occurring at the edges of the functional space.

To evaluate facet (iii), we compute pairwise beta-FD based on Jaccard's dissimilarity index (Baselga, 2010; Cardoso et al., 2014). Each pair of assemblages (A_i, A_j) shows a total trait dissimilarity that corresponds to the sum of the lengths of edges that are unique to each assemblage-specific dendrogram (Cardoso et al., 2014). Trait dissimilarity can be partitioned into two additive components (Baselga, 2010): replacement (Trait turnover) and richness differences (Trait nestedness). Trait dissimilarity values close to 1 indicate that two assemblages display functional dendrograms with very different number of non-overlapping branches. Since these indices are calculated for each community matrix, there are as many Trait dissimilarity values as pairs of assemblages, and they represent spatial patterns in copepod beta-FD. Here, we retained the average values of Trait dissimilarity, Trait turnover and Trait nestedness.

The indices described in Table 1 were calculated for every monthly community matrix representative of the contemporary ($n = 36$) and future ocean ($n = 180$). We also computed monthly species richness based on the same community matrices to investigate how the facets

of FD covary with taxonomic diversity and test if species-rich assemblages are more or less functionally diverse than species-poor assemblages (Stuart-Smith et al., 2013).

2.4. Proxies of marine ecosystem functioning

We gathered variables describing the spatial patterns of primary production, secondary production, and particulate organic carbon (POC) export outside of the euphotic zone to explore their covariance with zooplankton functional diversity on a global mean annual scale. To assess the covariance of FD with productivity, we used the recent observation-based product of mean annual epipelagic mesozooplankton biomass (MESOZOO, in mmol C m^{-3}) of Clerc et al. (2024). MESOZOO was generated with a habitat modelling pipeline tailored for continuous target variables (Knecht et al., 2023) which was trained with the monthly mesozooplankton biomass fields from the MARine Ecosystem DATa (MAREDAT) (Moriarty & O'Brien, 2013) in combination with monthly environmental predictors of mesozooplankton biomass (Clerc et al., 2024).

To assess the covariance of zooplankton FD with the productivity of phytoplankton, satellite-based ocean colour data (GlobColour) were sourced from the Copernicus Marine Environment Monitoring Service (CMEMS; data.marine.copernicus.eu). We retrieved the level 4-merged monthly concentrations (in mg m^{-3}) of chlorophyll-*a* (CHL-A) and the associated CHL-A concentrations in diatoms (DIATO), dinoflagellates (DINO), haptophytes (HAPTO), green algae (GREEN), *Prochlorococcus* (PROCHL) and prokaryotes (PROKAR), on a 100 km resolution (Xi et al., 2021). We used the monthly fields for the 2003-2022 period not to be biased by years where some months are missing and to match the period for which global NPP estimates are available as well. As the difference between gross primary production and respiration, NPP indicates the rate of biomass accumulation by phytoplankton that is available to zooplankton grazers. We retrieved the standard Vertically Generalized Production Model (VGPM) product from the Ocean Productivity website (oregonstate.edu; Behrenfeld & Falkowski, 1997). It provides surface NPP estimates based on MODIS observations for the 2002-2022 period, in mg C m^{-2} d^{-1}.

To assess how zooplankton functional diversity relates to the particle size distribution of plankton cells and particles, we retrieved the slope of the power-law particles size distribution (SLOPE) measured from satellite ocean color observations (Kostadinov et al., 2009). SLOPE values increase with the contribution of small cells and particles to the planktonic size spectrum. The GlobColour data, NPP estimates, and SLOPE estimates were re-sampled on the same 1° grid cell as the functional diversity estimates and monthly climatologies were computed based on all the data available.

To assess the covariance of zooplankton functional diversity with the strength and functioning of the biological carbon pump, we further retrieved the model-based estimates of mean annual sinking POC flux (POC FLUX) and mean annual POC export at the base of the euphotic zone (FPOC) of DeVries & Weber (2017) converted to mg C m^{-2} d^{-1}. We used the NPP estimates given by the latter study to estimate the efficiency of POC export fluxes through the E-RATIO (FPOC/NPP) which represents the fraction of POC that is exported below the euphotic zone relative to the initial productivity level. In the analyses below, we retained the VGPM-based NPP estimates as it very similar to the product of DeVries & Weber (2017) (Fig. S3). We compared the annual FPOC estimate to the more recent one of Clements et al. (2023) to ensure

that the emergent patterns investigated in this study are robust to various large-scale estimates of POC export (Fig. S4). The mean annual values of these indicator variables are shown in Fig. S5.

2.5. Analyses

All analyses were carried out in the R coding environment (R Core Team, 2021). First, mean annual ensemble values of species richness and FD indices were computed based on all the monthly values available and then mapped to visualize the main spatial patterns of marine copepod diversity for the contemporary period. For SES Faith, the spatial distribution and frequency of significant p-values at a risk of alpha = 0.05 was examined to identify the regions of the global ocean where Faith differs significantly from null expectations. For beta-FD, we computed the ratio between Trait turnover and Trait dissimilarity to identify the regions where functional traits dissimilarity is driven by trait replacement (i.e., ratio > 0.5). Covariance between species richness and FD indices was evaluated through linear models and second-degree polynomials. We retained the models showing the largest proportion of explained variance (adjusted R^2) based on variance analysis (ANOVA). This way, we investigated how mean annual taxonomic richness influences copepod FD and unveiled which species-rich assemblages also correspond to functionally diverse ones, along more than just one facet of FD (Stuart-Smith et al., 2013; McWilliam et al., 2017). We expected latitude to modulate the relationship between species richness and FD (Stuart-Smith et al., 2013; Benedetti, Wydler & Vogt, 2023). Therefore, we integrated an interaction term between species richness and absolute latitude in the linear models to test whether latitude imposes a strong effect on the covariance between taxonomic diversity and FD. Covariance between Faith and beta-FD indices were also examined to test if: (i) functionally rich assemblages show lower trait dissimilarity because of the co-occurrence of functionally redundant taxa, and (ii) the global gradient in functional richness is driven by Trait turnover or rather by Trait nestedness.

Second, we studied the covariance of the mean annual values of the ecosystem functioning proxies described in section 2.4 with our diversity estimates. The same regression-based approaches as above were used. Considering the multidimensionality of the dataset (23 variables), we focused on examining the emergent covariance of species richness and FD indices with MESOZOO and the indicators related to the biological carbon pump (NPP, POC FLUX, FPOC and E-RATIO). To explore the covariance of all variables together, we centered and scaled them to variance (i.e., Z-scores computation) and entered them into a principal component analysis (PCA). The ecosystem functioning proxies were used as quantitative supplementary variables and all of them were log10-transformed because they were skewed towards low values, except for SLOPE and MESOZOO. The Z-scores were displayed on a heatmap to illustrate the covariance structure between the FD indices and the ecosystem functioning proxies.

Finally, we investigated how climate change may impact copepod FD in the future. To do so, we computed the differences between the values of the monthly diversity indices calculated for the end-of-century period and the values calculated for the contemporary period, for each matching combination of assemblages (e.g., future monthly GAM-based assemblages were compared to contemporary GAM-based assemblages). These differences were standardized to the contemporary values to be expressed in relative changes. Then, mean annual ensemble

values of these relative changes were computed for each grid cell based on all ensemble members (n = 180). Prediction uncertainty was investigated to show where future changes in copepod FD are more, or less sensitive to ensemble member choice. The intra-annual variability, SDM-specific variability and ESM-specific variability were quantified and mapped through the standard deviation associated to their mean values.

3. Results

3.1. Distribution of mean annual copepod FD within and between assemblages

Copepod species richness displays a classic latitudinal diversity gradient on a mean annual scale (Figure 1), as extensively documented in previous work already (Benedetti, Wydler & Vogt, 2023; Benedetti, Gruber & Vogt, 2023). Richness increases from the poles to the equator, with peaks in the tropical oligotrophic gyres and the eastern Mediterranean Sea and dips in upwelling systems (Fig. 1a). More interestingly, we unveil an emergent functional richness pattern that departs from the species richness gradient towards higher latitudes (> 60°; Fig. 1b,c). Within the tropical band (0°-30°), the Faith pattern is very similar to the species richness gradient (Spearman's correlation coefficient = 0.94; $P < 0.001$), with peaks in the gyres and dips in upwelling systems. Average richness drops from 104.5 to 68.6 (-34.2%) when moving beyond the tropical band. Meanwhile, Faith shows a much weaker decrease (-2.5%) as annual mean Faith values > 2.8 remain frequent beyond the tropics, especially in the North Atlantic Ocean (Fig. 1b). SES Faith patterns show the regions where functional richness is higher or lower than null expectations for equal species richness levels (Fig. 1c). We unveil a clear latitudinal gradient in the sign and amplitude of SES Faith values supporting the view that environmental conditions are leading to functional clustering of copepod traits in the tropics by filtering out subsets of the functional space. Mean (± standard deviation) global SES Faith is equal to -1.23 (± 1.66), indicating that most of the ocean shows lower functional richness than null expectations. Indeed, negative mean annual SES Faith values are more widespread (62.5% of ocean cells) than positive ones; they go down to -5.18 and are concentrated in the tropical band. Meanwhile, positive SES Faith values are capped at 1.85 and 99% of these grid cells are located > 32° latitude. Inspecting the p-value distributions revealed that most of the negative SES Faith values observed in the tropics are significant, contrary to the positive ones which cannot be reliably separated from null expectations (Fig. S6). This means that the tropics show functional richness levels that are significantly lower than what could be expected from taxonomic richness.

We unveil a global gradient in mean annual FEve that is opposite to the gradient in species richness and functional richness (Fig. 1d). This means that the copepod assemblages located in the tropical gyres are characterized by scattered clouds of species in functional space whereas assemblages at higher latitudes show more regular distribution of HSI along trait dimensions. Lowest FEve values are found within the tropical gyres (0.34 ± 0.05) and are higher outside of the tropical band (0.55 ± 0.04) and in upwelling systems. Actually, the highest FEve values (> 0.5) are located in those transitional areas between the tropics and the high latitudes (around 40-45°).

The global FDis pattern is very similar to the species richness pattern (correlation coefficient = 0.89; $P < 0.001$; Fig. 1e). Regions showing higher FDis are characterized by copepod assemblages whose species are more spread out in functional space (i.e., co-occurrence of

functionally dissimilar species). The highest mean annual FDis values (> 0.32) are also found in the tropical oligotrophic gyres and the eastern Mediterranean Sea and lower values are found beyond the tropics, especially in the North Pacific Ocean and the Atlantic sector of the Southern Ocean. The lowest values (< 0.29) are located near the coasts and in eastern boundary upwelling systems. As expected, FDis patterns are nearly identical to Rao's Q patterns as both indices estimate the same facet of FD (Table 1; Figure S7).

Mean annual FDiv also shows a latitudinal gradient (Fig. 1f) but its values only range between 0.84 and 0.90 globally (0.88 ± 0.01). All FDiv values > 0.9 are located at latitudes < 30° and all values < 0.86 are located beyond 60°. However, mean FDiv does not show substantial variations within ($0.89 \pm 3.0*10^{-3}$) and outside the tropical band (0.87 ± 0.01). This means that species HSI values tend to be higher for extreme functional trait values in tropical assemblages but that extratropical assemblages can also show high HSI values at such extreme portions of the functional space.

The indices estimating facet (iii) of copepod FD highlight where the assemblages with the most dissimilar trait composition are located and whether such dissimilarity is driven by trait turnover or differences in trait richness (Figure 2). Globally, mean annual Trait dissimilarity (Fig. 2a) ranges from 0.24 to 0.47 (0.31 ± 0.06), meaning that no assemblage shows a completely dissimilar trait composition. Trait dissimilarity follows the opposite gradient to copepod species richness: it increases from the tropics (0.27 ± 0.03) to the poles (mean values > 60° = 0.39 ± 0.03). Its lowest values (< 0.25) are found in the oligotrophic gyres and its highest (> 0.40) are in the Southern Ocean, North Pacific Ocean and near coastal upwelling regions.

We find that mean annual Trait dissimilarity is largely driven by Trait turnover (Fig. 2b,c,d). Globally, mean Trait turnover follows the same gradient as Trait dissimilarity (correlation coefficient = 0.97; $P < 0.001$). Mean Trait nestedness is restricted to values < 0.10 (Fig. 2c) everywhere except in regions of the North Pacific Ocean and in coastal upwelling regions. Trait nestedness reflects differences in trait richness so it is logically opposite to Faith patterns (Fig. 1b). The ratio of Trait turnover to total Trait dissimilarity confirms the dominance of Trait turnover as a main driving process of functional dissimilarity as it if mostly > 0.5 globally (0.76 ± 0.04; Fig. 2d). It shows that the contribution of Trait turnover is highest (> 0.80) in the North Atlantic Ocean, the Arctic Ocean, and the Southern Ocean.

We here focus on mean annual patterns, but all indices show intra-annual variability which follows the amplitude of seasonal environmental variations seasonality, especially in terms of surface temperatures (Fig. S8). The uncertainty in FD indices that is driven by the choice of the species distribution model is of the same order of magnitude as seasonal variations but tends to show a different spatial pattern (Fig. S9): model choice generates more uncertainties towards higher latitudes, especially in the Southern Ocean.

3.2. Emergent relationships between species richness and FD

All FD facets show significant but varying responses to an increasing number of taxonomic units (Figure 3). We find that species-rich copepod assemblages are characterized by higher functional richness and more extreme trait values of functionally distant species compared to species-poor assemblages. Mean annual Faith, FDis and FDiv show significant increases with richness of varying strength (R^2 ranging between 0.57 and 0.74; Fig. 3a,d,e). Their relationship

to species richness is best described by second-degree polynomials that unveil how the increase rate in Faith, FDis and FDiv starts leveling off as richness increases. Based on the first derivative of the fitted polynomials, the rate of increase in Faith, FDis and FDiv decreases by more than 50% beyond richness values > 80.

Mean annual SES Faith, FEve and beta-FD indices show significant decreases of varying strength with species richness (R^2 ranging between 0.26 and 0.94; Fig. 3b,c,f,g,h). We find that species-rich copepod assemblages are more clustered in functional space (i.e., lower SES Faith and lower Trait dissimilarity) and are characterized by less regular trait expression (i.e., lower FEve) than species-poor assemblages. The gradient in taxonomic richness is associated with a decrease in Trait turnover, meaning that species-poor copepod assemblages display more dissimilar functional traits that are not found in species-rich assemblages. The relationship of SES Faith and FEve to species richness is best described by a linear decrease whereas the relationships between the three beta-FD indices and species richness are best described by second-degree polynomials. Again, the latter unveils how the rate of decrease in Trait dissimilarity and Trait turnover levels off by 50% beyond richness values > 80. The polynomial fit is weakest for Trait nestedness ($R^2 = 0.26$) and the fitted rate of decrease with richness is much weaker (from 0.10 to 0.06 only).

Figures 1 to 3 show that environmental factors associated with latitude have a potentially strong influence on the relationship between FD and species richness. To assess how strongly latitude modulates such covariance patterns, we include an interaction term between absolute latitude and richness in the linear and polynomial models above. We also perform covariance analysis (ANCOVA) to test if this interaction term improves the fit significantly. The strength of all covariance patterns varies significantly with latitude, but less so for FEve and Trait turnover. Adding absolute latitude improves the models' fit (all ANCOVA tests return $p < 0.001$) with varying degrees depending on how strong the initial fit was. The adjusted R^2 increased by 53.5% for Faith, 45.8% for SES Faith, 37.0% for FEve, 7.0% for FDis, 26.9% for FDiv, 1.1% for Trait dissimilarity, 9.4% for Trait turnover and 93.8% for Trait nestedness.

3.3. Emergent relationships between FD and indicators of ecosystem functioning

Next, we examine the covariance of species richness and FD with mean annual MESOZOO and an exhaustive suite of ecosystem functioning indicators (Figure 4; Fig. S10). Our analyses show that copepod species richness and FD are promoted under conditions of low primary production, but they do not favor the production mesozooplankton biomass or POC export efficiency (Fig. 4a). However, the latter two seem to be promoted when copepod assemblages display more dissimilar functional trait composition and more even trait expressions. MESOZOO and other indicators related to mean annual productivity and carbon export covary negatively with copepod richness and FD (Fig. S10). Phytoplankton biomass (CHL-A), the biomass production of most phytoplankton functional types (DIATO, DINO, HAPTO and GREEN) and the efficiency of carbon export below the euphotic zone (E-RATIO) covary positively with the three beta-FD indices, SES Faith and FEve, but they vary negatively with copepod species richness, Faith, FDis and FDiv (Figure S10). Mean annual NPP, PROCHL and indicators related to POC fluxes at depth show less marked patterns and mainly tend to covary negatively with Faith and SES Faith.

We focus on the most conspicuous patterns to test if copepod diversity has emergent positive or negative effects on zooplankton biomass production (Figure 4b to f). We find that emergent mesozooplankton production is lower in assemblages that display higher functional richness and more scattered species in functional space. Meanwhile, MESOZOO is favored in assemblages where trait expression is more balanced (i.e., higher FEve) and which show less common trait combinations (i.e., higher Trait dissimilarity and turnover). Globally, MESOZOO decreases with species richness, Faith, FDis and FDiv (Fig. 4a,b,d,e) but increases with FEve and Trait dissimilarity (and Trait turnover; Fig. 4c,f). The strongest negative relationship was found for FDis (R^2 = 0.62) and the weakest for FDiv (R^2 = 0.12). The strongest positive relationship was found for Trait dissimilarity (R^2 = 0.48). The strength of the covariance with MESOZOO varies significantly with latitude, but less so (< 10%) for species richness, FEve and FDis. Indeed, including an interaction term between the diversity index and absolute latitude improved the fit of the linear models (all ANCOVA tests returned $p < 0.001$), but less strongly than in the previous case. The adjusted R^2 increased by: 8.7% for species richness, 34.9% for Faith, 1.5% for FEve, 6.45% for FDis, 67.5% for FDiv and 23.9% for Trait dissimilarity. Finer regional patterns shown on Figure 4 are summarized in the Supplementary Results as well as Figs. S12 and S13.

3.4. Changes in copepod FD under global change

We examine how copepod mean annual FD will change in the future as a function of climate change projections averaged over 180 monthly ensemble members (Figure 5). On a global scale, our ensemble of SDMs predicts average relative increases in species richness (+6.0% ± 9.6; Fig. 5a), Faith (+0.7% ± 2.6; Fig. 5b), FDis (+0.3% ± 0.7; Fig. 5d), FDiv (+0.1% ± 0.4; Fig. 5e), but relative decreases in FEve (-2.4% ± 7.8; Fig. 5c). There is a marked spatial variability in the direction of changes in species richness and functional richness, as relative increases are offset by decreases in specific regions. Indeed, increases in richness are stronger at higher latitudes compared to the oligotrophic gyres (Kruskal-Wallis and post hoc pairwise Wilcoxon tests; Fig. S14). Differences in Faith follow a similar spatial trend, but they range mostly between -10% and +10%. Future SES Faith values and their associated p-values show the same distribution as for contemporary ocean conditions (Fig. S6), with negative SES Faith values prevailing in the tropical band, except in the coastal upwelling regions, and positive SES Faith values prevailing at high latitudes.

Future changes in FDiv only range ± 5% and changes in FDis are even weaker (mostly < ± 1.5%; Fig. 5d,e). Therefore, these two facets of copepod FD are not severely affected by future changes in oceanic environmental conditions. Meanwhile, changes in FEve are more severe (± 30%; Fig. 6c) and show marked variations across regions. Copepod assemblages will tend to become more similar in terms of functional trait composition, especially in the northern hemisphere. Indeed, changes in Trait dissimilarity are < 0 nearly everywhere (Fig. 5f). ΔTrait dissimilarity ranges between -5.5% (± 3.0) in the tropics and -0.7% (± 2.0) for latitudes > 60°. Again, changes in total Trait dissimilarity are mainly driven by changes in Trait turnover (correlation coefficient = 0.70, $P < 0.001$; Fig. 5f,g). The contribution of Trait nestedness to Trait dissimilarity will tend to increase in many regions, especially in the high latitudes of the northern hemisphere (Fig. 5h).

The spatial distribution of the uncertainty of our projections in future copepod FD is shown in Fig. S15 and are not homogeneous across FD indices. Regions showing weaker changes in future FD are those where ensemble members disagree the most on the direction of these changes (Fig. 5; Fig. S16). Usually, less than 75% of ensemble members agreed on the direction of changes in annual diversity depending on the index (Fig. S16). However, more than 50% of ensemble members always agreed on the direction of changes in FD across the globe. Previous work showed that this uncertainty is mainly driven by the choice of the SDM, followed by the choice of the ESM (Benedetti et al., 2021).

4. Discussion

4.1. Response of copepod FD to the global species richness gradient

This is the first study to map marine copepod FD on a fully global scale and to investigate its covariance with taxonomic diversity and proxies of ecosystem functioning. First, we asked how multiple facets of copepod FD changed as a function of increasing taxonomic diversity on a mean annual scale. By doing so, we evaluated to what extent changes in richness translate into changes in FD for marine mesozooplankton. Functional richness, divergence and dispersion increase with taxonomic diversity whereas functional evenness, trait dissimilarity and turnover decrease (Figs. 1, 2 & 3). These bivariate relationships show different directions, shapes and strengths. Consequently, species richness should not be viewed as a reliable indicator of all facets of FD and is therefore not sufficient to document changes in zooplankton biodiversity in space and time (Hillebrand et al., 2017; Blowes et al., 2019). The intra-annual variability of our diversity indices is lower than 20% over large parts of the global ocean (i.e., relative standard deviation to mean annual conditions; Fig. S8), suggesting that the patterns shown here on the annual scale are representative of the mean state. This first main result implies that field surveys should integrate the various facets of FD to exhaustively monitor zooplankton biodiversity.

The increase in functional richness with species richness is an emergent property that has been documented by previous field studies conducted on smaller scales for copepods (Becker et al., 2021; Tang et al., 2022; Li et al., 2022). We expected to confirm this pattern because our approach covers large environmental gradients that generate richness patterns through environmental filtering (e.g., warm-water taxa are sorted from cold-water taxa; Benedetti et al., 2021). As a result, speciose communities display larger species pools than non-speciose ones, allowing the emergence of more numerous trait combinations and thus higher functional richness (Mouchet et al., 2010; Chalmandrier et al., 2017; Suarez-Castro et al., 2022). This positive relationship was also observed across scales for several groups of marine ectotherms, from bivalves (Edie et al., 2018), corals (McWilliam et al., 2017) to tropical reef fishes (Stuart-Smith et al., 2013; Mouillot et al., 2014; Ferrari et al., 2023). Therefore, the increase of functional richness with species richness seems to be a universal property of marine ectotherms across scales.

More interestingly, previous studies also showed that the rate of increase of reef fish functional richness with taxonomic diversity varies with latitude (Stuart-Smith et al., 2013), a pattern observed here for marine copepods too (Fig. 3a,d). Indeed, we find that high latitude systems show steeper increases in functional richness and dispersion than tropical ones. In other words, adding taxonomic units has a stronger effect on functional richness in cold species-poor assemblages than in warm species-rich ones. In a context of global change, cold-water

communities will be progressively exposed to the intrusion of warm-water communities (Brun et al., 2019; Benedetti et al., 2021). Therefore, our finding that the zooplankton FD is more sensitive to changes in richness in polar regions than in tropical regions further highlights how exposed polar communities are to future changes in climate and biodiversity (but see section 4.3 for further discussion).

Tropical regions show weaker rates of changes in copepod FD with increasing richness as a result of functional clustering (or "niche convergence"; Mikryukov et al., 2023): the species progressively added in these assemblages display trait values that are already expressed, thus not increasing the coverage of the functional space. This is supported by the strong decrease in SES Faith with richness (Fig. 1 and 3b) which shows how the most species-rich communities from the tropics display significantly lower functional richness than expected. Plus, the strong turnover in traits associated with the global species richness gradient (Figs. 2 and 3) shows that some trait combinations are selected only under certain environmental conditions. We rely on models of abiotic habitats, so our zooplankton FD patterns reflect which trait combinations are more competitive than others under varying conditions of temperature and resource availability. Therefore, such functional clustering (i.e., SES Faith < 0) emerges as a result of environmental filtering (Freschet et al., 2011; McLean et al., 2021).

Analyzing the maps of community-weighted traits underlying the present FD patterns (see Benedetti, Wydler & Vogt, 2023) allows to unveil which trait combinations are selected in warm oligotrophic conditions and then progressively replaced by other combinations towards colder and more productive habitats. High latitudes are characterized by higher proportions of larger myelinated current-feeding copepods (Campbell et al., 2021; Brandão et al., 2021). As a result, high latitudes harbor more dissimilar sets of traits (Figs. 2, 3 and 4) that are not found in other regions (i.e., larger body sizes, more myelinated taxa and more current-feeding tactics that boost feeding rates; Benedetti, Wydler & Vogt, 2023). Meanwhile, the tropics show higher proportions of small amyelinated carnivorous copepods that rely on cruise-feeding or ambush-feeding tactics. We hypothesize that the copepod communities of these areas are characterized by higher levels of specialization likely driven by the strong competition for resources (de Bello et al. 2013; Kraft et al. 2015). This is supported by the fact that the tropical oligotrophic areas also show increased levels of FDis and FDiv (Figs. 3d,e and 5; Fig. S10). These two FD indices identify communities characterized by "extreme" and dispersed trait values occurring at the edges of the overall functional space. Such trait values emerge under enhanced resource competition due to conditions of low food availability, where stress-tolerant species are better adapted to feed. Our results support this view as regions of strongest environmental filtering (i.e., SES Faith < 0) and functional dispersion are characterized by conditions of low nutrient availability dominated by small phytoplankton (Figs. S6 & S10).

According to this hypothesis, enhanced resource availability should relax the selection of traits due to environmental filtering and enable more balanced trait expression, leading to higher functional evenness in the zooplankton. Our present FEve estimates support this expectation. Contrary to FDis and FDiv, FEve decreases with species richness and the rate of functional clustering (Fig. 3). FEve also increases with the turnover in trait composition but peaked right before the latter reaches its maximum (Figs. 1, 2 & 4). Copepod FEve peaks in upwelling systems and the transitional areas connecting the warm tropical gyres to the colder high latitudes (Fig. 4). Such regions display productive environmental conditions that allow a mixture of taxa

from very dissimilar environments and functionally dissimilar communities throughout the year, which promotes balance between dissimilar traits. Further supporting our hypothesis, FEve is higher in those productive environments where multiple phytoplankton functional types co-exist throughout the year, either through asynchronous blooms or co-occurrence (Fig. 5; Fig. S10). According to our results, the increased concentration and variety of phytoplankton cells (i.e., enhanced resource availability) promotes more balanced trait expression, instead of favoring only a small subset of the zooplankton community.

4.2. How may zooplankton FD influence ecosystem functioning?

We then examined the emergent relationships between copepod FD and multiple proxies of ecosystem functioning. By doing so, we tested whether communities with higher taxonomic and/or FD optimize the use of resources to convert them to biomass ("portfolio effect"; McCann, 2000). This hypothesis would be supported by positive relationships between our diversity estimates and productivity-related variables (i.e., MESOZOO, CHL-A, NPP, etc.). Conversely, if biomass production is mainly carried out by a few dominants whose traits are fitter under food replete conditions ("mass-ratio hypothesis"; Grime, 1998), we would find a negative relationship between our FD estimates and productivity-related variables. The present MESOZOO estimate is largely derived from field observations of copepod biomass (Strömberg et al., 2009; Clerc et al., 2024) so focusing on copepods to explore the links between MESOZOO and FD is a reasonable assumption.

We found that indicators of primary production, mesozooplankton production and POC export efficiency decrease with copepod species richness, functional richness, divergence and dispersion (Fig. 4; Fig. S10), supporting the "mass-ratio hypothesis". The fact that Trait dissimilarity due to turnover shows the opposite trend while decreasing with species richness (Fig. 3) further supports this hypothesis: less speciose communities, characterized by lower FD, are more productive and display traits that are not found in speciose communities (Fig. 4). Communities with fewer species characterized by larger body sizes and a higher prevalence of omnivorous and herbivorous current feeders (Benedetti, Wydler & Vogt, 2023) are associated with higher mesozooplankton biomass production and more efficient POC export. These specific traits were shown to sustain more efficient grazing and carbon storage (Kiørboe 2011; Brun et al., 2019) and to promote secondary production (Beaugrand et al., 2010; Brun et al., 2019). The emergent negative patterns between FD and productivity and export efficiency could be driven by a few keystone species, such as the large-bodied Calanidae, whose traits enable larger and faster growth as well as more efficient particles fluxes outside of the euphotic zone, promoting "high production-high export" regimes (Stamieszkin et al., 2015; Jónasdóttir et al., 2015; Henson et al., 2019). Contrary to the diversity indices mentioned above, copepod FEve showed a positive relationship with phytoplankton biomass, MESOZOO and the E-RATIO (Fig. 4; Fig. S10). This implies that the balance in copepod functional trait composition, on top of high phytoplankton biomasses (Knecht et al., 2023; Clerc et al., 2024), could be key to promote mesozooplankton biomass (Maureaud et al., 2019; Le Bagousse-Pinguet et al., 2021). Yet, FEve is a weaker covariate of MESOZOO compared to species richness, Faith and FDis (Fig. 4c) so this facet of FD may be less important for regulating zooplankton productivity at the scale of our study.

We deem the findings above sensible as they reflect the outcome expected from our current understanding of copepod species traits and ecology. Nonetheless, we cannot draw causal mechanisms between copepod FD and the performance of the biological carbon pump based on our correlative approach. The ecosystem functions studied are driven by a complex interplay of biological and physical factors whose contributions vary in space and time and that we cannot here disentangle from the effects of zooplankton FD (van der Plas, 2019; Boyd et al., 2019; Pinti et al., 2023). For instance, POC export efficiency alco covaried positively with the contribution of large and mineralized phytoplankton to phytoplankton biomass (Fig. S10). Such phytoplankton functional types are also known to favor and POC export efficiency (Tréguer et al., 2018; Henson et al., 2019; Nowicki et al., 2022). Nonetheless, our patterns can point towards the existence of interesting biodiversity–ecosystem functions relationships that were undocumented globally.

We did not detect a significant covariance between copepod FD and estimates of NPP and POC fluxes (Fig. 4; Fig. S10). Copepod traits may contribute to regulating the relative amount of NPP that gets exported below the euphotic zone (i.e., E-RATIO), but absolute NPP and POC fluxes may depend more on other important physical and biological factors: the concentration and biomass of zooplankton groups with specific traits, the quantity of large mineralized phytoplankton, the concentration of heterotrophic bacteria, how species interact with one another, or strong mixing events that inject particles below the mixed layer (Henschke et al., 2016; Jaspers et al., 2023; Tréguer et al., 2018; Boyd et al., 2019; Henson et al., 2019; Nowicki et al., 2022). We also acknowledge that export dynamics may be uncoupled from changes in copepod traits in time and throughout the water column (Jónasdóttir et al., 2015; Steinberg & Landry, 2017). For instance, members of the surface copepod community whose traits favor POC export can vertically migrate and excrete carbon-rich particles way below the euphotic zone, several months after their initial growth (Jónasdóttir et al., 2015; Pinti et al., 2023b). Such processes may weaken the potential imprint of surface zooplankton FD on absolute POC fluxes that we tried to recover through our approach.

Our findings support the existence of mechanistic links between trait combinations and ecosystem functions, reinforcing the pressing need to integrate functional trait measurements in zooplankton field surveys (Ratnarajah et al., 2023). New imaging techniques can simultaneously measure body size, shape, feeding activity and other relevant traits in an automatized fashion and at the scale of individuals (Orenstein et al., 2022). Through this process, the measurement of FD indices could also be integrated in field surveys to better assess the relative contribution of trait dimensions to services provided by zooplankton across scales, from production to ecosystem stability and resilience to environmental perturbations (Carmona et al., 2016; de Bello et al., 2021).

4.3. How will anthropogenic climate change reshuffle zooplankton FD?

Global warming may force warm-water zooplankton to migrate poleward, leading to the replacement of polar communities by more tropical ones in time (Benedetti et al., 2021). The effect of these changes in richness in composition on zooplankton trait expression and thus ecosystem functioning remains poorly known. As high latitudes display particular trait combinations that are not found in lower latitudes (Figs. 2 & 3), the compositional turnover associated with such poleward shifts could lower the functional dissimilarity of copepod

communities, which would imply a global functional homogenization of zooplankton, a pattern already observed for fishes (Villéger et al., 2014; Magurran et al., 2015). To test this hypothesis, we explored the response of global copepod FD to anthropogenic climate change based on 180 future monthly projections according to the same ESM simulations as Benedetti et al. (2021).

We find that anthropogenic climate change will have a varied set of impacts on copepod biodiversity, with very weak effects on FDis and FDiv (i.e., Δ values < 5%) but stronger effects on species richness, Faith, FEve and Trait dissimilarity (Fig. 5; Fig. S14). Most of the global ocean shows slight (< 10%) to strong (> 20%) projected increases in copepod species richness, which is in line with our previous projections (Benedetti et al., 2021). Since functional richness scales with species richness (Fig. 3), regions that will undergo species gains also undergo gains in functions. Yet patterns of FDis, FDiv and SES Faith (Fig. S6) remain relatively unaffected under climate change, suggesting that environmental filtering will continue to act as a strong driver of trait expression in copepod communities (as discussed in section 4.1). In the future, tropical systems will continue to host more speciose communities characterized by smaller carnivorous and omnivorous active and passive feeders better adapted to food-deplete conditions.

Future decreases in Trait turnover are partially set-off by increases in nestedness but not strongly enough to maintain contemporary levels of functional dissimilarity. As a result, Trait dissimilarity will decrease worldwide (Fig. 5f,g,h), meaning that high latitude communities are projected to become more functionally even, weakening the global gradient in Trait turnover (Fig. 5c,f,g). Consequently, anthropogenic climate change may drive functional homogenization among copepod communities, with an increasing prevalence of "tropical traits" over time (Villéger et al., 2014; Magurran et al., 2015).

Based on the findings discussed in section 4.2, what do our future projections in copepod FD imply for marine ecosystem functioning? Provided that mesozooplankton biomass and POC export efficiency are favored by the presence of certain trait combinations (i.e., large body size, myelination and current feeding) in communities of lower functional richness and higher evenness (Figs. 3 & 4), our results suggest that anthropogenic climate change will re-organize copepod trait expression in a way that decreases mesozooplankton productivity and POC export efficiency. We did not find any significant relationships between copepod FD and the amount of organic carbon exported below the euphotic zone, precluding us from drawing conclusions regarding to this ecosystem function. Taken together, our results fall in line with the current view that ongoing and future spatial re-organization of marine biodiversity may threaten biomass production and export efficiency (Beaugrand et al., 2010; Lotze et al., 2019). Through bottom-up processes and trophic amplification, global warming will alter resource availability, causing changes in primary production that propagate up the food-web and eventually decrease the size and biomass of higher trophic levels (Kwiatkowski et al., 2020; Tittensor et al., 2021; Atkinson et al., 2024). We here show that future changes in zooplankton trait expression may contribute to lowering the productivity and the health of the oceans.

4.4. Caveats

Our findings should be interpreted within the context of some key limitations that are inherent to a global correlative approach. One key limitation is that the availability of trait data and observations is often limited to adult stages (Brun et al., 2017; Benedetti, Wydler & Vogt, 2023;

Pata & Hunt, 2024). This bias towards adult stages implies that we underestimate the range of trait values (and thus functional richness patterns) expressed in true copepod communities where a large proportion of nauplii may occur. Those early life stages are smaller and display different morphologies and feeding strategies compared to adult stages (Kiørboe et al., 2011; Pata & Hunt, 2024). Therefore, intra-species variability in functional traits due to local adaptations or ontogeny could not be taken into account (Carmona et al., 2016).

Similarly, the wide species pool necessary to explore emergent global FD patterns (~300 species) limits the number of functional traits available across all copepod species (but see Benedetti, Wydler & Vogt, 2023). Missing functional traits implies that we might miss key dimensions of copepod FD and thus underestimate its spatial gradients (Maire et al., 2015; Mouillot et al., 2021). Nonetheless, many functional traits scale allometrically with body size among zooplankton and other marine ectotherms (Andersen et al., 2016; Pata & Hunt, 2024), especially those related to physiological rates (growth, respiration, ingestion or excretion; Kiørboe & Hirst, 2014; Pata & Hunt, 2024). Consequently, retaining body size as a continuous trait here may cover the inter-species variability in those traits. Copepods dominate mesozooplankton composition and concentration (Kiørboe, 2011; Brandão et al., 2021; Drago et al., 2022), so we cover significant dimensions of mesozooplankton FD. However, we did not account for the range of traits covered by other major meso- and macrozooplankton functional groups that show much larger body size, different body composition or alternative feeding strategies traits (i.e., krill, salps, jellyfishes, pteropods, foraminifera or chaetognaths). The very recent trait synthesis of Pata & Hunt (2024) will allow the community to explore zooplankton FD dynamics in a more holistic fashion.

Our approach relies on occurrence-based modelling and thus does not take the abundance of species and traits into account. As a result, indices associated with relative trait distribution in functional space (i.e., FDiv, FDis, FEve) may be underestimated in communities characterized by strong differences in concentrations between species displaying very contrasted trait values. Such biases should mainly prevail in very productive regions such as the poles where a few species with extreme size values and active current-feeding modes dominate copepod biomass while other smaller species remain by contributing more marginally to biomass (Brandão et al., 2021; Drago et al., 2022). High latitudes also showed higher uncertainty for species richness, functional richness and FEve due to SDM choice (Fig. S9). This means that more observational research on zooplankton FD and ecosystem functioning is necessary in these regions to improve the accuracy of our estimates. As these diversity indices are more influenced by algorithm choice than intra-annual variability at latitudes > 60° (Fig. S8), the trends shown here could become weaker or stronger with advancements in distribution modeling and the inclusion of more field observations of taxon-specific biomasses (Waldock et al., 2022; Lombard et al., 2019; Ratnarajah et al., 2023). Addressing this uncertainty is crucial since high latitude plankton ecosystems are the most threatened by future warming.

5. Conclusion

Our study suggests that zooplankton traits and FD depend on climate and resource availability and that changes in taxonomic diversity alone are insufficient to reveal the response of zooplankton biodiversity to changing environmental conditions (Hillebrand et al., 2017;

Blowes et al., 2019). Various facets of zooplankton FD relate differently to phytoplankton productivity, zooplankton biomass, and biological carbon pump efficiency. Relationships between biodiversity and ecosystem functioning vary with the facets of biodiversity, echoing patterns in other terrestrial and marine systems (Chalmandrier et al., 2017; La Bagousse-Pinguet et al., 2021). This calls for initiatives to better define what 'biodiversity' is in the context of the marine microbiome and especially when diversity metrics are used in conservation and policy applications. Our future projections suggest climate warming will globally reshape marine biodiversity, potentially reducing productivity across trophic levels (Tittensor et al., 2021; Atkinson et al., 2024). Our copepod FD estimates align with field observations from smaller scales (Becker et al., 2021; Tang et al., 2022) and may serve as benchmarks for testing biodiversity hypotheses. We advocate integrating FD into field surveys to better track plankton biodiversity responses across scales and habitats (Ratnarajah et al., 2023). Historical and future oceanographic data, combined with functional traits, can further elucidate plankton functional diversity patterns (Pata & Hunt, 2024). This will help ecosystem modelers assess the identity and number of traits and FD dimensions that are critical to model and monitor the response of marine ecosystems functioning to changes in plankton biodiversity (Kiørboe et al., 2018; Serra-Pompei et al., 2020).

Acknowledgements

We thank all contributors involved in plankton field sampling and identification and we acknowledge the efforts made to share such data through publicly available archives. We thank Alexandre Schickele for helping us choosing appropriate color palettes. This project has received funding from the European Union's Horizon 2020 Research and Innovation Programme under grant agreement no. 862923 (AtlantECO) and under grant agreement no. 101059915 (BIOceans5D). This output reflects only the author's view, and the European Union cannot be held responsible for any use that may be made of the information contained therein.

References

Albouy, C., Delattre, V. L., Mérigot, B., Meynard, C. N., & Leprieur, F. (2017). Multifaceted biodiversity hotspots of marine mammals for conservation priorities. *Diversity and distributions, 23*(6), 615-626. doi:https://doi.org/10.1111/ddi.12556

Andersen, K. H., Berge, T., Gonçalves, R. J., Hartvig, M., Heuschele, J., Hylander, S., . . . Kiørboe, T. (2016). Characteristic Sizes of Life in the Oceans, from Bacteria to Whales. *Annual Review of Marine Science, 8*(1), 217-241. doi:10.1146/annurev-marine-122414-034144

Atkinson, A., Rossberg, A. G., Gaedke, U., Sprules, G., Heneghan, R. F., Batziakas, S., . . . Frangoulis, C. (2024). Steeper size spectra with decreasing phytoplankton biomass indicate strong trophic amplification and future fish declines. *Nature Communications, 15*(1), 381. doi:10.1038/s41467-023-44406-5

Baselga, A. (2010). Partitioning the turnover and nestedness components of beta diversity. *Global Ecology and Biogeography, 19*(1), 134-143. doi:10.1111/j.1466-8238.2009.00490.x

Beaugrand, G., Edwards, M., & Legendre, L. (2010). Marine biodiversity, ecosystem functioning, and carbon cycles. *Proceedings of the National Academy of Sciences, 107*(22), 10120-10124. doi:10.1073/pnas.0913855107

Beaugrand, G., Edwards, M., Raybaud, V., Goberville, E., & Kirby, R. R. (2015). Future vulnerability of marine biodiversity compared with contemporary and past changes. *Nature Climate Change, 5*(7), 695-701. doi:10.1038/nclimate2650

Becker, É. C., Mazzocchi, M. G., de Macedo-Soares, L. C. P., Costa Brandão, M., & Santarosa Freire, A. (2021). Latitudinal gradient of copepod functional diversity in the South Atlantic Ocean. *Progress in Oceanography, 199*, 102710. doi:https://doi.org/10.1016/j.pocean.2021.102710

Behrenfeld, M. J., & Falkowski, P. G. (1997). Photosynthetic rates derived from satellite-based chlorophyll concentration. *Limnology and Oceanography, 42*(1), 1-20. doi:https://doi.org/10.4319/lo.1997.42.1.0001

Benedetti, F., Gasparini, S., & Ayata, S.-D. (2016). Identifying copepod functional groups from species functional traits. *Journal of Plankton Research, 38*(1), 159-166. doi:10.1093/plankt/fbv096

Benedetti, F., Vogt, M., Elizondo, U. H., Righetti, D., Zimmermann, N. E., & Gruber, N. (2021). Major restructuring of marine plankton assemblages under global warming. *Nature Communications, 12*(1), 5226. doi:10.1038/s41467-021-25385-x

Benedetti, F., Wydler, J., & Vogt, M. (2023). Copepod functional traits and groups show divergent biogeographies in the global ocean. *Journal of Biogeography, 50*(1), 8-22. doi:https://doi.org/10.1111/jbi.14512

Benedetti, F., Gruber, N., & Vogt, M. (2023). Global gradients in species richness of marine plankton functional groups. *Journal of Plankton Research*. doi:10.1093/plankt/fbad044

Blowes, S. A., Supp, S. R., Antão, L. H., Bates, A., Bruelheide, H., Chase, J. M., . . . Dornelas, M. (2019). The geography of biodiversity change in marine and terrestrial assemblages. *Science, 366*(6463), 339-345. doi:doi:10.1126/science.aaw1620

Boyd, P. W., Claustre, H., Levy, M., Siegel, D. A., & Weber, T. (2019). Multi-faceted particle pumps drive carbon sequestration in the ocean. *Nature, 568*(7752), 327-335. doi:10.1038/s41586-019-1098-2

Brandão, M. C., Benedetti, F., Martini, S., Soviadan, Y. D., Irisson, J.-O., Romagnan, J.-B., . . . Tara Oceans Consortium, C. (2021). Macroscale patterns of oceanic zooplankton composition and size structure. *Scientific Reports, 11*(1), 15714. doi:10.1038/s41598-021-94615-5

Brun, P., Payne, M. R., & Kiørboe, T. (2016). Trait biogeography of marine copepods–an analysis across scales. *Ecology Letters, 19*(12), 1403-1413.

Brun, P., Payne, M. R., & Kiørboe, T. (2017). A trait database for marine copepods. *Earth Syst. Sci. Data, 9*(1), 99-113. doi:10.5194/essd-9-99-2017

Brun, P., Stamieszkin, K., Visser, A. W., Licandro, P., Payne, M. R., & Kiørboe, T. (2019). Climate change has altered zooplankton-fuelled carbon export in the North Atlantic. *Nature Ecology & Evolution, 3*(3), 416-423. doi:10.1038/s41559-018-0780-3

Campbell, M. D., Schoeman, D. S., Venables, W., Abu-Alhaija, R., Batten, S. D., Chiba, S., . . . Richardson, A. J. (2021). Testing Bergmann's rule in marine copepods. *Ecography, 44*(9), 1283-1295. doi:https://doi.org/10.1111/ecog.05545

Cardinale, B. J., Duffy, J. E., Gonzalez, A., Hooper, D. U., Perrings, C., Venail, P., . . . Wardle, D. A. (2012). Biodiversity loss and its impact on humanity. *Nature, 486*(7401), 59-67.

Cardoso, P., Rigal, F., Carvalho, J. C., Fortelius, M., Borges, P. A. V., Podani, J., & Schmera, D. (2014). Partitioning taxon, phylogenetic and functional beta diversity into replacement and richness difference components. *Journal of Biogeography, 41*(4), 749-761. doi:https://doi.org/10.1111/jbi.12239

Carmona, C. P., de Bello, F., Mason, N. W. H., & Lepš, J. (2016). Traits Without Borders: Integrating Functional Diversity Across Scales. *Trends in ecology & evolution, 31*(5), 382-394. doi:10.1016/j.tree.2016.02.003

Chalmandrier, L., Münkemüller, T., Colace, M.-P., Renaud, J., Aubert, S., Carlson, B. Z., . . . Thuiller, W. (2017). Spatial scale and intraspecific trait variability mediate assembly rules in alpine grasslands. *Journal of Ecology, 105*(1), 277-287. doi:https://doi.org/10.1111/1365-2745.12658

Clements, D. J., Yang, S., Weber, T., McDonnell, A. M. P., Kiko, R., Stemmann, L., & Bianchi, D. (2023). New Estimate of Organic Carbon Export From Optical Measurements Reveals the Role of Particle Size Distribution and Export Horizon. *Global Biogeochemical Cycles, 37*(3), e2022GB007633. doi:https://doi.org/10.1029/2022GB007633

Clerc, C., Bopp, L., Benedetti, F., Knecht, N., Vogt, M., & Aumont, O. (2023). Effects of mesozooplankton growth and reproduction on plankton and organic carbon dynamics in a marine biogeochemical model. *ESS Open Archive.* March 07, 2024. doi: 10.22541/essoar.170983160.00886471/v1 (submitted to *Global Biogeochemical Cycles*, minor revisions)

Daru, B. H., Karunarathne, P., & Schliep, K. (2020). phyloregion: R package for biogeographical regionalization and macroecology. *Methods in Ecology and Evolution, 11*(11), 1483-1491. doi:https://doi.org/10.1111/2041-210X.13478

de Bello, F., Vandewalle, M., Reitalu, T., Lepš, J., Prentice, H. C., Lavorel, S., & Sykes, M. T. (2013). Evidence for scale- and disturbance-dependent trait assembly patterns in dry semi-natural grasslands. *Journal of Ecology, 101*(5), 1237-1244. doi:https://doi.org/10.1111/1365-2745.12139

de Bello, F., Lavorel, S., Hallett, L. M., Valencia, E., Garnier, E., Roscher, C., . . . Lepš, J. (2021). Functional trait effects on ecosystem stability: assembling the jigsaw puzzle. *Trends in ecology & evolution, 36*(9), 822-836. doi:10.1016/j.tree.2021.05.001

de Vargas, C., Audic, S., Henry, N., Decelle, J., Mahé, F., Logares, R., . . . Velayoudon, D. (2015). Eukaryotic plankton diversity in the sunlit ocean. *Science, 348*(6237), 1261605. doi:doi:10.1126/science.1261605

DeVries, T., & Weber, T. (2017). The export and fate of organic matter in the ocean: New constraints from combining satellite and oceanographic tracer observations. *Global Biogeochemical Cycles, 31*(3), 535-555. doi:10.1002/2016gb005551

Djeghri, N., Boyé, A., Ostle, C., & Hélaouët, P. (2023). Reinterpreting two regime shifts in North Sea plankton communities through the lens of functional traits. *Global Ecology and Biogeography, 32*(6), 962-975. doi:https://doi.org/10.1111/geb.13659

Dormann, C. F., Elith, J., Bacher, S., Buchmann, C., Carl, G., Carré, G., . . . Leitão, P. J. (2013). Collinearity: a review of methods to deal with it and a simulation study evaluating their performance. *Ecography, 36*(1), 27-46.

Drago, L., Panaïotis, T., Irisson, J.-O., Babin, M., Biard, T., Carlotti, F., . . . Kiko, R. (2022). Global Distribution of Zooplankton Biomass Estimated by In Situ Imaging and Machine Learning. *Frontiers in Marine Science, 9*. doi:10.3389/fmars.2022.894372

Edie, S. M., Jablonski, D., & Valentine, J. W. (2018). Contrasting responses of functional diversity to major losses in taxonomic diversity. *Proceedings of the National Academy of Sciences, 115*(4), 732-737. doi:doi:10.1073/pnas.1717636115

Elith, J., & Leathwick, J. R. (2009). Species Distribution Models: Ecological Explanation and Prediction Across Space and Time. *Annual Review of Ecology, Evolution, and Systematics, 40*(1), 677-697. doi:10.1146/annurev.ecolsys.110308.120159

Eriksson, D., Righetti, D., Benedetti, F., Gruber, N., R., Paoli, L., Salazar, G., Sunagawa, S. & Vogt, M. (2023). Nitrogen fixation rates increase with diazotroph richness in the global ocean. *EcoEvoRxiv*. https://doi.org/10.32942/X2Z323 (submitted to *Science Advances*)

Faith, D. P. (1992). Conservation evaluation and phylogenetic diversity. *Biological Conservation, 61*(1), 1-10.

Ferrari, D. S., Floeter, S. R., Leprieur, F., & Quimbayo, J. P. (2023). A trait-based approach to marine island biogeography. *Journal of Biogeography, 50*(3), 528-538. doi:https://doi.org/10.1111/jbi.14549

Freschet, G. T., Dias, A. T. C., Ackerly, D. D., Aerts, R., van Bodegom, P. M., Cornwell, W. K., . . . Cornelissen, J. H. C. (2011). Global to community scale differences in the prevalence of convergent over divergent leaf trait distributions in plant assemblages. *Global Ecology and Biogeography, 20*(5), 755-765. doi:https://doi.org/10.1111/j.1466-8238.2011.00651.x

Gamfeldt, L., Lefcheck, J. S., Byrnes, J. E. K., Cardinale, B. J., Duffy, J. E., & Griffin, J. N. (2015). Marine biodiversity and ecosystem functioning: what's known and what's next? *Oikos, 124*(3), 252-265. doi:https://doi.org/10.1111/oik.01549

Garcia, H. E., R. A. Locarnini, T. P. Boyer, J. I. Antonov, O.K. Baranova, M.M. Zweng, J.R. Reagan, D.R. Johnson, 2014. World Ocean Atlas 2013, Volume 4: Dissolved Inorganic Nutrients (phosphate, nitrate, silicate). S. Levitus, Ed., A. Mishonov Technical Ed.; NOAA Atlas NESDIS 76, 25 pp.

Gonzalez, A., Germain, R. M., Srivastava, D. S., Filotas, E., Dee, L. E., Gravel, D., . . . Loreau, M. (2020). Scaling-up biodiversity-ecosystem functioning research. *Ecology Letters, 23*(4), 757-776. doi:https://doi.org/10.1111/ele.13456

Grime, J. P. (1998). Benefits of plant diversity to ecosystems: immediate, filter and founder effects. *Journal of Ecology, 86*(6), 902-910. doi:https://doi.org/10.1046/j.1365-2745.1998.00306.x

Henschke, N., Everett, J. D., Richardson, A. J., & Suthers, I. M. (2016). Rethinking the Role of Salps in the Ocean. *Trends in ecology & evolution, 31*(9), 720-733. doi:https://doi.org/10.1016/j.tree.2016.06.007

Henson, S., Le Moigne, F., & Giering, S. (2019). Drivers of Carbon Export Efficiency in the Global Ocean. *Global Biogeochemical Cycles, 33*(7), 891-903. doi:10.1029/2018gb006158

Hillebrand, H., Blasius, B., Borer, E. T., Chase, J. M., Downing, J. A., Eriksson, B. K., . . . Ryabov, A. B. (2017). Biodiversity change is uncoupled from species richness trends: Consequences for conservation and monitoring. *Journal of Applied Ecology, 55*(1), 169-184. doi:https://doi.org/10.1111/1365-2664.12959

Jaspers, C., Hopcroft, R. R., Kiørboe, T., Lombard, F., López-Urrutia, Á., Everett, J. D., & Richardson, A. J. (2023). Gelatinous larvacean zooplankton can enhance trophic transfer and carbon sequestration. *Trends in ecology & evolution*. doi:https://doi.org/10.1016/j.tree.2023.05.005

Jónasdóttir, S. H., Visser, A. W., Richardson, K., & Heath, M. R. (2015). Seasonal copepod lipid pump promotes carbon sequestration in the deep North Atlantic. *Proceedings of the National Academy of Sciences, 112*(39), 12122-12126. doi:10.1073/pnas.1512110112

Kembel, S. W., Cowan, P. D., Helmus, M. R., Cornwell, W. K., Morlon, H., Ackerly, D. D., . . . Webb, C. O. (2010). Picante: R tools for integrating phylogenies and ecology. *Bioinformatics, 26*(11), 1463-1464. doi:10.1093/bioinformatics/btq166

Kiørboe, T., & Hirst, A. G. (2014). Shifts in Mass Scaling of Respiration, Feeding, and Growth Rates across Life-Form Transitions in Marine Pelagic Organisms. *The American Naturalist, 183*(4), E118-E130. doi:10.1086/675241

Kiørboe, T. (2011). How zooplankton feed: mechanisms, traits and trade-offs. *Biological Reviews, 86*(2), 311-339.

Kiørboe, T., Visser, A., & Andersen, K. H. (2018). A trait-based approach to ocean ecology. *ICES Journal of marine science, 75*(6), 1849-1863. doi:10.1093/icesjms/fsy090

Knecht, N. S., Benedetti, F., Elizondo, U. H., Bednaršek, N., Chaabane, S., de Weerd, C., . . . Vogt, M. (2023). The impact of zooplankton calcifiers on the marine carbon cycle. *Global Biogeochemical Cycles, n/a*(n/a), e2022GB007685. doi:https://doi.org/10.1029/2022GB007685

Kostadinov, T., Siegel, D., & Maritorena, S. (2009). Retrieval of the particle size distribution from satellite ocean color observations. *Journal of Geophysical Research: Oceans, 114*(C9).

Kraft, N. J. B., Godoy, O., & Levine, J. M. (2015). Plant functional traits and the multidimensional nature of species coexistence. *Proceedings of the National Academy of Sciences, 112*(3), 797-802. doi:doi:10.1073/pnas.1413650112

Kwiatkowski, L., Torres, O., Bopp, L., Aumont, O., Chamberlain, M., Christian, J. R., . . . Ziehn, T. (2020). Twenty-first century ocean warming, acidification, deoxygenation, and upper-ocean nutrient and primary production decline from CMIP6 model projections. *Biogeosciences, 17*(13), 3439-3470. doi:10.5194/bg-17-3439-2020

Le Bagousse-Pinguet, Y., Gross, N., Saiz, H., Maestre, F. T., Ruiz, S., Dacal, M., . . . García-Palacios, P. (2021). Functional rarity and evenness are key facets of biodiversity to boost multifunctionality. *Proceedings of the National Academy of Sciences, 118*(7), e2019355118. doi:10.1073/pnas.2019355118

Laliberté, E., & Legendre, P. (2010). A distance-based framework for measuring functional diversity from multiple traits. *Ecology, 91*(1), 299-305. doi:https://doi.org/10.1890/08-2244.1

977 Laliberté, E., Legendre, P., Shipley, B., & Laliberté, M. E. (2014). Package 'fd'. *Measuring functional diversity*
978 *from multiple traits, and other tools for functional ecology, 1*, 0-12.
979 Lehtinen, S., Tamminen, T., Ptacnik, R., & Andersen, T. (2017). Phytoplankton species richness, evenness, and
980 production in relation to nutrient availability and imbalance. *Limnology and Oceanography, 62*(4),
981 1393-1408. doi:https://doi.org/10.1002/lno.10506
982 Le Moigne, F. A. C., Henson, S. A., Cavan, E., Georges, C., Pabortsava, K., Achterberg, E. P., . . . Sanders, R.
983 J. (2016). What causes the inverse relationship between primary production and export efficiency in the
984 Southern Ocean? *Geophysical Research Letters, 43*(9), 4457-4466.
985 doi:https://doi.org/10.1002/2016GL068480
986 Lenz, P. H. (2012). The biogeography and ecology of myelin in marine copepods. *Journal of Plankton Research,*
987 *34*(7), 575-589.
988 Li, Y., Ge, R., Chen, H., Zhuang, Y., Liu, G., & Zheng, Z. (2022). Functional diversity and groups of crustacean
989 zooplankton in the southern Yellow Sea. *Ecological Indicators, 136*, 108699.
990 doi:https://doi.org/10.1016/j.ecolind.2022.108699
991 Litchman, E., Ohman, M. D., & Kiørboe, T. (2013). Trait-based approaches to zooplankton communities. *Jour-*
992 *nal of Plankton Research, 35*(3), 473-484.
993 Lombard, F., Boss, E., Waite, A. M., Vogt, M., Uitz, J., Stemmann, L., . . . Appeltans, W. (2019). Globally
994 Consistent Quantitative Observations of Planktonic Ecosystems. *Frontiers in Marine Science, 6*.
995 doi:10.3389/fmars.2019.00196
996 Lotze, H. K., Tittensor, D. P., Bryndum-Buchholz, A., Eddy, T. D., Cheung, W. W. L., Galbraith, E. D., . . .
997 Worm, B. (2019). Global ensemble projections reveal trophic amplification of ocean biomass declines
998 with climate change. *Proceedings of the National Academy of Sciences, 116*(26), 12907-12912.
999 doi:doi:10.1073/pnas.1900194116
1000 Magurran, A. E., Dornelas, M., Moyes, F., Gotelli, N. J., & McGill, B. (2015). Rapid biotic homogenization of
1001 marine fish assemblages. *Nature Communications, 6*(1), 8405. doi:10.1038/ncomms9405
1002 Maire, E., Grenouillet, G., Brosse, S., & Villéger, S. (2015). How many dimensions are needed to accurately
1003 assess functional diversity? A pragmatic approach for assessing the quality of functional spaces. *Global*
1004 *Ecology and Biogeography, 24*(6), 728-740.
1005 Mason, N. W. H., Mouillot, D., Lee, W. G., & Wilson, J. B. (2005). Functional richness, functional evenness
1006 and functional divergence: the primary components of functional diversity. *Oikos, 111*(1), 112-118.
1007 doi:https://doi.org/10.1111/j.0030-1299.2005.13886.x
1008 Maureaud, A., Hodapp, D., van Denderen, P. D., Hillebrand, H., Gislason, H., Spaanheden Dencker, T., . . .
1009 Lindegren, M. (2019). Biodiversity–ecosystem functioning relationships in fish communities: biomass
1010 is related to evenness and the environment, not to species richness. *Proceedings of the Royal Society B:*
1011 *Biological Sciences, 286*(1906), 20191189. doi:doi:10.1098/rspb.2019.1189
1012 McCann, K. S. (2000). The diversity–stability debate. *Nature, 405*(6783), 228-233. doi:10.1038/35012234
1013 McLean, M., Stuart-Smith, R. D., Villéger, S., Auber, A., Edgar, G. J., MacNeil, M. A., . . . Mouillot, D. (2021).
1014 Trait similarity in reef fish faunas across the world's oceans. *Proceedings of the National Academy of*
1015 *Sciences, 118*(12), e2012318118. doi:10.1073/pnas.2012318118
1016 McWilliam, M., Hoogenboom, M. O., Baird, A. H., Kuo, C.-Y., Madin, J. S., & Hughes, T. P. (2018). Biogeo-
1017 graphical disparity in the functional diversity and redundancy of corals. *Proceedings of the National*
1018 *Academy of Sciences, 115*(12), 3084-3089.
1019 Mikryukov, V., Dulya, O., Zizka, A., Bahram, M., Hagh-Doust, N., Anslan, S., . . . Tedersoo, L. (2023). Con-
1020 necting the multiple dimensions of global soil fungal diversity. *Science Advances, 9*(48), eadj8016.
1021 doi:doi:10.1126/sciadv.adj8016
1022 Moriarty, R., & O'Brien, T. D. (2013). Distribution of mesozooplankton biomass in the global ocean. *Earth Syst.*
1023 *Sci. Data, 5*(1), 45-55. doi:10.5194/essd-5-45-2013

Mouchet, M. A., Villéger, S., Mason, N. W. H., & Mouillot, D. (2010). Functional diversity measures: an overview of their redundancy and their ability to discriminate community assembly rules. *Functional Ecology, 24*(4), 867-876. doi:https://doi.org/10.1111/j.1365-2435.2010.01695.x

Mouillot, D., Graham, N. A. J., Villéger, S., Mason, N. W. H., & Bellwood, D. R. (2013). A functional approach reveals community responses to disturbances. *Trends in ecology & evolution, 28*(3), 167-177. doi:https://doi.org/10.1016/j.tree.2012.10.004

Mouillot, D., Villéger, S., Parravicini, V., Kulbicki, M., Arias-González, J. E., Bender, M., . . . Vigliola, L. (2014). Functional over-redundancy and high functional vulnerability in global fish faunas on tropical reefs. *Proceedings of the National Academy of Sciences, 111*(38), 13757-13762.

Mouillot, D., Loiseau, N., Grenié, M., Algar, A. C., Allegra, M., Cadotte, M. W., . . . Auber, A. (2021). The dimensionality and structure of species trait spaces. *Ecology Letters, 24*(9), 1988-2009. doi:https://doi.org/10.1111/ele.13778

Nowicki, M., DeVries, T., & Siegel, D. A. (2022). Quantifying the Carbon Export and Sequestration Pathways of the Ocean's Biological Carbon Pump. *Global Biogeochemical Cycles, 36*(3), e2021GB007083. doi:https://doi.org/10.1029/2021GB007083

Oksanen, J., Blanchet, F. G., Kindt, R., Legendre, P., Minchin, P. R., O'hara, R., . . . Wagner, H. (2013). Package 'vegan'. *Community ecology package, version, 2*(9).

Orenstein, E. C., Ayata, S.-D., Maps, F., Becker, É. C., Benedetti, F., Biard, T., . . . Irisson, J.-O. (2022). Machine learning techniques to characterize functional traits of plankton from image data. *Limnology and Oceanography, 67*(8), 1647-1669. doi:https://doi.org/10.1002/lno.12101

Paquette, A., & Messier, C. (2011). The effect of biodiversity on tree productivity: from temperate to boreal forests. *Global Ecology and Biogeography, 20*(1), 170-180. doi:https://doi.org/10.1111/j.1466-8238.2010.00592.x

Paradis, E., & Schliep, K. (2019). ape 5.0: an environment for modern phylogenetics and evolutionary analyses in R. *Bioinformatics, 35*(3), 526-528. doi:10.1093/bioinformatics/bty633

Pata, P. R., & Hunt, B. P. V. (2024). Harmonizing marine zooplankton trait data toward a mechanistic understanding of ecosystem functioning. *Limnology and Oceanography*. doi:https://doi.org/10.1002/lno.12478

Phillips, S. J., Dudik, M., Elith, J., Graham, C. H., Lehmann, A., Leathwick, J., & Ferrier, S. (2009). Sample selection bias and presence-only distribution models: implications for background and pseudo-absence data. *Ecological Applications, 19*(1), 181-197.

Pimiento, C., Leprieur, F., Silvestro, D., Lefcheck, J. S., Albouy, C., Rasher, D. B., . . . Griffin, J. N. (2020). Functional diversity of marine megafauna in the Anthropocene. *Science Advances, 6*(16), eaay7650. doi:doi:10.1126/sciadv.aay7650

Pinti, J., DeVries, T., Norin, T., Serra-Pompei, C., Proud, R., Siegel, D. A., . . . Visser, A. W. (2023). Model estimates of metazoans' contributions to the biological carbon pump. *Biogeosciences, 20*(5), 997-1009. doi:10.5194/bg-20-997-2023

Prowe, A. F., Visser, A. W., Andersen, K. H., Chiba, S., & Kiørboe, T. (2019). Biogeography of zooplankton feeding strategy. *Limnology and Oceanography, 64*(2), 661-678.

R Studio Team (2021). RStudio: Integrated Development for R. RStudio, PBC, Boston, MA URL http://www.rstudio.com/

Ratnarajah, L., Abu-Alhaija, R., Atkinson, A., Batten, S., Bax, N. J., Bernard, K. S., . . . Yebra, L. (2023). Monitoring and modelling marine zooplankton in a changing climate. *Nature Communications, 14*(1), 564. doi:10.1038/s41467-023-36241-5

Rombouts, I., Beaugrand, G., Ibanez, F., Gasparini, S., Chiba, S., & Legendre, L. (2010). A multi-variate approach to large-scale variation in marine planktonic copepod diversity and its environmental correlates. *Limnology and Oceanography, 55*(5), 2219.

Sailley, S. F., Vogt, M., Doney, S. C., Aita, M. N., Bopp, L., Buitenhuis, E. T., . . . Yamanaka, Y. (2013). Comparing food web structures and dynamics across a suite of global marine ecosystem models. *Ecological modelling, 261-262*, 43-57. https://doi.org/10.1016/j.ecolmodel.2013.04.006

Sarmiento, J. L. and Gruber, N. (2006) Ocean Biogeochemical Dynamics, Princeton University Press, Princeton.

Schleuter, D., Daufresne, M., Massol, F., & Argillier, C. (2010). A user's guide to functional diversity indices. *Ecological monographs, 80*(3), 469-484. doi:https://doi.org/10.1890/08-2225.1

Serra-Pompei, C., Soudijn, F., Visser, A. W., Kiørboe, T., & Andersen, K. H. (2020). A general size- and trait-based model of plankton communities. *Progress in Oceanography, 189*, 102473. doi:https://doi.org/10.1016/j.pocean.2020.102473

Stamieszkin, K., Pershing, A. J., Record, N. R., Pilskaln, C. H., Dam, H. G., & Feinberg, L. R. (2015). Size as the master trait in modeled copepod fecal pellet carbon flux. *Limnology and Oceanography, 60*(6), 2090-2107.

Steinberg, D. K., & Landry, M. R. (2017). Zooplankton and the Ocean Carbon Cycle. *Annual Review of Marine Science, 9*(1), 413-444. doi:10.1146/annurev-marine-010814-015924

Strömberg, K. H. P., Smyth, T. J., Allen, J. I., Pitois, S., & O'Brien, T. D. (2009). Estimation of global zooplankton biomass from satellite ocean colour. *Journal of Marine Systems, 78*(1), 18-27. doi:https://doi.org/10.1016/j.jmarsys.2009.02.004

Stuart-Smith, R. D., Bates, A. E., Lefcheck, J. S., Duffy, J. E., Baker, S. C., Thomson, R. J., . . . Airoldi, L. (2013). Integrating abundance and functional traits reveals new global hotspots of fish diversity. *Nature, 501*(7468), 539-542.

Suárez-Castro, A. F., Raymundo, M., Bimler, M., & Mayfield, M. M. (2022). Using multi-scale spatially explicit frameworks to understand the relationship between functional diversity and species richness. *Ecography, 2022*(6), e05844. doi:https://doi.org/10.1111/ecog.05844

Takahashi, K., Ichikawa, T., Saito, H., Kakehi, S., Sugimoto, Y., Hidaka, K., & Hamasaki, K. (2013). Sapphirinid copepods as predators of doliolids: Their role in doliolid mortality and sinking flux. *Limnology and Oceanography, 58*(6), 1972-1984.

Tang, Q., Yang, J., & Sun, D. (2022). Functional diversity of copepod assemblages along a basin-scale latitudinal gradient in the North Pacific Ocean. *Ecological Indicators, 141*, 109112. doi:https://doi.org/10.1016/j.ecolind.2022.109112

Taylor, K. E., Stouffer, R. J., & Meehl, G. A. (2012). An overview of CMIP5 and the experiment design. *Bulletin of the American Meteorological Society, 93*(4), 485.

Thuiller, W., Guéguen, M., Renaud, J., Karger, D. N., & Zimmermann, N. E. (2019). Uncertainty in ensembles of global biodiversity scenarios. *Nature Communications, 10*(1), 1446. doi:10.1038/s41467-019-09519-w

Tittensor, D. P., Novaglio, C., Harrison, C. S., Heneghan, R. F., Barrier, N., Bianchi, D., . . . Blanchard, J. L. (2021). Next-generation ensemble projections reveal higher climate risks for marine ecosystems. *Nature Climate Change, 11*(11), 973-981. doi:10.1038/s41558-021-01173-9

Tréguer, P., Bowler, C., Moriceau, B., Dutkiewicz, S., Gehlen, M., Aumont, O., . . . Pondaven, P. (2018). Influence of diatom diversity on the ocean biological carbon pump. *Nature Geoscience, 11*(1), 27-37. doi:10.1038/s41561-017-0028-x

Turner, J. T. (2015). Zooplankton fecal pellets, marine snow, phytodetritus and the ocean's biological pump. *Progress in Oceanography, 130*, 205-248.

van der Plas, F. (2019). Biodiversity and ecosystem functioning in naturally assembled communities. *Biological Reviews, 94*(4), 1220-1245. doi:https://doi.org/10.1111/brv.12499

van Someren Gréve, H., Almeda, R., & Kiørboe, T. (2017). Motile behavior and predation risk in planktonic copepods. *Limnology and oceanography, 62*(5), 1810-1824. doi:https://doi.org/10.1002/lno.10535

Villéger, S., Mason, N. W. H., & Mouillot, D. (2008). New multidimensional functional diversity indices for a multifaceted framework in functional ecology. *Ecology, 89*(8), 2290-2301. doi:https://doi.org/10.1890/07-1206.1

Villéger, S., Novack-Gottshall, P. M., & Mouillot, D. (2011). The multidimensionality of the niche reveals functional diversity changes in benthic marine biotas across geological time. *Ecology Letters, 14*(6), 561-568. doi:https://doi.org/10.1111/j.1461-0248.2011.01618.x

Villéger, S., Grenouillet, G., & Brosse, S. (2014). Functional homogenization exceeds taxonomic homogenization among European fish assemblages. *Global Ecology and Biogeography, 23*(12), 1450-1460. doi:https://doi.org/10.1111/geb.12226

Violle, C., Navas, M.-L., Vile, D., Kazakou, E., Fortunel, C., Hummel, I., & Garnier, E. (2007). Let the concept of trait be functional! *Oikos, 116*(5), 882-892. doi:https://doi.org/10.1111/j.0030-1299.2007.15559.x

Waldock, C., Stuart-Smith, R. D., Albouy, C., Cheung, W. W. L., Edgar, G. J., Mouillot, D., . . . Pellissier, L. (2022). A quantitative review of abundance-based species distribution models. *Ecography, 2022*(1). doi:https://doi.org/10.1111/ecog.05694

Woodd-Walker, R. S., Ward, P., & Clarke, A. (2002). Large-scale patterns in diversity and community structure of surface water copepods from the Atlantic Ocean. *Marine Ecology Progress Series, 236*, 189-203.

Xi, H., Losa, S. N., Mangin, A., Garnesson, P., Bretagnon, M., Demaria, J., . . . Bracher, A. (2021). Global Chlorophyll a Concentrations of Phytoplankton Functional Types With Detailed Uncertainty Assessment Using Multisensor Ocean Color and Sea Surface Temperature Satellite Products. *Journal of Geophysical Research: Oceans, 126*(5), e2020JC017127. doi:https://doi.org/10.1029/2020JC017127

Yan, P., Fernández-Martínez, M., Van Meerbeek, K., Yu, G., Migliavacca, M., & He, N. (2023). The essential role of biodiversity in the key axes of ecosystem function. *Global Change Biology, 29*(16), 4569-4585. doi:https://doi.org/10.1111/gcb.16666

Data availability statement

The copepod species occurrence data used to train the species distribution models are publicly available on Zenodo (https://doi.org/10.5281/zenodo.5101349). The copepod species functional traits table is available as Supplementary Table S1. All R codes are accessible on the GitHub account of F.B. (https://github.com/benfabio/Global-cOpepoD-functionaL-diversitY).

FD facet	Index	Meaning	Input data	HSI weighing?	Computation method	Main R packages used	References
(i) Functional richness (**fraction of the total functional space occupied by the species assemblage?**)	Faith's index (**Faith**)	Assemblages with higher Faith values are those where the present species represent more distant and more numerous branches on the total functional dendrogram (i.e., more functional volume filled by the assemblage)	Gower distance matrix (section 2.1) + Community matrices with species' presence-absence data inferred from the species HSI (using the probability threshold that maximizes the agreement between observed and modelled distributions)	No	Sum of the lengths of all those branches of the functional dendrogram that are members of the corresponding minimum spanning path covered by the species constituting an assemblage	*gawdis* v.0.1.5 (de Bello et al., 2021) *picante* v.1.8.2 (Kembel et al., 2010) *ape* v.5.7-1 (Paradis & Schliep, 2019)	Faith (1992) Schleuter et al. (2010)
	Standardized-effect-size of Faith (**SES Faith**)	SES Faith values < 0 indicate that functional clustering (or functional convergence) occurs due to environmental filtering in the copepod assemblage whereas values > 0 indicate that there is functional overdispersion		No	SES Faith were calculated by randomly reshuffling the tips of the functional dendrogram (i.e., the species names) 999 times. The 999 random Faith values provided a null distribution of Faith's index against which observed Faith's index values were compared. The ensuing global monthly SES Faith values and p-values indicate where functional richness is significantly higher or lower than the values dictated by species richness alone		
(ii) Functional evenness**,** dispersion and divergence **(how is the functional space occupied by the species assemblage?**)	Functional evenness (**FEve**)	Higher FEve values indicate that species in the assemblage display similar HSI at equal distances between nearest neighbors in the functional space. Lower FEve values indicate the co-existence of scattered clouds of functional units	Multidimensional functional space obtained by projecting a Gower distance matrix (section 2.1) into a principal coordinates analysis (PCoA) FD indices based on the first four axes of a PCoA (Figure S1)	Yes	FEve uses the HSI-weighted distances between all species pairs to calculate the minimum spanning tree that connects all said species in the multidimensional functional space (Villéger et al., 2008). Then, FEve measures the regularity of the branch lengths	*gawdis* v.0.1.5 (de Bello et al., 2021) *vegan* v.2.6-4 (Oksanen et al., 2022) *FD* v.1.0-12.3 (Laliberté et al., 2014)	Mason et al. (2005) Villéger et al. (2008) Laliberté & Legendre (2010) Schleuter et al. (2010) Mouillot et al. (2021)
	Functional dispersion (**FDis**) and Rao's quadratic entropy (**Rao's Q**)	FDis and Rao's Q estimate a similar facet of FD. Assemblages with higher FDis and Rao's Q values are those whose species are further away from each other and from the centroid in the functional space (i.e., more specialized species)			FDis measures the mean distance of the species to the centroid of the functional space occupied by the assemblage, using the species' HSI as weighs for the distances		
					Rao's Q computes the variance of trait dissimilarity per species pairs (i.e., similar to a Simpson index) and weighs this variance by the product of the species' HSI		
	Functional divergence (**FDiv**)	Assemblages with higher FDiv values are characterized by					

		higher HSI values at the vertices of their convex hull (i.e., more extreme traits values			FDiv defines the vertices and gravity center of a convex hull in functional space, based of the species present in the assemblage, and then measures the HSI-weighted deviances of each species present to the species' mean distance to that center of gravity		
(iii) **Beta-FD** (How do assemblages overlap in functional space?)	Total trait dissimilarity based on Jaccard's dissimilarity index (**Trait dissimilarity**)	Trait dissimilarity values close to 1 indicate that two assemblages display functional dendrograms with very different number of branches that are non-overlapping	Same as Faith	No	Each pair of assemblages (A_i, A_j) shows a total trait dissimilarity that corresponds to the sum of the lengths of edges that are unique to each assemblage-specific dendrogram	*gawdis* v.0.1.5 (de Bello et al., 2021) *picante* v.1.8.2 (Kembel et al., 2010) *ape* v.5.7-1 (Paradis & Schliep, 2019) *phyloregion* v.1.0.8 (Daru et al., 2020)	Baselga (2010) Cardoso et al. (2014)
	Trait dissimilarity driven by turnover (i.e., replacement) (**Trait turnover**)	Trait turnover values close to 1 indicate that total trait dissimilarity is driven by the replacement of branches			For every (A_i, A_j), Trait turnover corresponds to the substitution of branches exclusive to A_i by the other branches with the same total length that are exclusive to A_j		
	Trait dissimilarity driven by nestedness (i.e., differences in trait richness) (**Trait turnover**)	Trait nestedness values close to 1 indicate that total trait dissimilarity is driven by different number of branches, whatever their identity			Trait nestedness is equal to the absolute difference between the branch lengths of A_i and A_j		

Table 1: Summary of the metrics (name, meaning, underlying input data, methodology and R packages used) used in the present study to estimate the various facets of marine copepod functional diversity (FD).

Figure captions

Figure 1: Distribution of contemporary mean annual a) species richness, b) Faith index (Faith), c) standardized effect sizes (SES) of Faith, d) functional evenness (FEve), e) functional dispersion (FDis) and f) functional divergence (FDiv). Faith estimates functional richness. SES Faith measures the difference between observed Faith and null Faith estimates obtained from a randomly assembled community of the species same richness. Species richness and Faith were calculated on presence-absence data whereas FEve, FDis and FDiv were weighed by habitat suitability indices ranging between 0 and 1 to better represent the distribution of habitat suitability in functional space. Mean annual values are derived from monthly values (n = 12) computed for assemblages whose species composition was modelled through three species distribution models.

Figure 2: Distribution of contemporary mean annual pairwise a) total functional trait dissimilarity, b) trait turnover, c) trait nestedness, and d) the ratio between trait turnover and total trait dissimilarity. The beta diversity indices were all computed on presence-absence data and were based on Jaccard's dissimilarity index. Mean annual values are derived from monthly values (n = 12) computed for assemblages whose species composition was modelled through three species distribution models.

Figure 3: Emergent relationships between global mean annual values of copepod species richness and a) Faith index (Faith), b) standardized-effect-sizes (SES) of Faith, c) functional evenness (FEve), d) functional dispersion (FDis), e) functional divergence (FDiv), f) total functional trait dissimilarity, g) trait turnover, and (h) trait nestedness. Mean annual values are derived from monthly values (n = 12) computed for assemblages whose species composition was modelled through three species distribution models. Species richness, Faith and functional beta diversity indices were based on presence-absence data whereas FEve, FDis and FDiv were weighed by habitat suitability indices ranging between 0 and 1. Each point was colored as a function of absolute latitude to illustrate where spatial variations have the strongest effects. The statistics of the fitted regressions are given.

Figure 4: Emergent relationships between global mean annual values of copepod diversity indices and indicator variables of ecosystem functioning based on the a) Z-score profiles (number of standard deviations below or above the annual mean) showing where variables display higher (red) or lower (blue) values relative to the mean. We focus on the most conspicuous patterns enabling us to test the emergent relationships between zooplankton biomass production and b) total trait dissimilarity, c) functional evenness (FEve), d) species richness, e) functional divergence (FDiv), f) Faith index (Faith) and g) functional dispersion (FDis). Grid cells were colored as a function of absolute latitude to illustrate where spatial variations have the strongest effects. The sorting of the variables is based on the similarity of the spatial patterns of the Z-scores: variables on the Y axis are close if they show similar Z-scores patterns (according to Euclidean distances). The X axis represents the ocean grid cells (i.e., space). The acronyms are given in section 2.4., indicators of ecosystem functioning are given in capital letters.

Figure 5: Distribution of the relative differences (Δ, in %) in mean annual copepod a) species richness, b) Faith index (Faith), c) functional evenness (FEve), d) functional dispersion (FDis), e) functional divergence (FDiv), f) total trait dissimilarity, g) trait turnover and h) trait nestedness between the contemporary (2012-2031) and end-of-century (2081-2100) periods. End-of-century estimates were based on an ensemble of monthly values obtained for three species distribution models and five earth system models (n = 180). Species richness, Faith and functional beta diversity indices were based on presence-absence data whereas FEve, FDis and FDiv were weighed by habitat suitability indices ranging between 0 and 1. For a), c) and h) values > 30% are plotted in a darker shade of red.

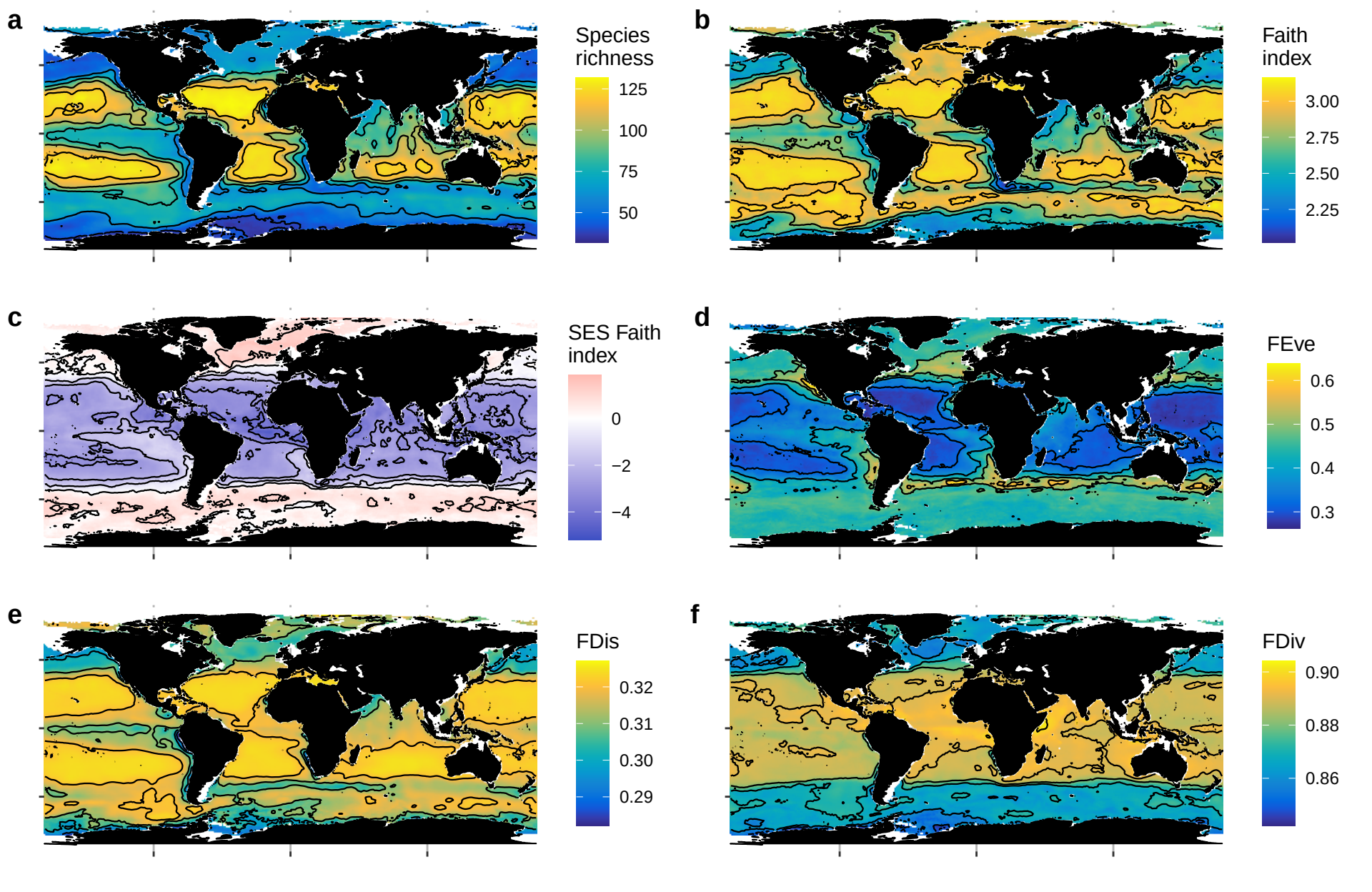
a
Species richness
125
100
75
50
b
Faith index
3.00
2.75
2.50
2.25
c
SES Faith index
0
−2
−4
d
FEve
0.6
0.5
0.4
0.3
e
FDis
0.32
0.31
0.30
0.29
f
FDiv
0.90
0.88
0.86

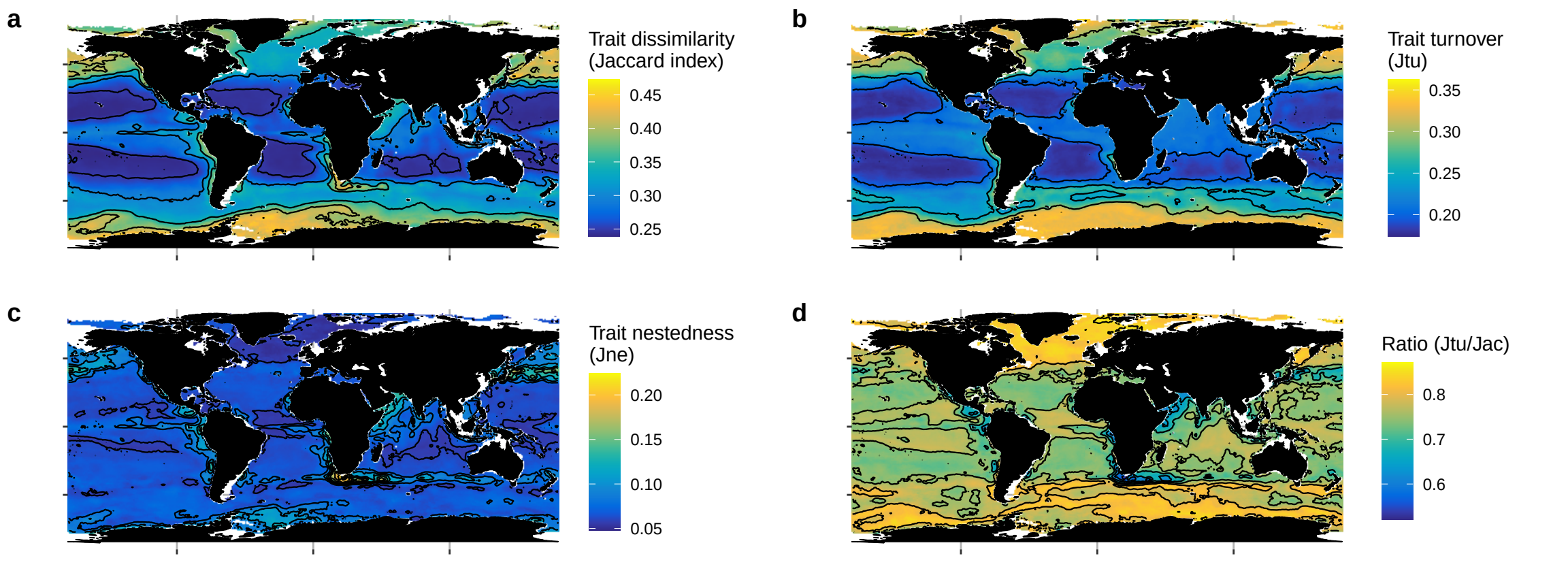
a
Trait dissimilarity
(Jaccard index)
0.45
0.40
0.35
0.30
0.25
b
Trait turnover
(Jtu)
0.35
0.30
0.25
0.20
c
Trait nestedness
(Jne)
0.20
0.15
0.10
0.05
d
Ratio (Jtu/Jac)
0.8
0.7
0.6

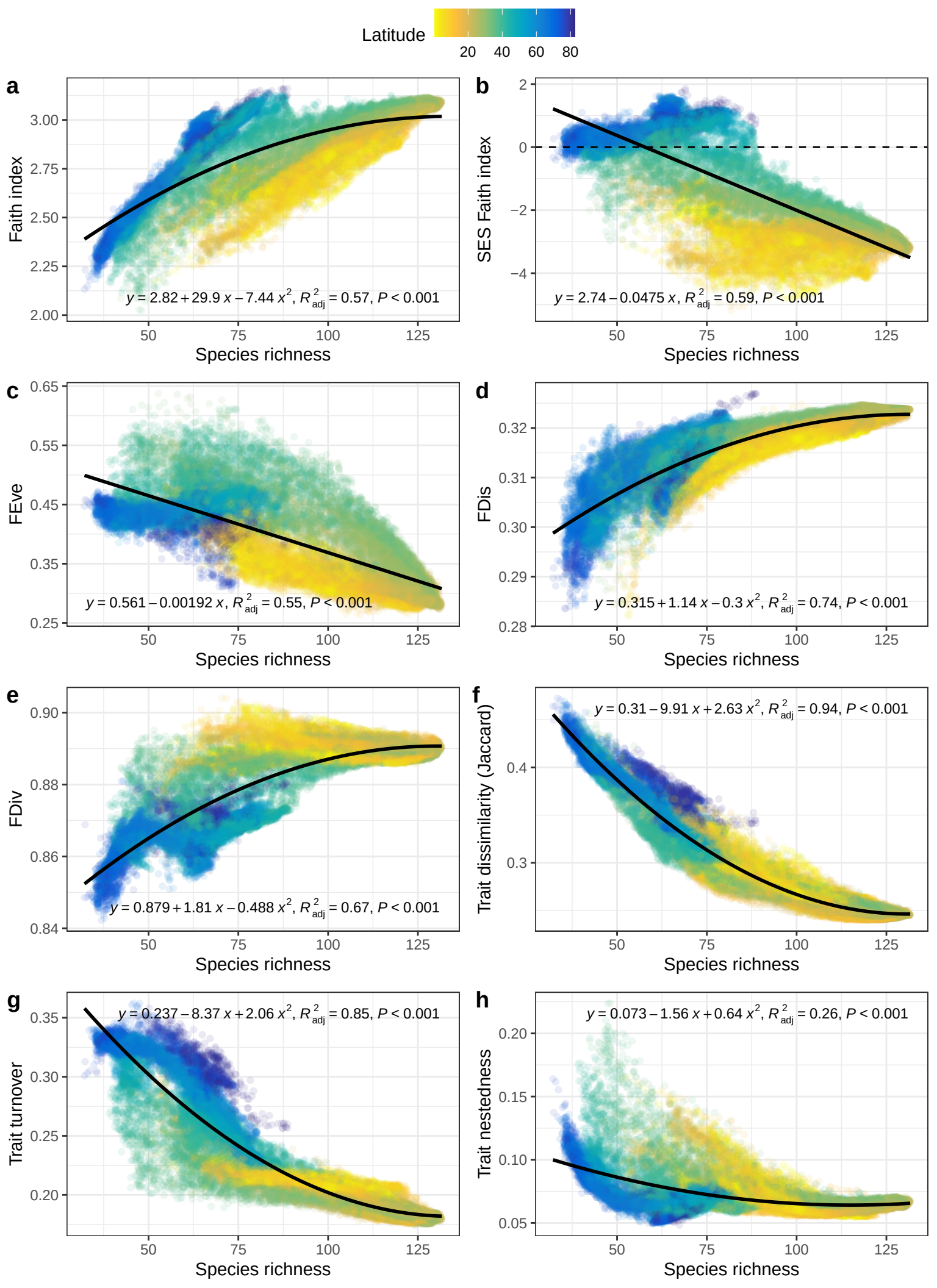
Latitude
20 40 60 80
a
Faith index
3.00
2.75
2.50
2.25
2.00
$y = 2.82 + 29.9\,x - 7.44\,x^2$, $R^2_{adj} = 0.57$, $P < 0.001$
50 75 100 125
Species richness
b
SES Faith index
2
0
−2
−4
$y = 2.74 - 0.0475\,x$, $R^2_{adj} = 0.59$, $P < 0.001$
50 75 100 125
Species richness
c
FEve
0.65
0.55
0.45
0.35
0.25
$y = 0.561 - 0.00192\,x$, $R^2_{adj} = 0.55$, $P < 0.001$
50 75 100 125
Species richness
d
FDis
0.32
0.31
0.30
0.29
0.28
$y = 0.315 + 1.14\,x - 0.3\,x^2$, $R^2_{adj} = 0.74$, $P < 0.001$
50 75 100 125
Species richness
e
FDiv
0.90
0.88
0.86
0.84
$y = 0.879 + 1.81\,x - 0.488\,x^2$, $R^2_{adj} = 0.67$, $P < 0.001$
50 75 100 125
Species richness
f
Trait dissimilarity (Jaccard)
0.4
0.3
$y = 0.31 - 9.91\,x + 2.63\,x^2$, $R^2_{adj} = 0.94$, $P < 0.001$
50 75 100 125
Species richness
g
Trait turnover
0.35
0.30
0.25
0.20
$y = 0.237 - 8.37\,x + 2.06\,x^2$, $R^2_{adj} = 0.85$, $P < 0.001$
50 75 100 125
Species richness
h
Trait nestedness
0.20
0.15
0.10
0.05
$y = 0.073 - 1.56\,x + 0.64\,x^2$, $R^2_{adj} = 0.26$, $P < 0.001$
50 75 100 125
Species richness

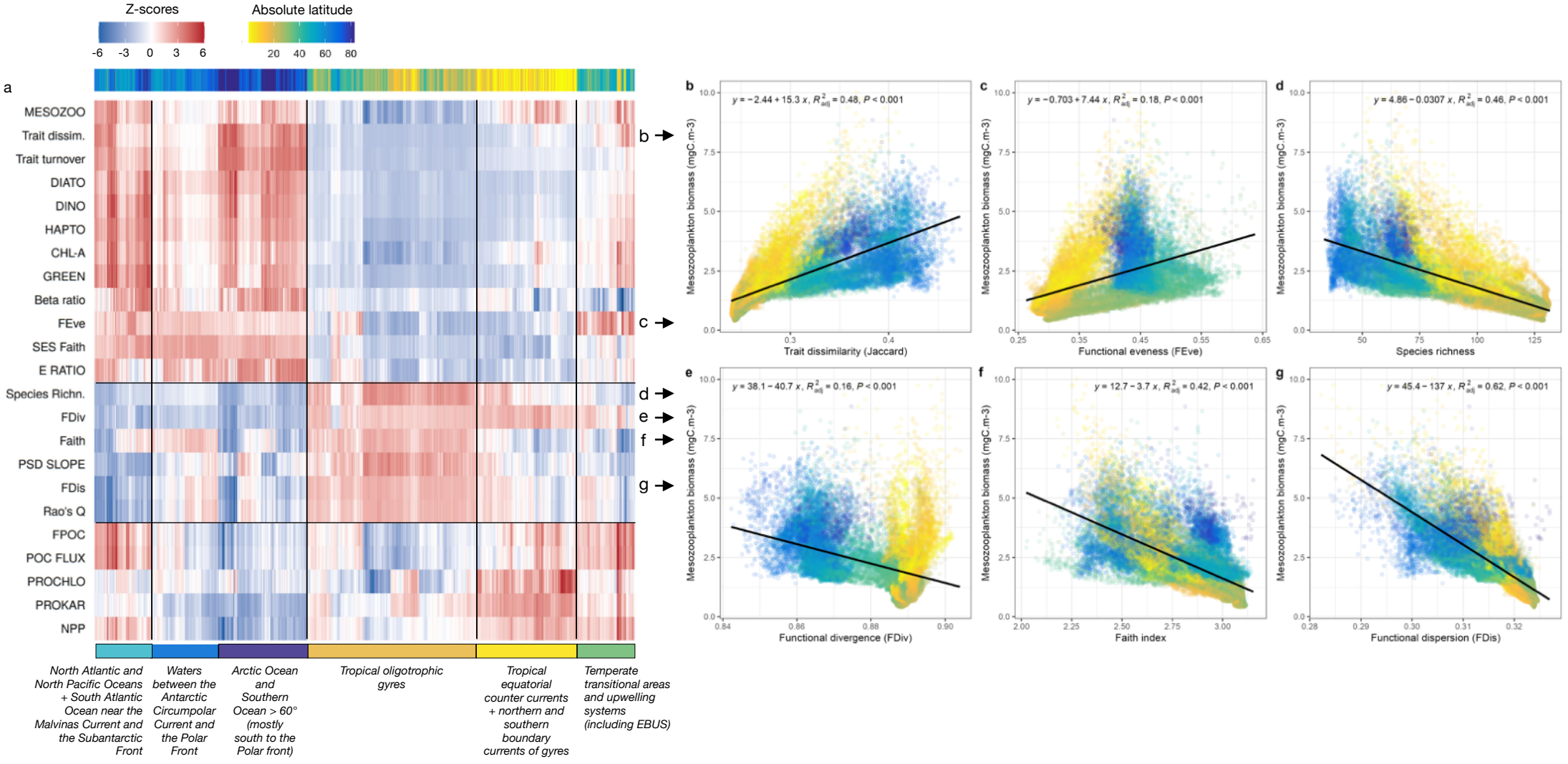
Z-scores
-6 -3 0 3 6
Absolute latitude
20 40 60 80
a
MESOZOO
Trait dissim.
Trait turnover
DIATO
DINO
HAPTO
CHL-A
GREEN
Beta ratio
FEve
SES Faith
E RATIO
Species Richn.
FDiv
Faith
PSD SLOPE
FDis
Rao's Q
FPOC
POC FLUX
PROCHLO
PROKAR
NPP
b
c
d
e
f
g
North Atlantic and North Pacific Oceans + South Atlantic Ocean near the Malvinas Current and the Subantarctic Front
Waters between the Antarctic Circumpolar Current and the Polar Front
Arctic Ocean and Southern Ocean > 60° (mostly south to the Polar front)
Tropical oligotrophic gyres
Tropical equatorial counter currents + northern and southern boundary currents of gyres
Temperate transitional areas and upwelling systems (including EBUS)
b
y = −2.44 + 15.3 x, R^2_{adj} = 0.48, P < 0.001
Mesozooplankton biomass (mgC.m-3)
Trait dissimilarity (Jaccard)
c
y = −0.703 + 7.44 x, R^2_{adj} = 0.18, P < 0.001
Functional eveness (FEve)
d
y = 4.86 − 0.0307 x, R^2_{adj} = 0.46, P < 0.001
Species richness
e
y = 38.1 − 40.7 x, R^2_{adj} = 0.16, P < 0.001
Functional divergence (FDiv)
f
y = 12.7 − 3.7 x, R^2_{adj} = 0.42, P < 0.001
Faith index
g
y = 45.4 − 137 x, R^2_{adj} = 0.62, P < 0.001
Functional dispersion (FDis)

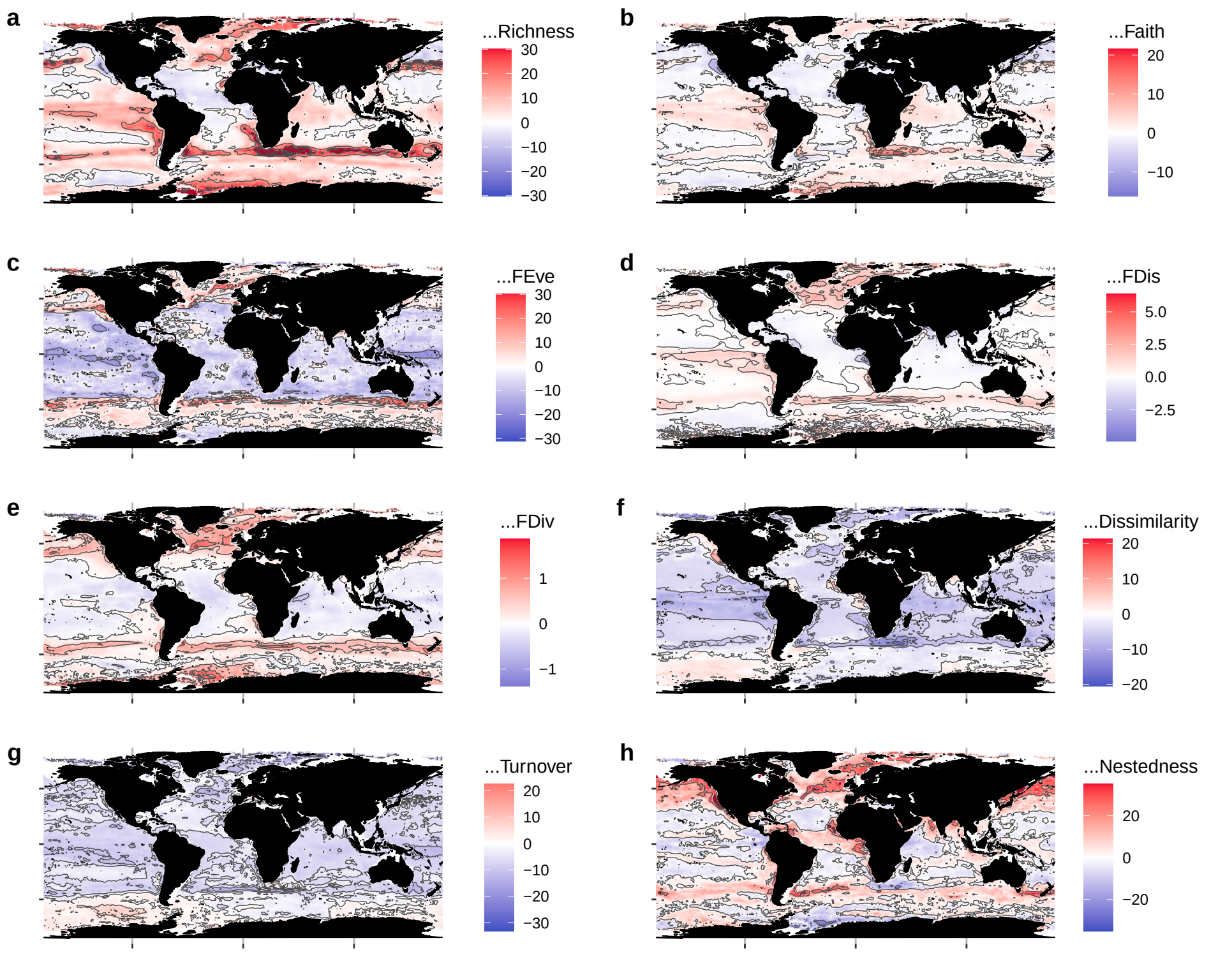
a
...Richness
30
20
10
0
−10
−20
−30
b
...Faith
20
10
0
−10
c
...FEve
30
20
10
0
−10
−20
−30
d
...FDis
5.0
2.5
0.0
−2.5
e
...FDiv
1
0
−1
f
...Dissimilarity
20
10
0
−10
−20
g
...Turnover
20
10
0
−10
−20
−30
h
...Nestedness
20
0
−20

Supplementary Materials to « *Emergent relationships between the functional diversity of marine zooplankton and ecosystem functioning in the global ocean* »

by Fabio Benedetti, Jonas Wydler, Corentin Clerc, Nielja Knecht & Meike Vogt.

The following .pdf document contains three types of Supplementary Materials:

- Supplementary Methods
- Supplementary Results
- Supplementary Figures (S1 to S16)

The Supplementary Table 1 (the copepod species traits table with references) is given separately in an excel sheet.

Supplementary Methods: Exhaustive description of why and how were the various functional diversity (FD) indices computed in the present study.

FD is a multidimensional and multifaceted concept embedding changes in composition within (alpha-diversity) and between (beta-diversity) assemblages (Mason et al., 2005; Mouillot et al., 2013). Consequently, we chose to compute indices that describe the following facets of FD: (i) how much of the total functional space is filled by the composition of each assemblage (functional richness), (ii) how are the HSI and/or inferred presences/absences of species distributed within the functional spaces (functional dispersion, evenness or divergence), and (iii) how much do assemblages overlap in functional space (beta-FD; Villéger et al., 2011). We also computed monthly species richness based on the same community matrices to investigate how the facets of FD covary with taxonomic diversity and test if species-rich assemblages are more or less functionally diverse than species-poor assemblages (Stuart-Smith et al., 2013).

To evaluate facet (i), we computed Faith's index (Faith) as a proxy for functional richness using the Gower distance matrix described above as the reference functional dendrogram (Faith, 1992). For each assemblage, Faith was computed as the sum of the lengths of all those branches of the functional dendrogram that are members of the corresponding minimum spanning path covered by the species constituting said assemblage. Assemblage composition was described by species' mean HSI (i.e., continuous probabilities) but Faith requires binary presence-absence data (i.e., distributions). We thus converted the HSI to 1 and 0 based on the probability threshold that maximizes the agreement between the observed and the modelled distribution (Thuiller et al., 2023). Assemblages displaying higher species richness are automatically represented by more branches on the functional dendrogram. Differences in Faith are thus biased by differences in taxonomic richness and standardized-effect-sizes (SES) must be calculated to study functional richness patterns that are not biased by species richness (Schleuter et al., 2010). SES of Faith (SES Faith) were calculated on the same data by randomly reshuffling the tips of the functional dendrogram (i.e., the species names) 999 times. The 999 random Faith values provided a null distribution of Faith's index against which observed Faith's index values were compared. The ensuing global monthly SES Faith values and P-values indicate where functional richness is significantly higher or lower than the values dictated by species richness alone. SES Faith values < 0 indicate that functional clustering (or functional convergence) occurs due to environmental filtering occurs in the copepod assemblage whereas values > 0

indicate that functional overdispersion occurs (Mikryukov et al., 2023). Faith and SES Faith values were computed using the *picante* R package (Kembel et al., 2010).

To evaluate facet (ii), we computed four complementary FD indices widely used in the literature (Mason et al., 2005; Villéger et al., 2008): functional evenness (FEve), functional dispersion (FDis), Rao's quadratic entropy (Rao's Q) and functional divergence (FDiv). FEve describes whether species traits are distributed regularly within the functional space occupied by the assemblage, with higher FEve values indicating more regular trait distributions. Here, FEve uses the HSI-weighted distances between all species pairs to calculate the minimum spanning tree that connects all said species in the multidimensional functional space (Villéger et al., 2008). Then, FEve measures the regularity of the branch lengths. Higher FEve values indicate that species occur in the assemblage with similar HSI at equal distances between nearest neighbors in the functional space, whereas lower values indicate the co-existence of scattered clouds of functional units.

FDis and Rao's Q estimate a similar facet of FD. FDis measures the mean distance of the species to the centroid of the functional space occupied by the assemblage, using the species-specific HSI as weighs for the distances (Laliberté & Legendre, 2010). Rao's Q computes the variance of trait dissimilarity per species pairs (similar to a Simpson index) and weighs this variance by the product of the species' HSI. Assemblages characterized by higher FDis and Rao's Q are assemblages whose species are further away from each other and from the centroid in the functional space (i.e., more specialized species).

FDiv uses the species present in the assemblage to define the vertices and gravity center of a convex hull in functional space (Villéger et al., 2008). Then, FDiv measures the HSI-weighted deviances of each species present to the species' mean distance to that center of gravity. Assemblages displaying higher FDiv values are characterized by higher HSI values at the vertices of their convex hull (i.e., more extreme traits values).

By construction, these four indices are not affected by differences in species richness (Schleuter et al., 2010; Laliberté & Legendre, 2010) so SES were not calculated. Contrary to Faith's index, computing these four indices requires a multidimensional functional space by projecting the Gower distance matrix into a principal coordinates analysis (PCoA; Villéger et al., 2008). The hyper-dimensionality of PCoA spaces makes the computation of hypervolume-based indices challenging (Mouillot et al., 2021). Therefore, following recent community guidelines (Mouillot et al., 2021), we calculated those FD indices based on the first four axes of the PCoA as these retained a similar level of functional dissimilarity as the original Gower distance matrix

(**Figure S1**). Functional richness is more commonly quantified through the FRic index than by Faith (Villéger et al., 2008). Therefore we made sure that Faith provided similar functional richness patterns as standardized FRic values on a mean annual scale (**Figure S2**). We preferred Faith over FRic because it is less sensible to SDM choice and because FRic is only representative of changes in species composition occurring at the edges of the functional space.

To evaluate facet (iii), we rely on the framework proposed by Baselga (2010) and Cardoso et al. (2014) to compute pairwise beta-FD based on Jaccard's dissimilarity index. In this framework, each copepod assemblage A_x is a subset of the functional dendrogram described in section 2.1. Each pair of assemblages (A_i, A_j) shows a total trait dissimilarity that corresponds to the sum of the lengths of edges that are unique to each assemblage-specific dendrogram (Cardoso et al., 2014). We hereby refer to this total dissimilarity values as trait dissimilarity (Trait dissimilarity). Similar as in Baselga (2010), Trait dissimilarity can be partitioned into two additive components: replacement (hereby: Trait turnover) and richness differences (hereby: Trait nestedness). For every (A_i, A_j), Trait turnover corresponds to the substitution of branches exclusive to A_i by the other branches with the same total length that are exclusive to A_j (Cardoso et al., 2014). The remaining dissimilarity fraction (Trait nestedness) is equal to the absolute difference between the branch lengths of A_i and A_j. These beta-FD indices were computed with the function phylobeta() of the *phyloregion* R package (Daru et al., 2020) using the same presence-absence community matrices as those used for calculating Faith values. Trait dissimilarity, Trait turnover and Trait nestedness are all bounded between 0 and 1. Trait dissimilarity values close to 1 indicate that two assemblages display functional dendrograms with very different number of branches that are non-overlapping. Since these indices are calculated for each community matrix, there are as many index values as pairs of assemblages (i.e., pairs of ocean grid cells) and they represent emergent spatial patterns in copepod beta-FD. For each assemblage, we retained the average values of Trait dissimilarity, Trait turnover and Trait nestedness. Like what is done with taxonomic diversity, exploring the covariance of these beta-FD indices together with Faith allows to test if the emergent functional richness pattern is driven by turnover in traits composition or differences in number of traits.

References

Baselga, A. (2010). Partitioning the turnover and nestedness components of beta diversity. *Global Ecology and Biogeography, 19*(1), 134-143. doi:10.1111/j.1466-8238.2009.00490.x

Cardoso, P., Rigal, F., Carvalho, J. C., Fortelius, M., Borges, P. A. V., Podani, J., & Schmera, D. (2014). Partitioning taxon, phylogenetic and functional beta diversity into replacement and richness difference components. *Journal of Biogeography, 41*(4), 749-761. https://doi.org/10.1111/jbi.12239

Daru, B. H., Karunarathne, P., & Schliep, K. (2020). phyloregion: R package for biogeographical regionalization and macroecology. *Methods in Ecology and Evolution, 11*(11), 1483-1491. https://doi.org/10.1111/2041-210X.13478

Faith, D. P. (1992). Conservation evaluation and phylogenetic diversity. *Biological Conservation, 61*(1), 1-10.

Kembel, S. W., Cowan, P. D., Helmus, M. R., Cornwell, W. K., Morlon, H., Ackerly, D. D., . . . Webb, C. O. (2010). Picante: R tools for integrating phylogenies and ecology. *Bioinformatics, 26*(11), 1463-1464.

Laliberté, E., & Legendre, P. (2010). A distance-based framework for measuring functional diversity from multiple traits. *Ecology, 91*(1), 299-305. https://doi.org/10.1890/08-2244.1

Mason, N. W. H., Mouillot, D., Lee, W. G., & Wilson, J. B. (2005). Functional richness, functional evenness and functional divergence: the primary components of functional diversity. *Oikos, 111*(1), 112-118. https://doi.org/10.1111/j.0030-1299.2005.13886.x

Mikryukov, V., Dulya, O., Zizka, A., Bahram, M., Hagh-Doust, N., Anslan, S., . . . Tedersoo, L. (2023). Connecting the multiple dimensions of global soil fungal diversity. *Science Advances, 9*(48), eadj8016. doi:doi:10.1126/sciadv.adj8016

Mouillot, D., Graham, N. A. J., Villéger, S., Mason, N. W. H., & Bellwood, D. R. (2013). A functional approach reveals community responses to disturbances. *Trends in ecology & evolution, 28*(3), 167-177. https://doi.org/10.1016/j.tree.2012.10.004

Mouillot, D., Loiseau, N., Grenié, M., Algar, A. C., Allegra, M., Cadotte, M. W., . . . Auber, A. (2021). The dimensionality and structure of species trait spaces. *Ecology Letters, 24*(9), 1988-2009. https://doi.org/10.1111/ele.13778

Schleuter, D., Daufresne, M., Massol, F., & Argillier, C. (2010). A user's guide to functional diversity indices. *Ecological monographs, 80*(3), 469-484. https://doi.org/10.1890/08-2225.1

Stuart-Smith, R. D., Bates, A. E., Lefcheck, J. S., Duffy, J. E., Baker, S. C., Thomson, R. J., . . . Airoldi, L. (2013). Integrating abundance and functional traits reveals new global hotspots of fish diversity. *Nature, 501*(7468), 539-542.

Thuiller, W., Georges, D., Gueguen, M., Engler, R., Breiner, F., Lafourcade, B., Patin, R. (2023). biomod2: Ensemble Platform for Species Distribution Modeling. R package version 4.2-4, https://CRAN.R-project.org/package=biomod2

Villéger, S., Mason, N. W. H., & Mouillot, D. (2008). New multidimensional functional diversity indices for a multifaceted framework in functional ecology. *Ecology, 89*(8), 2290-2301. https://doi.org/10.1890/07-1206.1

Villéger, S., Novack-Gottshall, P. M., & Mouillot, D. (2011). The multidimensionality of the niche reveals functional diversity changes in benthic marine biotas across geological time. *Ecology Letters, 14*(6), 561-568. https://doi.org/10.1111/j.1461-0248.2011.01618.x

Supplementary Results: Finer regional description of the copepod diversity patterns and how their covary with indicator variables of ecosystem functioning (complementary to Figure 4).

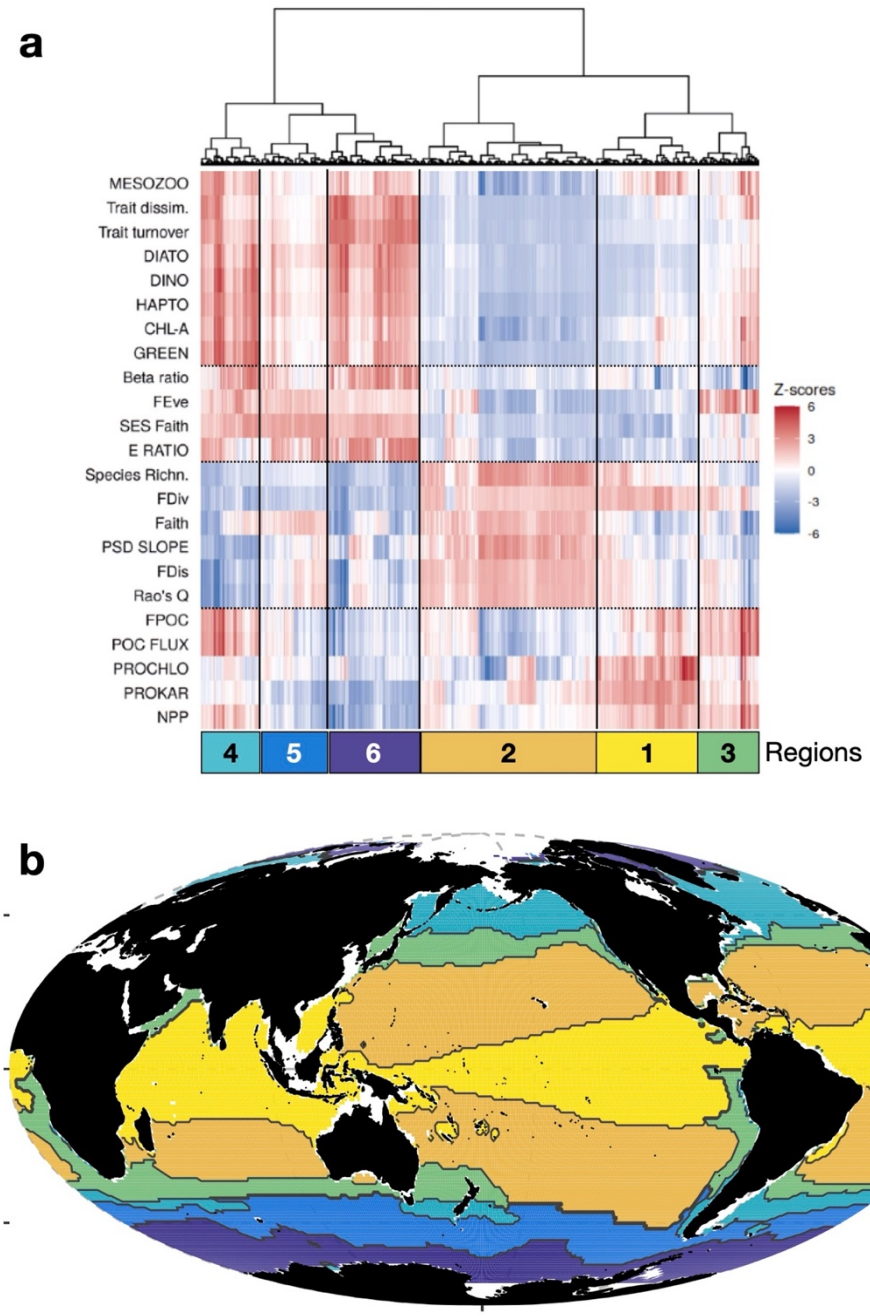

***Figure**: Hierarchical clustering of the global ocean based on the a) Z-score profiles of the copepod functional diversity (FD) indices and the indicator variables of marine ecosystem functioning. The Z-scores profiles show where variables display higher (red) or lower (blue) values relative to the mean. They were used to calculate a pairwise Euclidean distance matrix between ocean grid cells (1°x1°) that were then clustered into b) regions of similar emergent patterns of copepod FD and indicators of ecosystem functioning. Z-scores were computed on mean annual values. The hierarchical clustering of the Euclidean distance matrix was based on Ward's linkage. The suite of acronyms is give in section 2.4. of the main text, indicators of ecosystem functioning are given in capital letters.*

The results in Figures 1 to 3 indicate that the covariance patterns between the facets of copepod FD and ecosystem functioning indicators are spatially structured. To identify regions that share similar covariance structure and pinpoint those where higher FD values overlap with higher performance of ecosystem functions, we cluster the ocean in a hierarchical fashion based on the Z-scores of the variables studied here. A Euclidean distance matrix was computed from the Z-scores and hierarchical clustering was performed based on Ward's linkage because the latter is a synoptic criterion that minimizes intra-cluster variance and enables to disentangle large regional differences (Legendre & Legendre, 2012). We here focus on six regions (Figure 5b) because these are: (i) robust clusters based on intra-variance to inter-variance ratios (Benedetti et al., 2021), and (ii) spatially-coherent regions that are clearly interpretable in a global oceanographic context (i.e., regions similar to Benedetti, Wydler & Vogt, 2023). The larger/smaller regions obtained when choosing higher/lower cutting levels are shown in Figure S11.

The six regions are highly similar to those defined in Benedetti, Wydler & Vogt (2023). Regions 2 and 1 are the largest in terms of grid cell coverage (31.4% and 18.6%, respectively), followed by region 6 (16.4%), 5 (12.2%), 3 (10.8%) and 4 (10.6%). Region 1 is exclusively tropical (0-25° latitude) and gathers warm-water areas that are influenced by major oceanographic features such as equatorial counter currents and the southern or northern boundary currents of the tropical gyres. Region 2 comprises the large tropical oligotrophic gyres of the Pacific, Atlantic and Indian Oceans. Region 3 gathers the more coastal parts of upwelling systems (i.e., the eastern boundary upwellings and the northern upwelling of the Indian Ocean) and the transitional areas that separate the warm tropical gyres from the colder waters of the North Pacific, North Atlantic and Southern Oceans. Region 4 gathers the North Atlantic and North Pacific Oceans, as well as the part of the South Atlantic Ocean that experiences the retroflexion of the Malvinas Current and the Subantarctic front. Region 5 comprises the waters confined between the Antarctic Circumpolar Current to the north and the Polar Front to the south. Region 6 is almost exclusively polar (> 60° latitude) and gathers the Arctic Ocean and the waters south to the Polar Front.

At a high similarity level, the main dichotomy separates the regions mainly occurring < 45° latitude (1-3) from those occurring > 40° (4-6). Relative to regions 1-3, regions 4-6 show higher SES Faith, FEve, Trait dissimilarity/turnover, higher MESOZOO, higher E RATIO and higher phytoplankton biomass mainly ensured by larger functional types (CHL-A, DIATOM, DINO, HAPTO, lower PSD SLOPE; Fig. 5a). Meanwhile, regions 1-3 are mainly characterized by lower Trait dissimilarity/turnover and higher species richness, Faith, FDiv, FDis, and larger

PSD SLOPE values due to a stronger contribution of very small plankton to primary production (i.e., higher PROKAR and PROCHL).

More interestingly, we also find significant variations in copepod FD and ecosystem functioning indicators among the low latitude and the high latitude regions (based on Kruskal-Wallis tests; Figure S12). Among regions 1-3, region 2 shows the highest levels of species and functional richness (Figure S12h,i) but the lowest levels of FEve, MESOZOO, CHL-A and POC export fluxes. Meanwhile, region 3 displays the highest levels of FEve, MESOZOO, CHL-A, and POC export fluxes and the lowest species richness and functional richness (Figure S12h,i,j,k,l,n). Region 1 is an intermediate case between 2 and 3. It shows higher levels of NPP, PROKAR and PROCHL. Among regions 4-6, region 5 shows the highest levels functional richness and FDis (Figure S12a,b) but the lowest levels of total Trait dissimilarity, MESOZOO and CHL-A (Figure S12c,d,f). Meanwhile, region 4 stands out for its higher phytoplankton productivity (CHL-A and NPP), higher MESOZOO and POC export fluxes below the euphotic zone (Figure S12d,e,f,g).

The direction of the linear relationships fitted between copepod diversity and MESOZOO (Fig. 4) are mostly conserved on a regional level (Figure S13). However, they vary in strength between regions (pairwise ANCOVA tests, $P < 0.01$; but see Figure S13). The negative fit between species richness and MESOZOO is strongest for regions 2 and 4 but barely significant ($R^2 < 0.1$) for regions 3, 4 and 6. Similarly, the decrease in MESOZOO with Faith becomes weaker with latitude: it is strongest for region 1, remains relatively similar in regions 2, 3 and 4 and then becomes very weak ($R^2 < 0.05$) in regions 5 and 6. The increase in MESOZOO with Trait dissimilarity and turnover is highest for regions 1 and 2 and becomes very weak in region 6. The decrease in MESOZOO with FDis does not vary so clearly with latitude. It is strongest for regions 3 and 4 (both $R^2 > 0.45$) and weakest for region 5 ($R^2 < 0.15$). However, contrary to what we observed on a global scale (Fig. 4), MESOZOO actually decreases with FEve in regions 3 and 4 with varying rates and shows barely no linear relationship with FEve in regions 5 and 6 (Figure S13). The positive covariance between FEve and MESOZOO is thus mainly driven by the copepod assemblages of regions 1 and 2 ($R^2 = 0.45$ and 0.28, respectively).

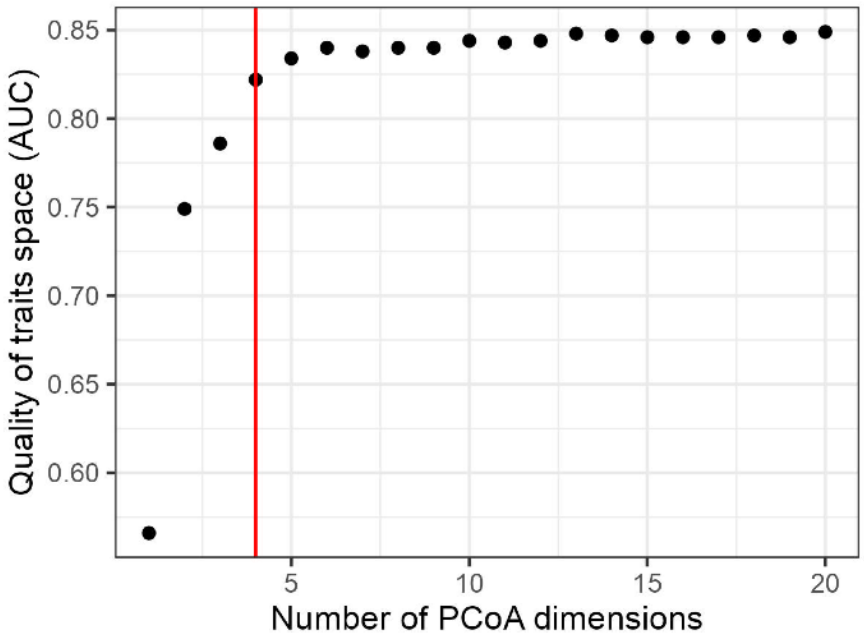

Figure S1: Variation of the quality of the multidimensional trait space based on the area under the curve (AUC) criterion, described in Mouillot et al. (2021), as a function of the number of dimensions of a principal coordinates analysis (PCoA) retained for computing an Euclidean distance matrix. AUC is unitless and ranges between 0 and 1. A value of 1 represents the best case scenario where the ranking of species pairs would be perfectly preserved between the reference Gower distance matrix and the Euclidean distances matrices of lower dimensionality. As a rule of thumb, dimensionality reduction is considered to be « acceptable » when AUC > 0.7. AUC > 0.8 is considered as « excellent ». The lower dimensional space is a poor representation of the initial trait space when AUC < 0.5 and AUC = 0 means as good as random. The vertical red line indicates the number of PCoA dimensions (n = 4) we retained for computing some of our functional diversity indices.

Mouillot, D., Loiseau, N., Grenié, M., Algar, A. C., Allegra, M., Cadotte, M. W., . . . Auber, A. (2021). The dimensionality and structure of species trait spaces. *Ecology Letters, 24*(9), 1988-2009. doi:https://doi.org/10.1111/ele.13778

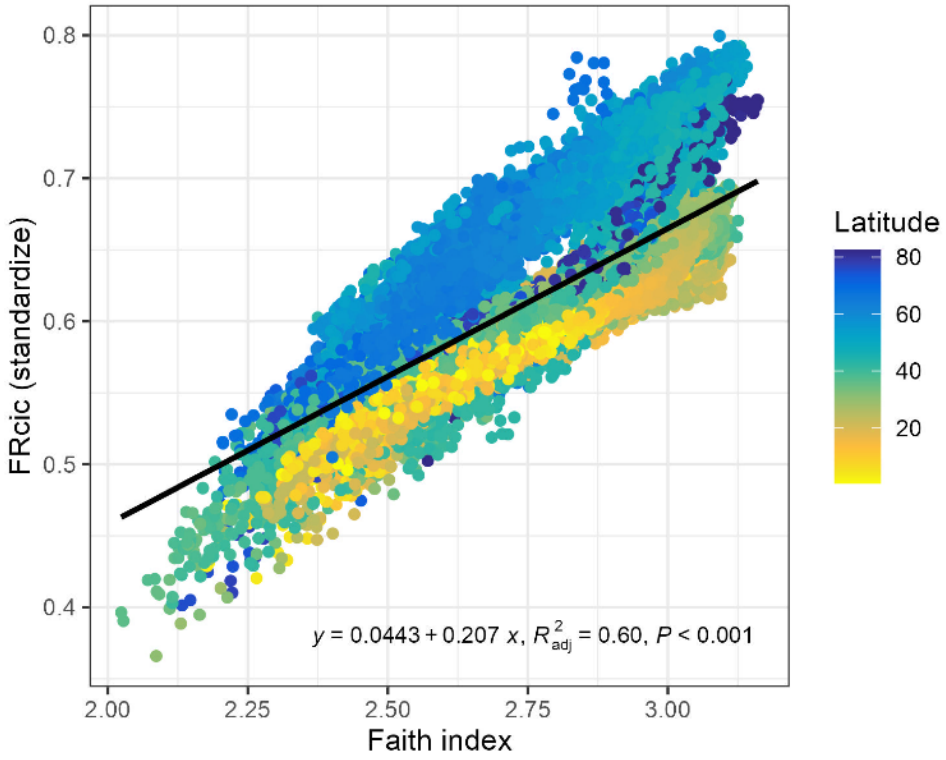

Figure S2: Agreement between our Faith index values and the functional richness (FRic) index of Villéger et al. (2008) on a mean annual scale. The indices were computed based on presence-absence data and mean annual values are derived from monthly values (n = 12) computed for assemblages whose species composition was modelled through three species distribution models. Spearman's rank correlation coefficient between the two functional richness indices is equal to 0.69 ($P < 0.001$) on a mean annual scale.

Villéger, S., Mason, N. W. H., & Mouillot, D. (2008). New multidimensional functional diversity indices for a multifaceted framework in functional ecology. *Ecology, 89*(8), 2290-2301. doi:https://doi.org/10.1890/07-1206.1

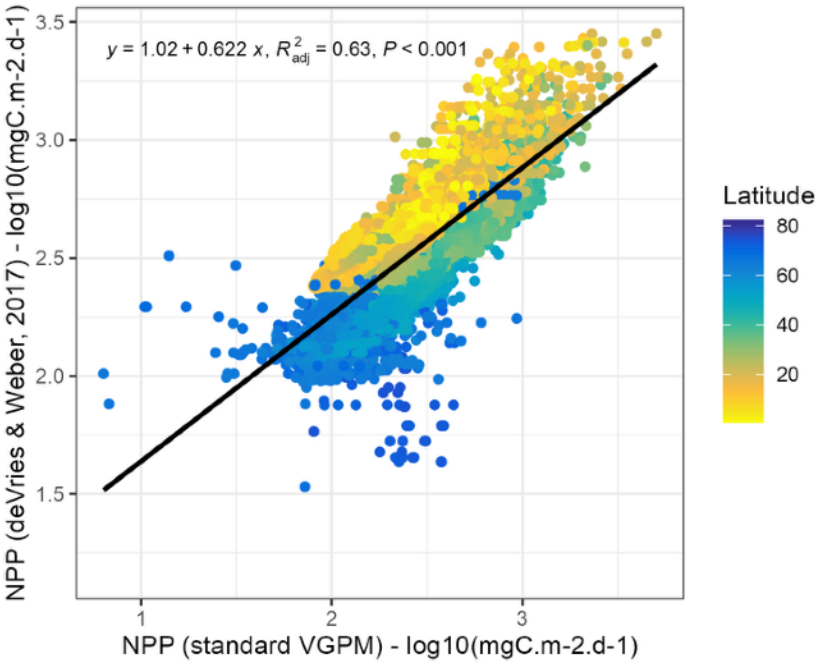

Figure S3: Agreement between the mean annual values of surface net primary production (NPP) issued from the standard VGPM algorithm (available at: https://sites.science.oregonstate.edu/ocean.productivity/index.php) and those from DeVries & Weber (2017), on a log10 scale. The Spearman's rank correlation coefficient between the two products of mean annual NPP is equal to 0.80 ($P < 0.001$). The bold line corresponds to the fitted linear regression.

DeVries, T., & Weber, T. (2017). The export and fate of organic matter in the ocean: New constraints from combining satellite and oceanographic tracer observations. *Global Biogeochemical Cycles, 31*(3), 535-555. doi:10.1002/2016gb005551

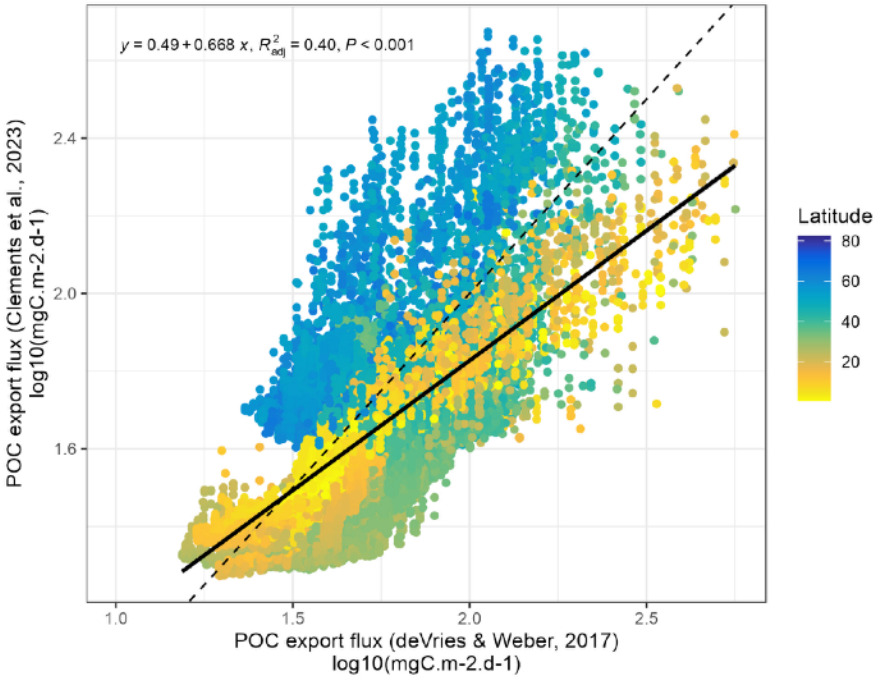

Figure S4: Agreement between the global mean annual values of particulate organic carbon (POC) export flux from DeVries & Weber (2017) and those from Clements et al. (2023) (on a log10 scale). The Spearman's rank correlation coefficient between the two products is equal to 0.54 ($P < 0.001$). The dashed line corresponds to the 1:1 line. The bold line corresponds to the fitted linear regression.

Clements, D. J., Yang, S., Weber, T., McDonnell, A. M. P., Kiko, R., Stemmann, L., & Bianchi, D. (2023). New Estimate of Organic Carbon Export From Optical Measurements Reveals the Role of Particle Size Distribution and Export Horizon. *Global Biogeochemical Cycles, 37*(3), e2022GB007633. doi:https://doi.org/10.1029/2022GB007633

DeVries, T., & Weber, T. (2017). The export and fate of organic matter in the ocean: New constraints from combining satellite and oceanographic tracer observations. *Global Biogeochemical Cycles, 31*(3), 535-555. doi:10.1002/2016gb005551

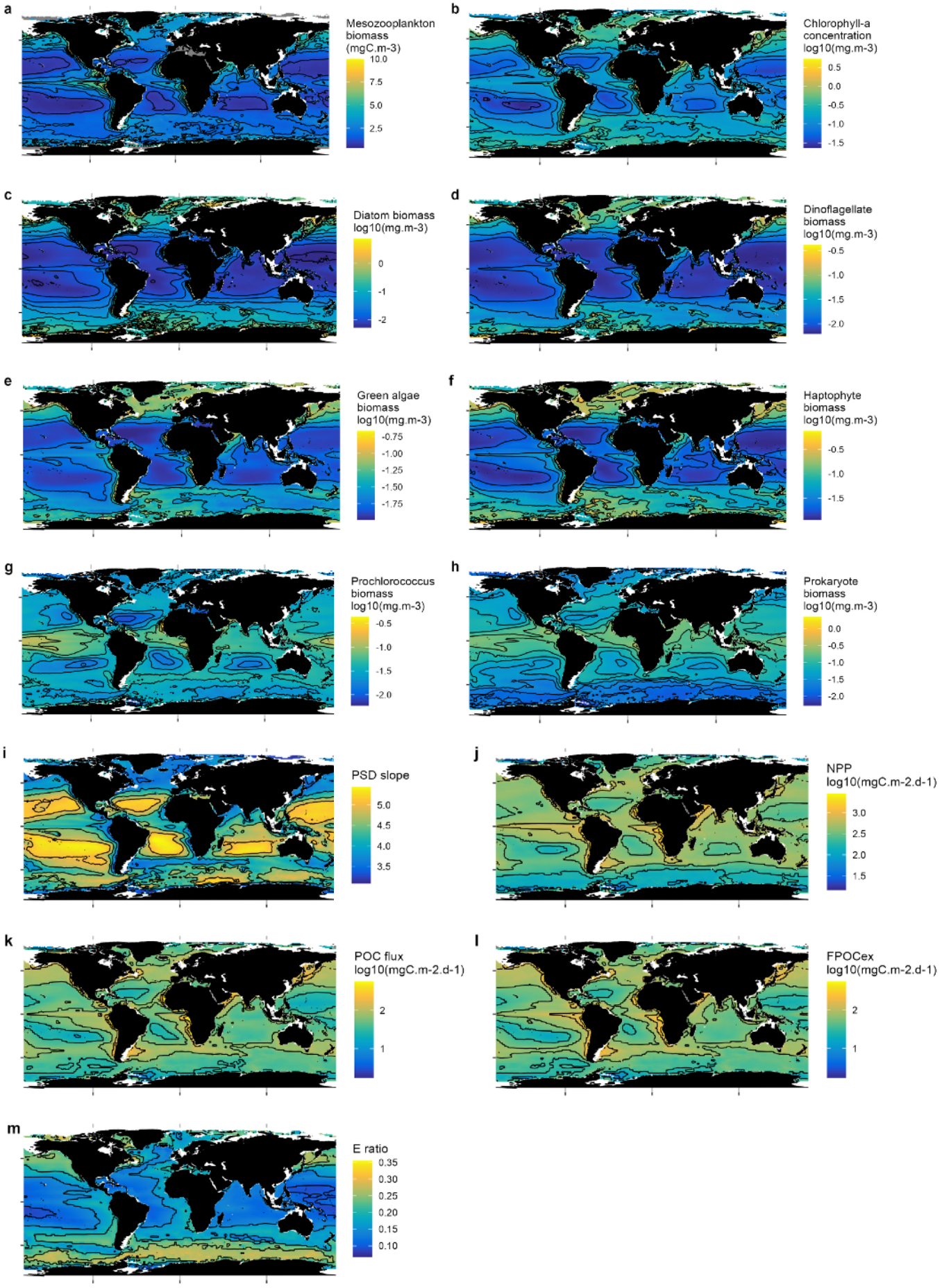
a
Mesozooplankton biomass (mgC.m-3)
10.0
7.5
5.0
2.5
b
Chlorophyll-a concentration log10(mg.m-3)
0.5
0.0
-0.5
-1.0
-1.5
c
Diatom biomass log10(mg.m-3)
0
-1
-2
d
Dinoflagellate biomass log10(mg.m-3)
-0.5
-1.0
-1.5
-2.0
e
Green algae biomass log10(mg.m-3)
-0.75
-1.00
-1.25
-1.50
-1.75
f
Haptophyte biomass log10(mg.m-3)
-0.5
-1.0
-1.5
g
Prochlorococcus biomass log10(mg.m-3)
-0.5
-1.0
-1.5
-2.0
h
Prokaryote biomass log10(mg.m-3)
0.0
-0.5
-1.0
-1.5
-2.0
i
PSD slope
5.0
4.5
4.0
3.5
j
NPP log10(mgC.m-2.d-1)
3.0
2.5
2.0
1.5
k
POC flux log10(mgC.m-2.d-1)
2
1
l
FPOCex log10(mgC.m-2.d-1)
2
1
m
E ratio
0.35
0.30
0.25
0.20
0.15
0.10

Figure S5: Spatial distribution of mean annual a) surface mesozooplankton biomass concentration (MESOZOO), b) surface chlorophyll-a concentration (CHL-A), c) surface diatom biomass concentration (DIATO), d) surface dinoflagellates biomass concentration (DINO), e) surface green algae biomass concentration (GREEN), f) surface haptophyte biomass concentration (HAPTO), g) surface *Prochlorococcus* biomass concentration (PROCHL), h) surface prokaryote biomass concentration (PROKAR), i) surface values of the slope of the particle size distribution (PSD SLOPE), j) surface net primary production (NPP), k) surface flux of sinking particulate organic carbon (POC flux), l) POC export flux at the basis of the euphotic zone (FPOCex), and m) the efficiency of POC export at the basis of the euphotic zone relative to surface NPP (E ratio = FPOCex/NPP).

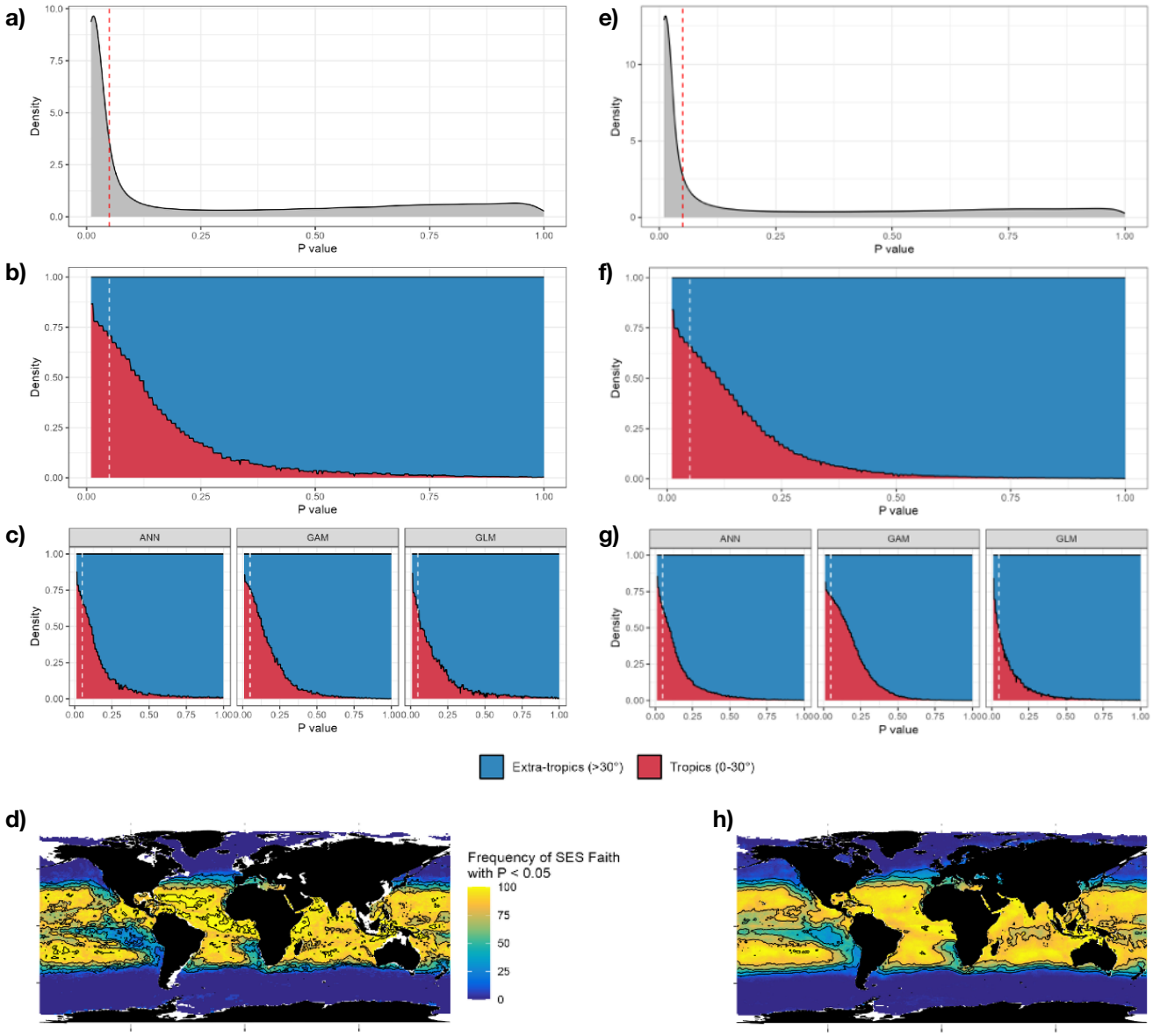

Figure S6: Density of the P-values of the standardized-effect-size of the Faith index (SES Faith) based on the observed Faith and the distribution of 999 null Faith values, in terms of a) absolute distribution and b) relative distribution across tropical (red) and extra-tropical (blue) copepod assemblages. c) same as b) but across the three different species distribution models used in our study (GLM = generalized linear model, GAM = generalized additive model, ANN = artificial neural network). d) show the global surface spatial distribution of the frequency of $P < 0.05$ (in %) based on the same data as a) and b). e) to h) are the same as a) to d) but for the end-of-century period (2081-2100) instead of the contemporary period. Faith and SES Faith were computed from the species' monthly presence-absence maps. The red and white dashed vertical lines indicate the positon of the chosen significance threshold ($P = 0.05$).

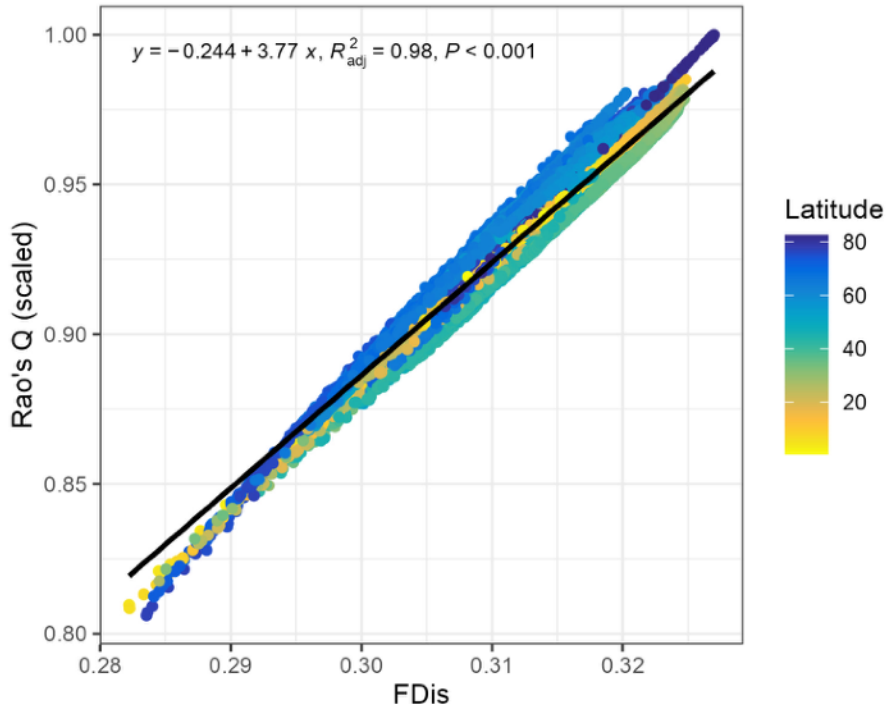

Figure S7: Comparison between mean annual functional dispersion (FDis) and mean annual Rao's quadratic entropy (Rao's Q, scaled to its maximal values). The indices were computed on species habitat suitability data and mean annual values are derived from monthly values (n = 12) computed for assemblages whose species composition was modelled through three species distribution models. Spearman's rank correlation coefficient between the two indices is equal to 0.98 ($P < 0.001$) on a mean annual scale. The bold line corresponds to the fitted linear regression.

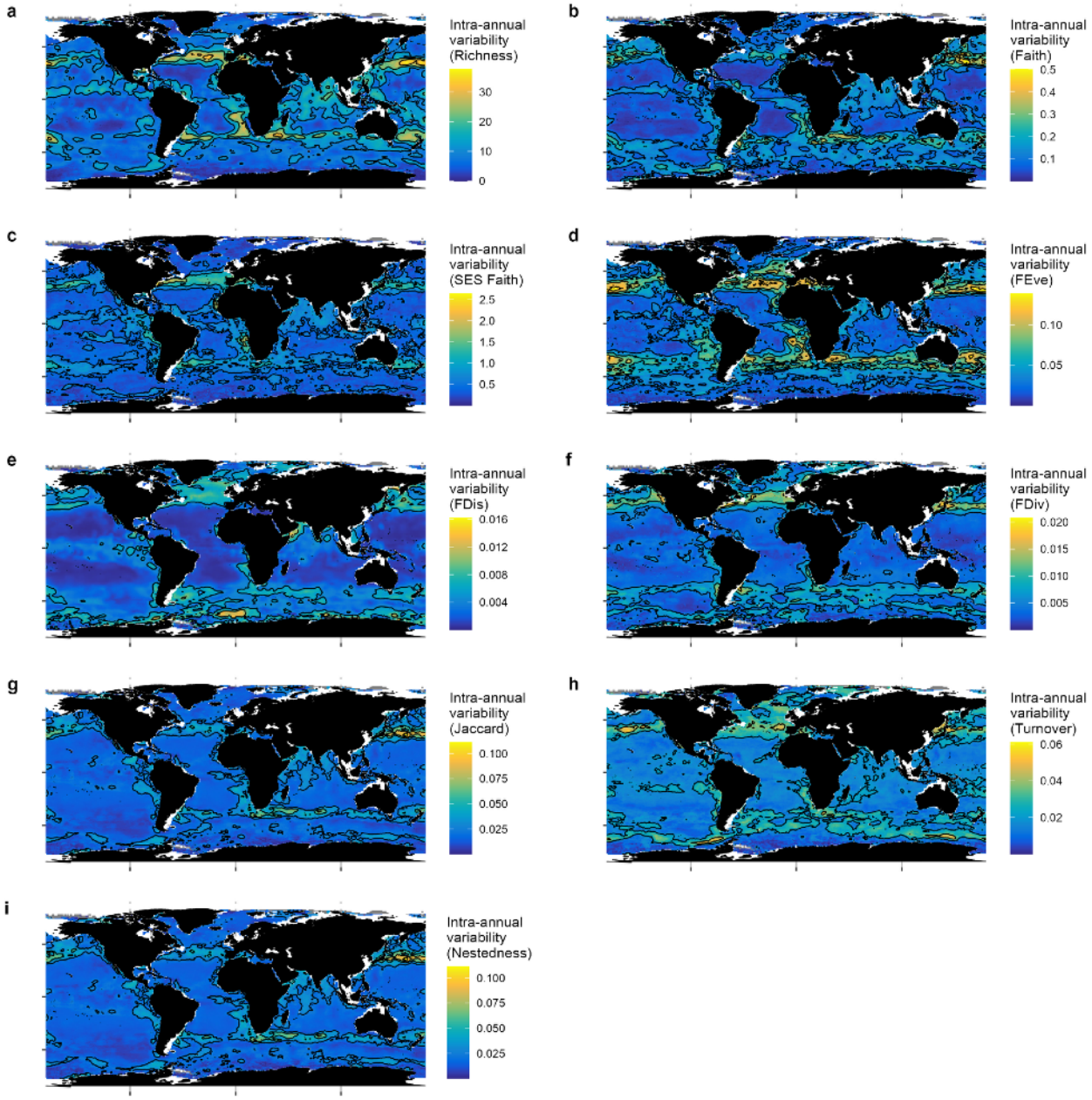

Figure S8: Spatial distribution of the intra-annual variability in global surface estimates of a) copepod species richness, b) functional richness (Faith index), c) standardized-effect-sizes of the Faith index (SES Faith), d) functional evenness (FEve), e) functional dispersion (FDis), f) functional divergence (FDiv), g) total trait dissimilarity (based on Jaccard's index), h) trait turnover, and i) trait nestedness. Mean annual values were derived from monthly values (n = 12) computed for assemblages whose species composition was modelled through three species distribution models. Copepod species richness, Faith, SES Faith and the three functional beta diversity indices (based on Jaccard's dissimilarity index) were based on presence-absence data whereas FEve, FDis and FDiv were weighed by species habitat suitability indices ranging between 0 and 1 (i.e., presence probability).

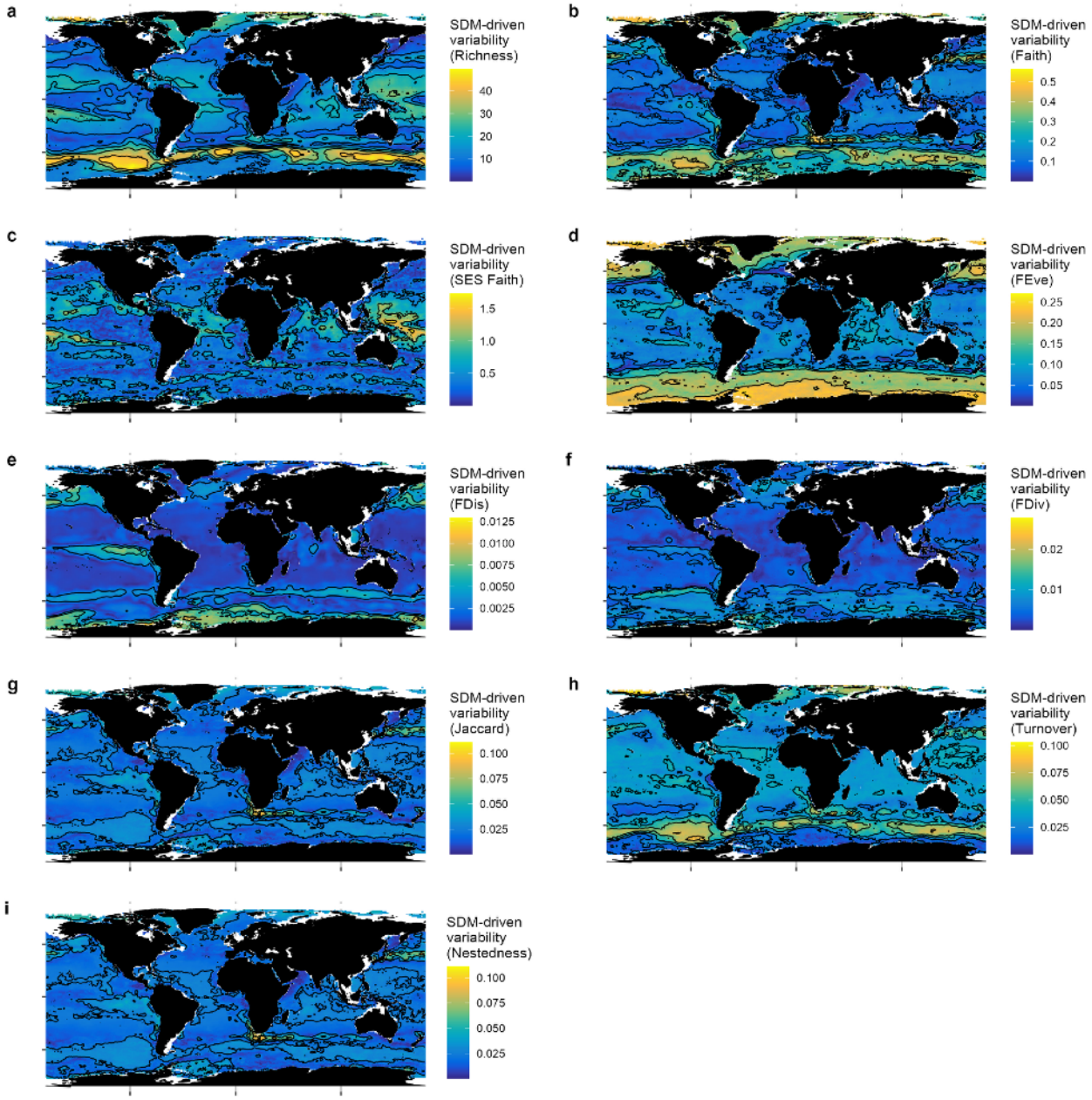

Figure S9: Spatial distribution of the variability (i.e., uncertainty) that is driven by the choice of the species distribution model (SDM) for our global surface estimates of a) copepod species richness, b) functional richness (Faith index), c) standardized effect sizes of the Faith index (SES Faith), d) functional evenness (FEve), e) functional dispersion (FDis), f) functional divergence (FDiv), g) total trait dissimilarity (based on Jaccard's index), h) trait turnover, and i) trait nestedness. Mean annual values were derived from monthly values (n = 12) computed for assemblages whose species composition was modelled through three types of species distribution models (GLMs, GAMs and ANN). Copepod species richness, Faith, SES Faith and the three functional beta diversity indices (based on Jaccard's dissimilarity index) were based on presence-absence data whereas FEve, FDis and FDiv were weighed by species habitat suitability indices ranging between 0 and 1 (i.e., presence probability).

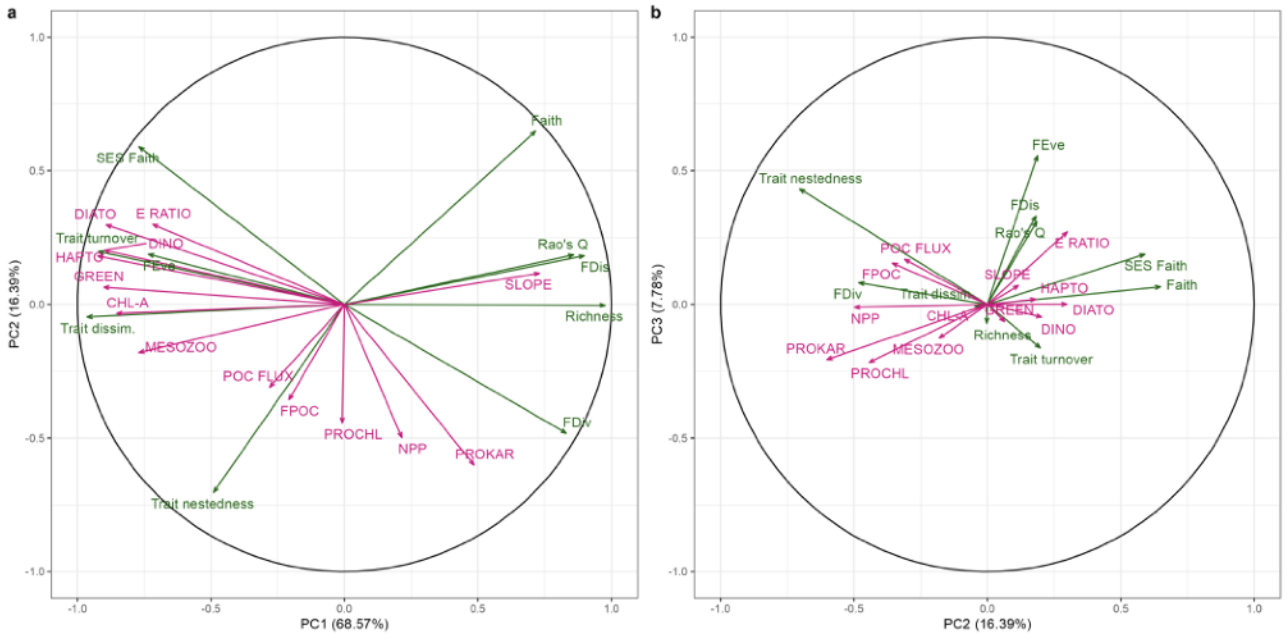

Figure S10: Principal component analysis (PCA) showing the covariance between mean annual values of copepod diversity indices (green) and indicators of marine ecosystem functioning (pink; Figure S5). a) shows principal components (PC) 1 and 2 (84.96% of total variance) and b) shows PC 2 and 3 (24.17% of total variance). Richness = copepod species richness, Faith = Faith richness (index of functional richness), SES Faith = standardized-effect-size of Faith index, FEve = functional evenness, FDis = functional dispersion, FDiv = functional divergence, Rao's Q = Rao's quadratic entropy, Trait dissim. = total trait dissimilarity (based on Jaccard's index), MESOZOO = surface concentration of mesozooplankton biomass, CHL-A = surface chlorophyll-a concentration, DIATO = surface concentration of diatom biomass, DINO = surface concentration of dinoflagellate biomass, HAPTO = surface concentration of haptophyte biomass, GREEN = surface concentration of green algae biomass, PROCHL = surface concentration of *Prochlorococcus* biomass, PROKAR = surface concentration of prokaryote biomass, SLOPE = slope of the spectrum of the particles size distribution, NPP = net primary production, POC FLUX = surface flux of sinking particulate organic carbon (POC), FPOC = export flux of POC out of the euphotic zone, E RATIO = efficiency of POC export relative to the surface NPP (FPOC/NPP).

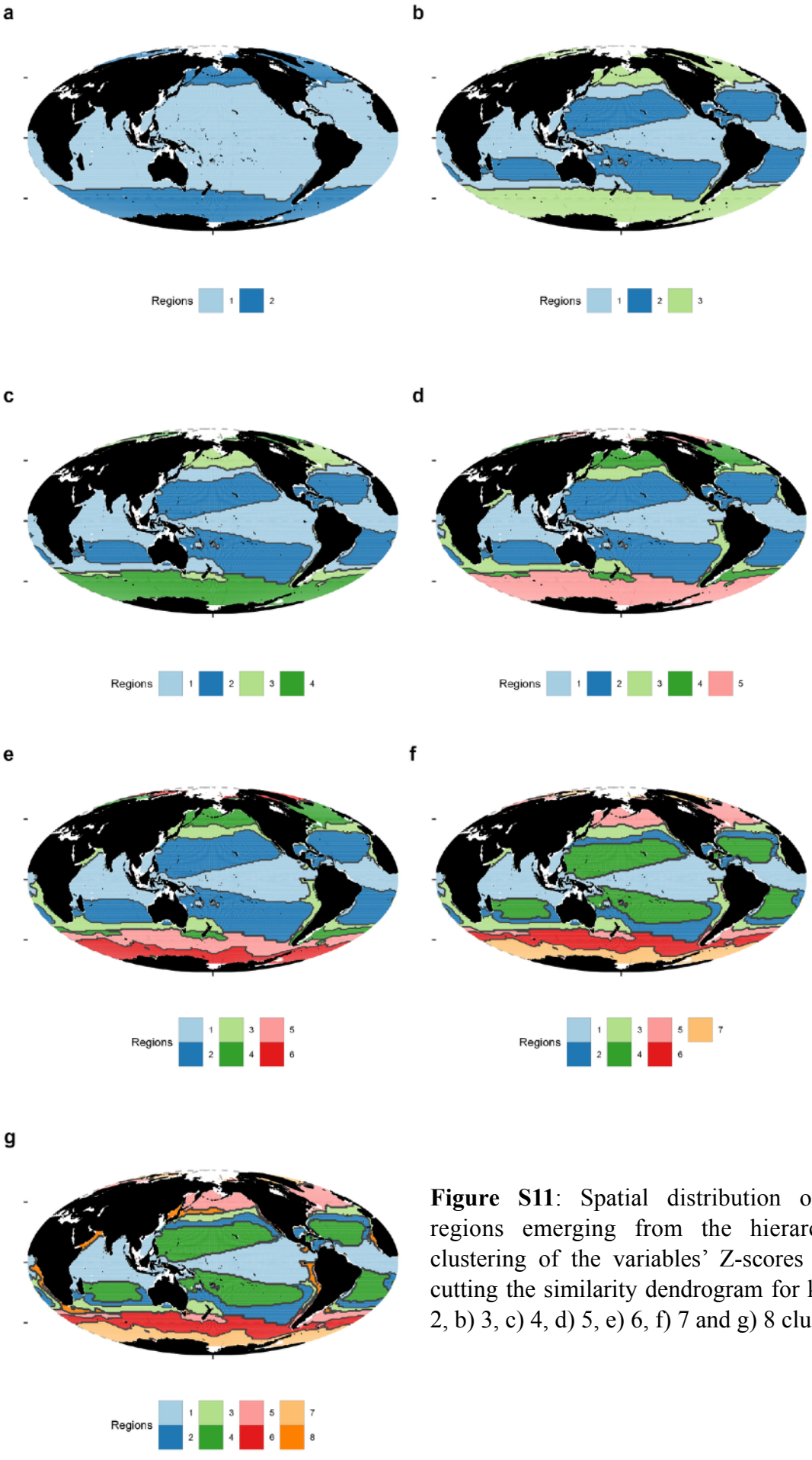

Figure S11: Spatial distribution of the regions emerging from the hierarchical clustering of the variables' Z-scores when cutting the similarity dendrogram for k = a) 2, b) 3, c) 4, d) 5, e) 6, f) 7 and g) 8 clusters.

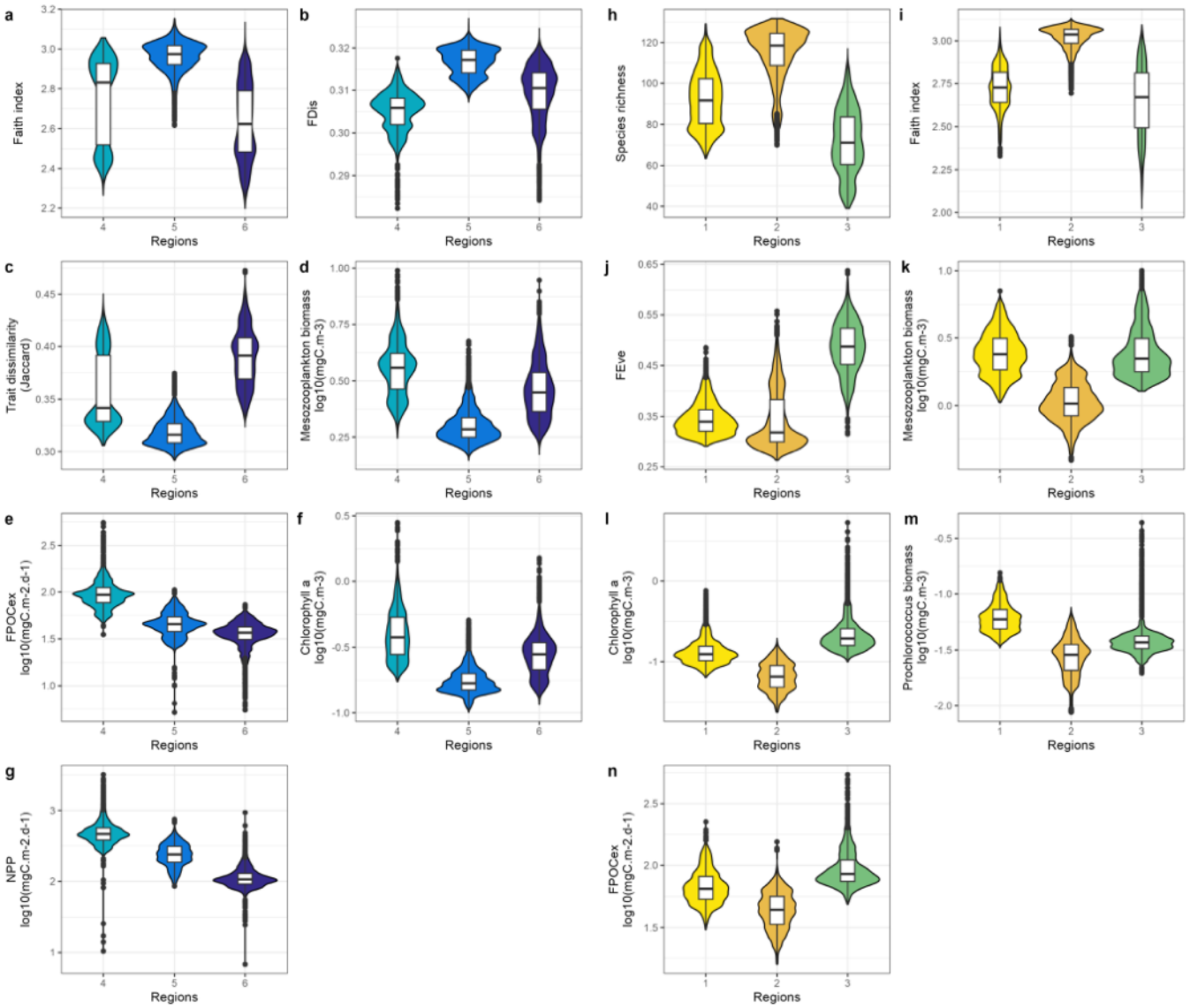

Figure S12: Distribution of mean annual a) Faith index (functional richness), b) Functional dispersion (FDis), c) total trait dissimilarity (based on Jaccard's index), d) mesozooplankton biomass surface concentration (MESOZOO), e) flux of particulate organic carbon (POC) out of the euphotic zone (FPOCex), f) surface chlorophyll-a concentration (CHL-A) and g) surface net primary production (NPP) between regions 4, 5 and 6 shown in Figure 5 (high latitude regions); distribution of mean annual h) surface copepod species richness, i) Faith index, j) functional evenness (FEve), k) MESOZOO, l) CHL-A, m) surface *Prochlorococcus* biomass concentration and n) FPOCex between regions 1, 2 and 3 shown in Figure 5 (tropical regions). Non parametric variance analyses (Kruskal-Wallis tests) and pairwise Wilcoxon tests were applied with Bonferroni's method for P values correction to test for differences in the distributions shown here. They all returned significant P values ($P < 0.001$).

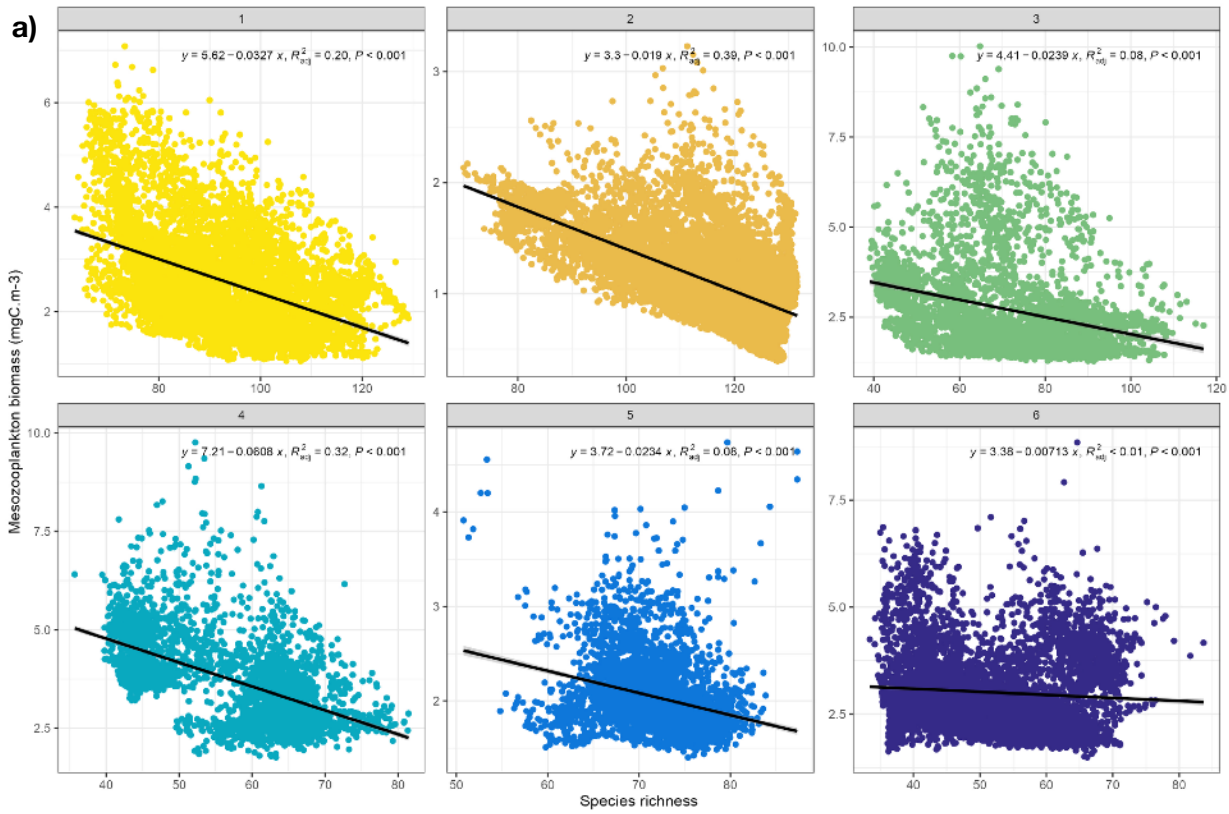
a)
1
2
3
4
5
6
y = 5.62 − 0.0327 x, R^2_{adj} = 0.20, P < 0.001
y = 3.3 − 0.019 x, R^2_{adj} = 0.39, P < 0.001
y = 4.41 − 0.0239 x, R^2_{adj} = 0.08, P < 0.001
y = 7.21 − 0.0608 x, R^2_{adj} = 0.32, P < 0.001
y = 3.72 − 0.0234 x, R^2_{adj} = 0.06, P < 0.001
y = 3.38 − 0.00713 x, R^2_{adj} < 0.01, P < 0.001
Mesozooplankton biomass (mgC.m-3)
Species richness

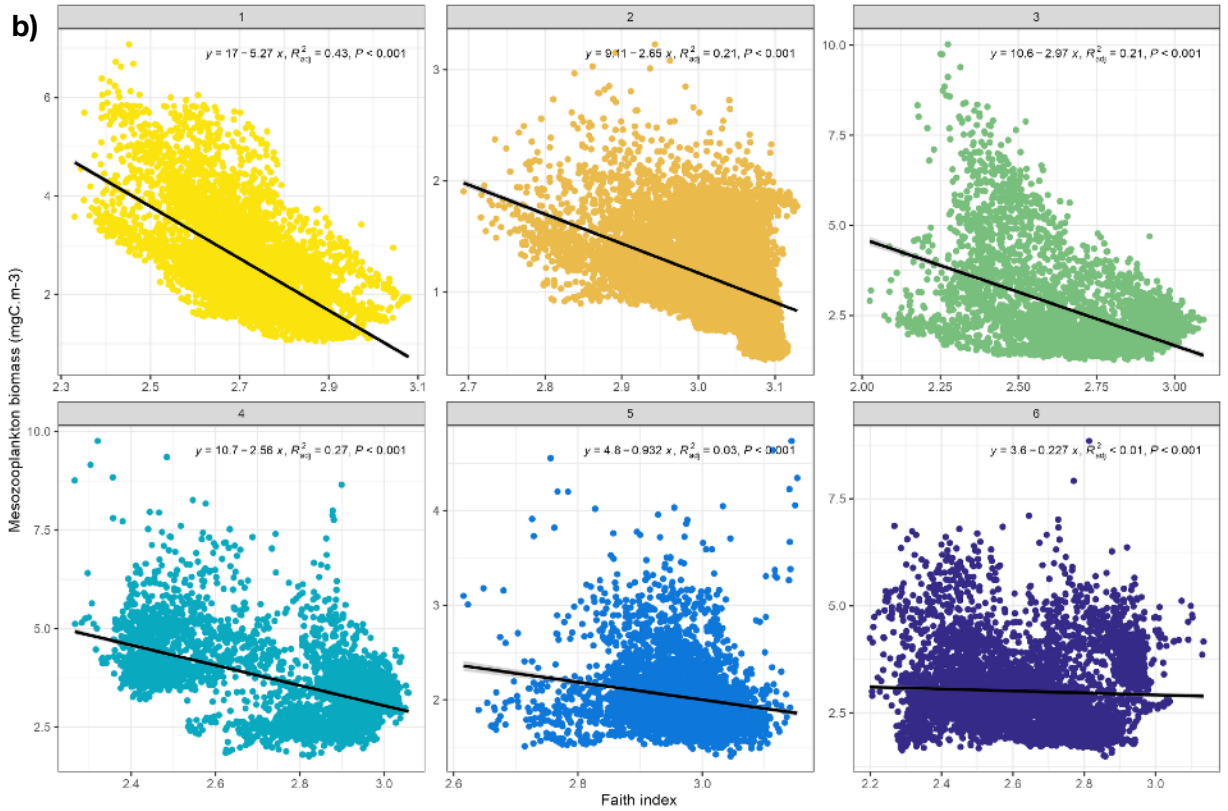
b)
1
2
3
4
5
6
y = 17 − 5.27 x, R^2_{adj} = 0.43, P < 0.001
y = 9.11 − 2.65 x, R^2_{adj} = 0.21, P < 0.001
y = 10.6 − 2.97 x, R^2_{adj} = 0.21, P < 0.001
y = 10.7 − 2.58 x, R^2_{adj} = 0.27, P < 0.001
y = 4.8 − 0.932 x, R^2_{adj} = 0.03, P < 0.001
y = 3.6 − 0.227 x, R^2_{adj} < 0.01, P < 0.001
Mesozooplankton biomass (mgC.m-3)
Faith index

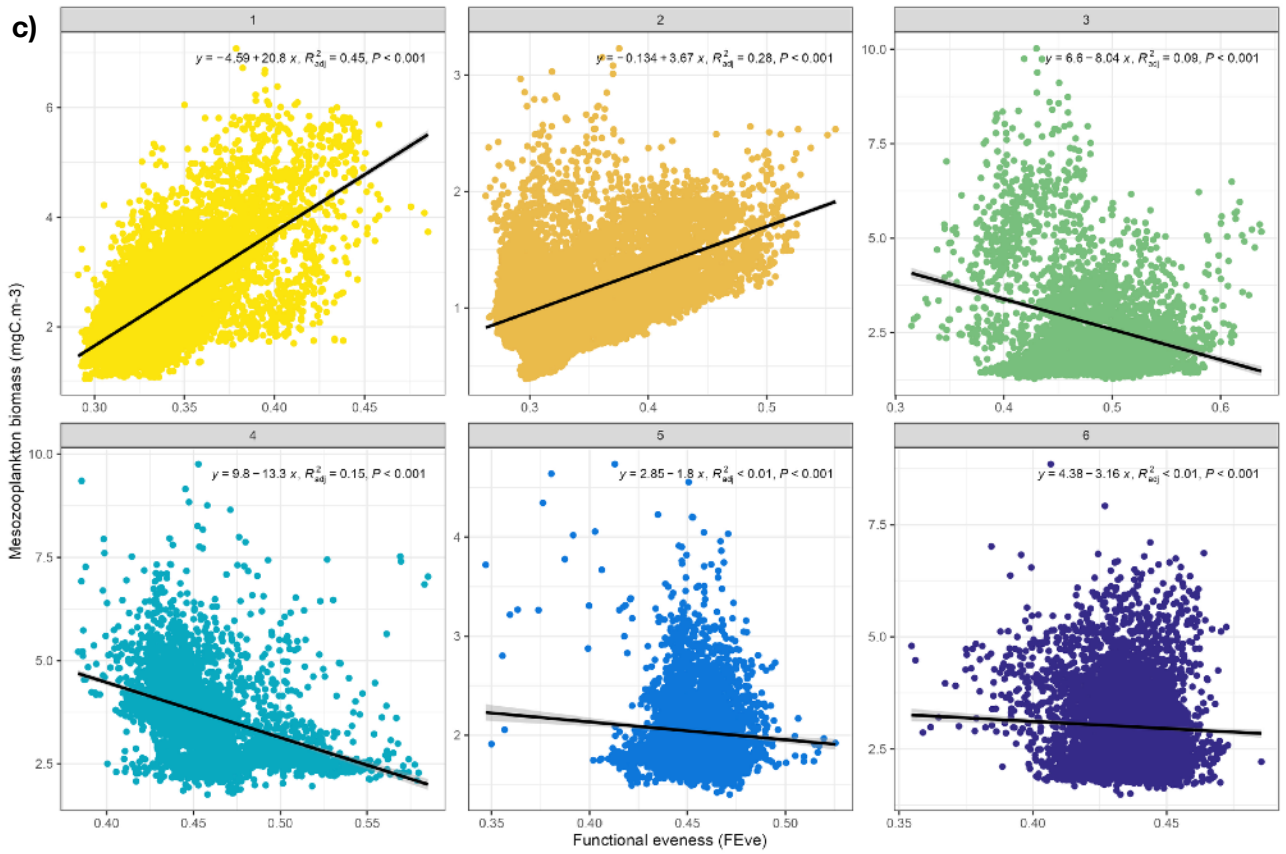
c)
1
2
3
4
5
6
y = −4.59 + 20.8 x, R^2_{adj} = 0.45, P < 0.001
y = −0.134 + 3.67 x, R^2_{adj} = 0.28, P < 0.001
y = 6.6 − 8.04 x, R^2_{adj} = 0.09, P < 0.001
y = 9.8 − 13.3 x, R^2_{adj} = 0.15, P < 0.001
y = 2.85 − 1.8 x, R^2_{adj} < 0.01, P < 0.001
y = 4.38 − 3.16 x, R^2_{adj} < 0.01, P < 0.001
Mesozooplankton biomass (mgC.m-3)
Functional eveness (FEve)

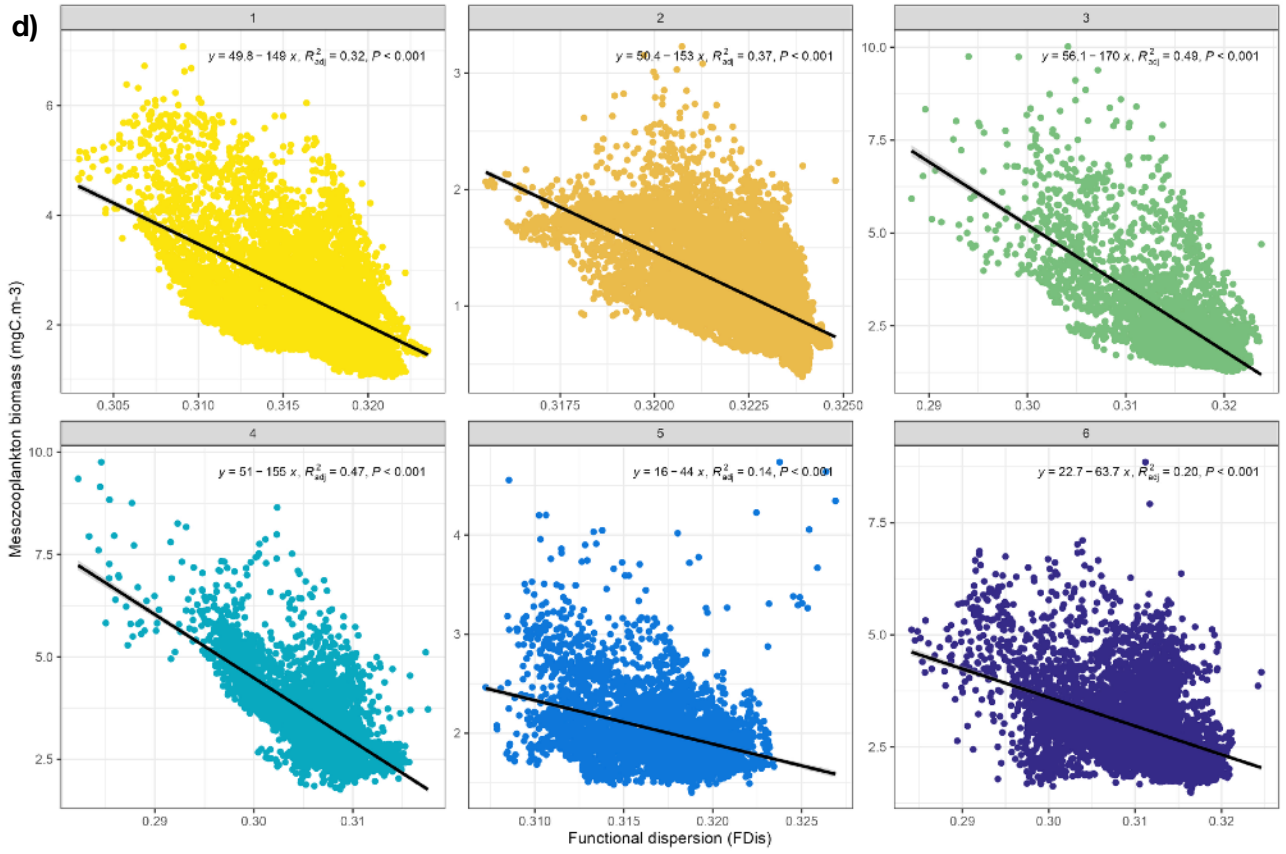
d)
1
2
3
4
5
6
y = 49.8 − 148 x, R^2_{adj} = 0.32, P < 0.001
y = 50.4 − 153 x, R^2_{adj} = 0.37, P < 0.001
y = 56.1 − 170 x, R^2_{adj} = 0.49, P < 0.001
y = 51 − 155 x, R^2_{adj} = 0.47, P < 0.001
y = 16 − 44 x, R^2_{adj} = 0.14, P < 0.001
y = 22.7 − 63.7 x, R^2_{adj} = 0.20, P < 0.001
Mesozooplankton biomass (mgC.m-3)
Functional dispersion (FDis)

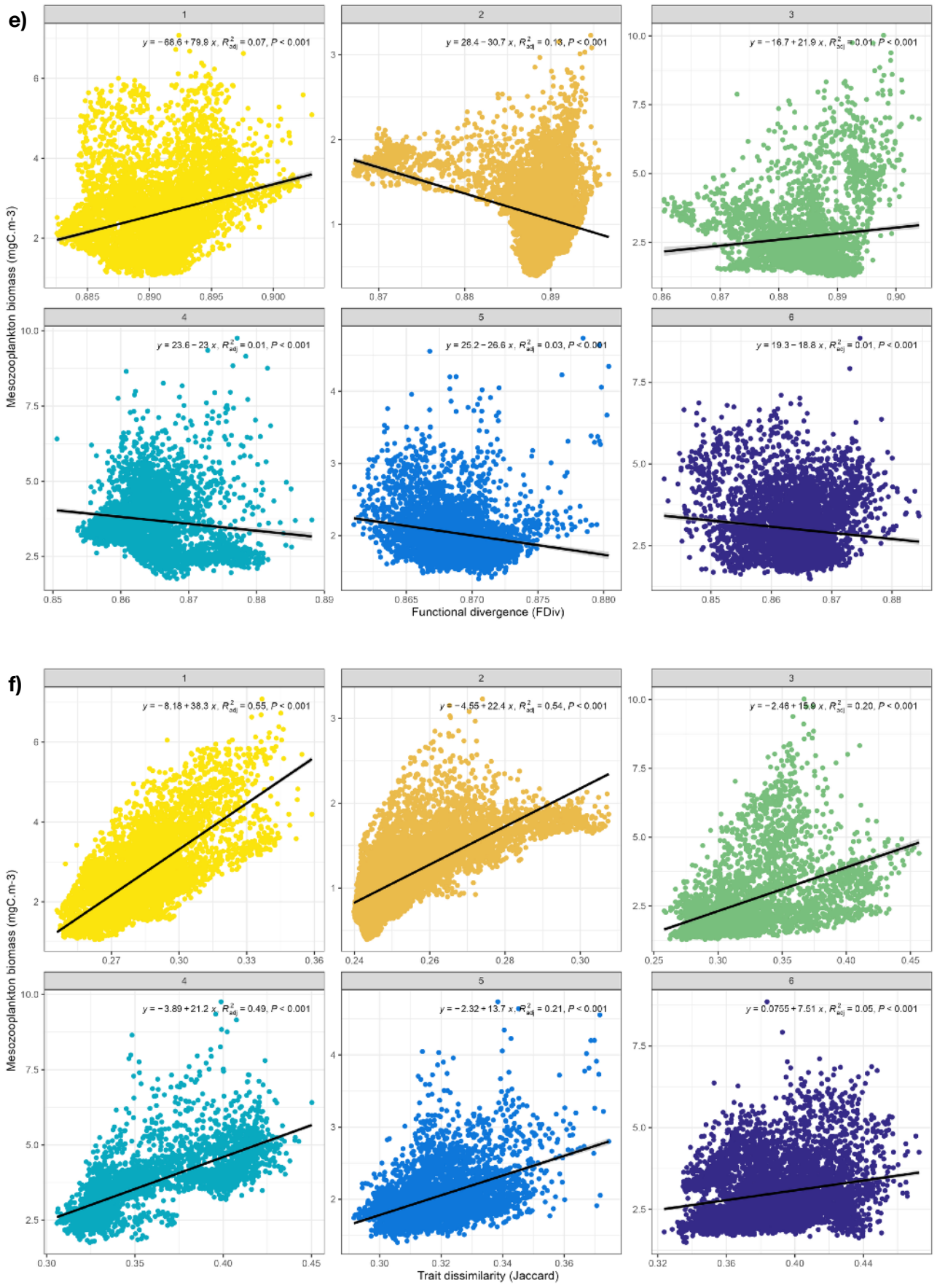

Figure S13: Emergent relationships between mean annual surface estimates of mesozooplankton biomass concentration and a) copepod species richness, b) Faith index (functional richness index), c) functional evenness (FEve), d) functional dispersion (FDis), e) functional divergence (FDiv) and

f) total trait dissimilarity (based on Jaccard's index) between the six regions defined in Figure 5. The black bold lines correspond to the fitted linear regressions. Copepod species richness, Faith and total trait dissimilarity were based on presence-absence data whereas FEve, FDis and FDiv were weighed by species habitat suitability indices ranging between 0 and 1.

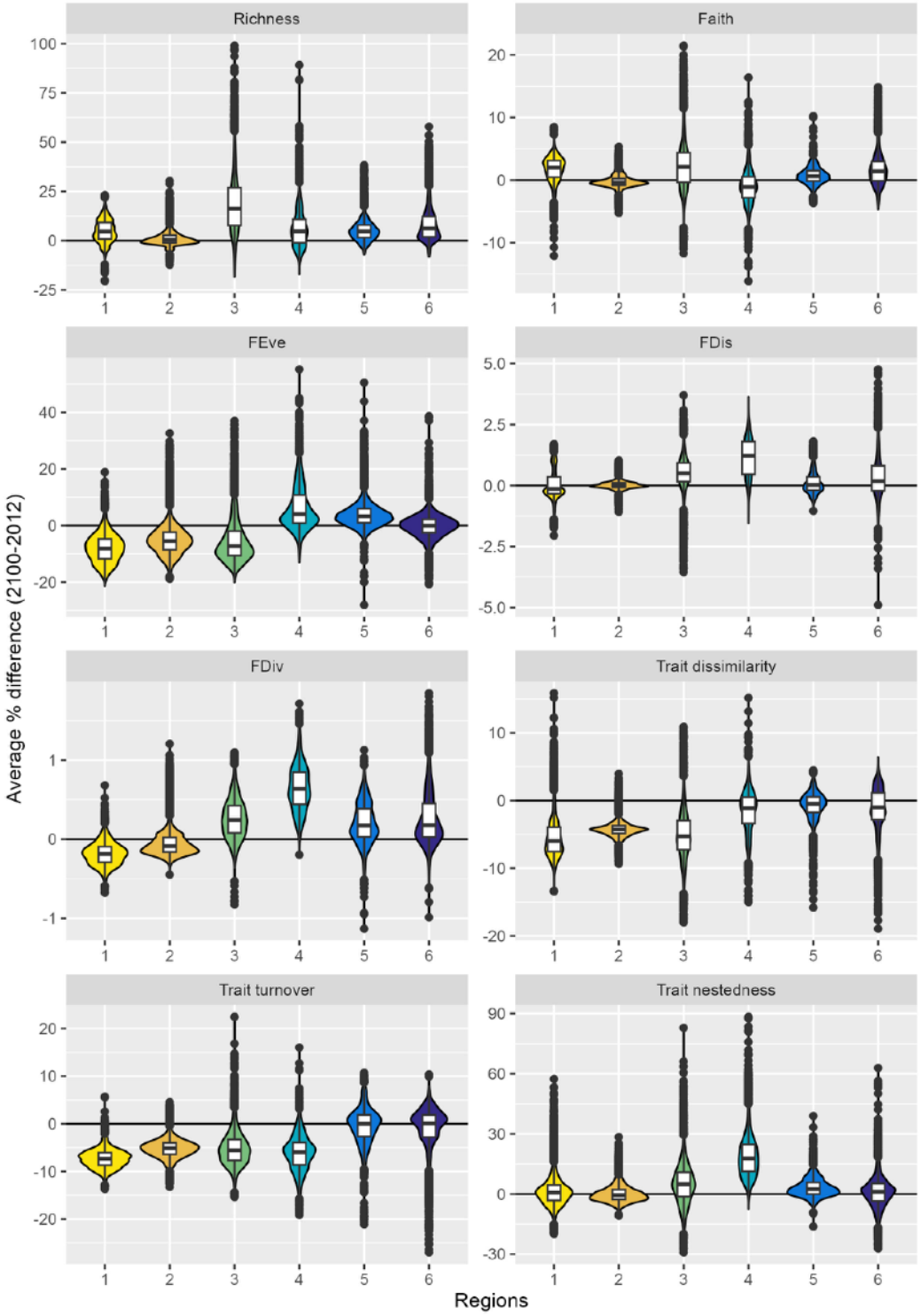

Figure S14: Distribution of the relative differences (Δ, in %) in copepod species richness, Faith index, functional evenness (FEve), functional dispersion (FDis), functional divergence (FDiv), total trait dissimilarity, trait turnover and trait nestedness between the contemporary (2012-2031) and end-of-century (2081-2100) periods, across the six regions of Figure 5. End-of-century estimates were based on an ensemble of monthly values obtained for three species distribution models and five earth system models (n = 180). Species richness, Faith and functional beta diversity indices were based on presence-absence data whereas FEve, FDis and FDiv were weighed by habitat suitability indices.

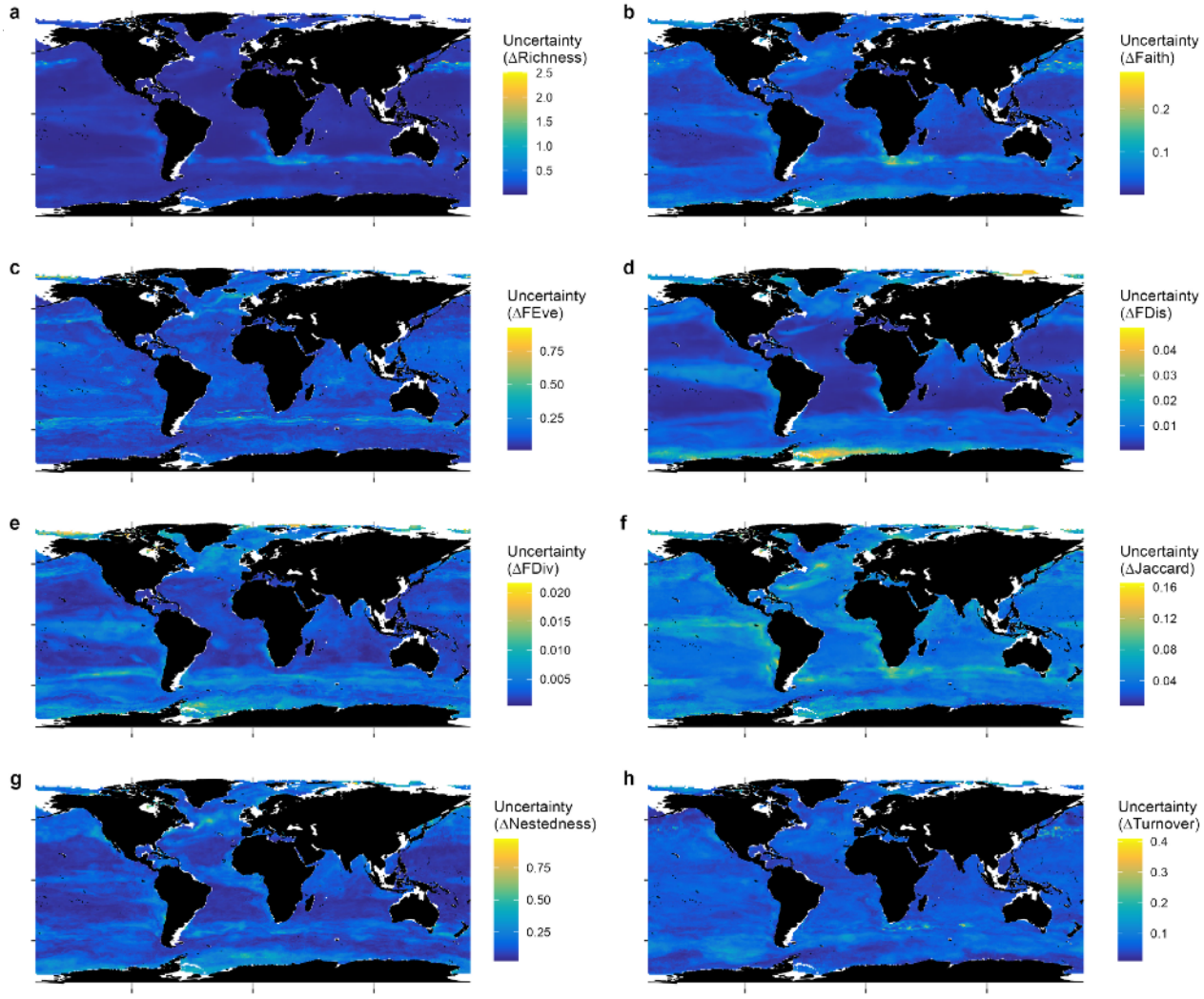

Figure S15: Spatial distribution of uncertainty (i.e., standard deviation associated to the ensemble mean) of the relative difference (Δ, in %) in a) copepod species richness, b) Faith index (functional richness index), c) functional evenness (FEve), d) functional dispersion (FDis), e) functional divergence (FDiv), f) total trait dissimilarity (based on Jaccard's index), g) trait nestedness and h) trait turnover between the contemporary (2012-2031) and end-of-century (2081-2100) periods. End-of-century estimates were based on an ensemble of monthly values obtained for three species distribution models and five earth system models (n = 180). Species richness, Faith and functional beta diversity indices were based on presence-absence data whereas FEve, FDis and FDiv were weighed by habitat suitability indices.

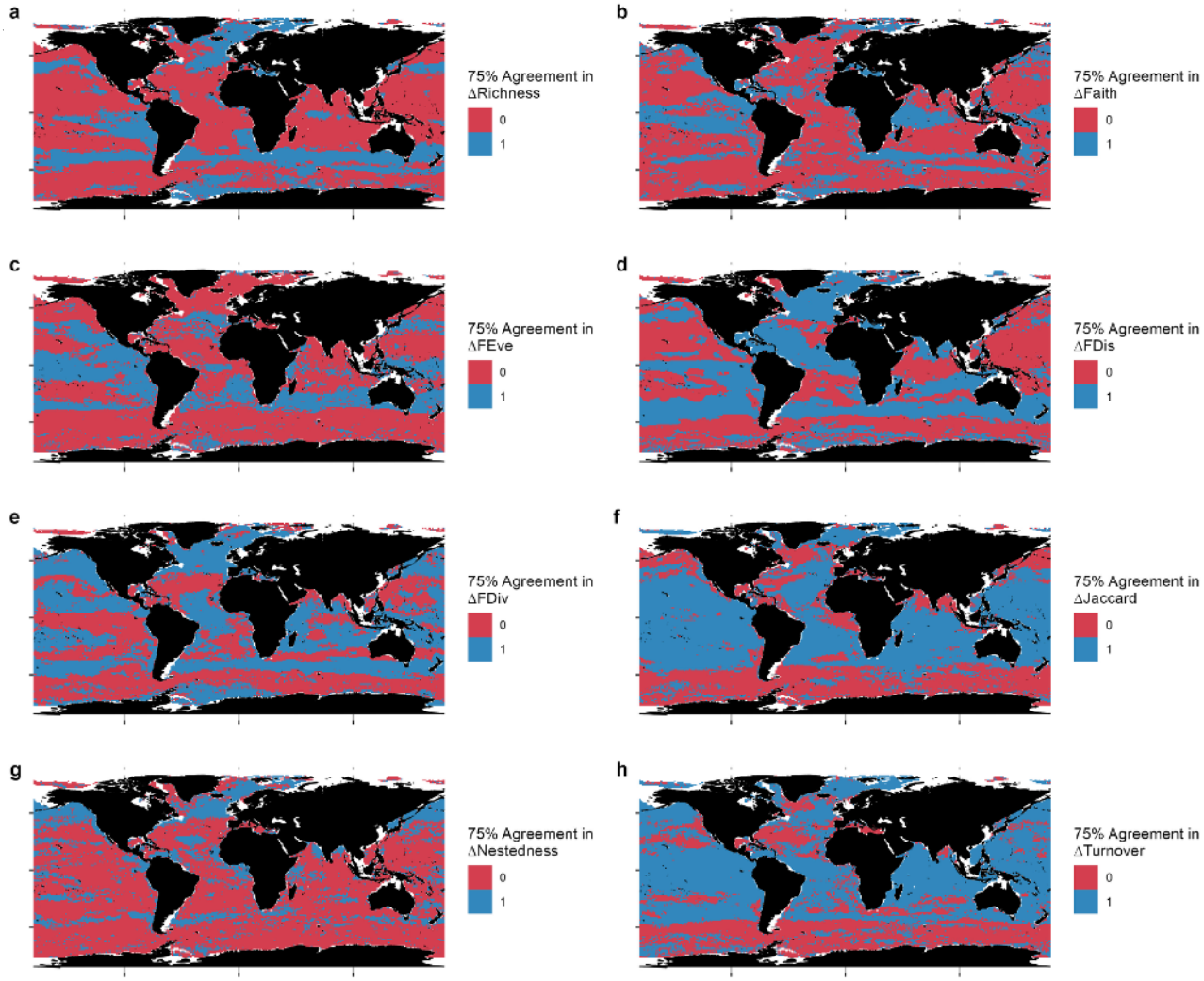

Figure S16: Regions where more than 75% of the ensemble members (n = 15 on a mean annual scale, highlighted in blue on the maps) agree on the sign of the relative difference (Δ, in %) in a) copepod species richness, b) Faith index (functional richness index), c) functional evenness (FEve), d) functional dispersion (FDis), e) functional divergence (FDiv), f) total trait dissimilarity (based on Jaccard's index), g) trait nestedness and h) trait turnover between the contemporary (2012-2031) and end-of-century (2081-2100) periods. End-of-century estimates were based on an ensemble of monthly values obtained for three species distribution models and five earth system models (n = 180).